HARVARD UNIVERSITY
Graduate School of Arts and Sciences

DISSERTATION ACCEPTANCE CERTIFICATE

The undersigned, appointed by the

Division of Medical Sciences

in the subject of Biological Chemistry and Molecular Pharmacology

have examined a dissertation entitled

The Role of Pericyte Loss in Adult Retinal Microvascular Stability:
Implications for Diabetic Retinopathy

presented by Cammi Nicole Valdez

candidate for the degree of Doctor of Philosophy and hereby certify that it is worthy of acceptance.

Signature:
Typed Name: Dr. Guillermo Garcia-Cardeña

Signature:
Typed Name: Dr. Diane Bielenberg

Signature:
Typed Name: Dr. Matthew Nugent

Dr. Susan Dymecki, Program Head

Date: May 01, 2014

Dr. David Lopes Cardozo, Director of Graduate Studies

The Role of Pericyte Loss in Adult Retinal Microvascular Stability: Implications for Diabetic Retinopathy

A dissertation presented

by

Cammi Nicole Valdez

to

The Division of Medical Sciences

in partial fulfillment of the requirements
for the degree of
Doctor of Philosophy
in the subject of
Biological Chemistry and Molecular Pharmacology

Harvard University
Cambridge, Massachusetts
May 2014

Dissertation Advisor: Dr. Patricia A. D’Amore Cammi Valdez

The Role of Pericyte Loss in Adult Retinal Microvascular Stability: Implications for Diabetic Retinopathy

ABSTRACT

Diabetes affects more than 382 million people worldwide and can lead to vision loss as a result of progressive degeneration of the neurovascular unit in the retina, a condition known as diabetic retinopathy (DR). Early stage DR is characterized by microangiopathies including microaneurysms, microhemorrhages, and hyper-permeability. Analyses of postmortem human retinal tissue and retinas from animal models indicate that degeneration of the pericytes, the cells that make up the outer layer of capillaries, is an early event in DR; however, the relative contribution of specific cellular components to DR pathobiology has been difficult to dissect due to the complexity of existing models.

To directly assess the consequences of pericyte death on retinal microvascular integrity, I used a mouse model (iDTR; M-Cre) conditionally expressing a simian diphtheria toxin receptor (DTR) controlled by the smooth muscle myosin heavy chain Cre (M-Cre) promoter. Upon induction of Cre, the simian DTR is expressed in pericytes and smooth muscle cells, which therefore become diphtheria toxin (DT) sensitive. Administration of DT to these mice causes mural cell loss. Five days after the first DT injection, iDTR; M-Cre mice developed microaneurysms, acellular capillaries, and increased vascular permeability, vascular changes that are characteristic of background DR.

To measure pericyte loss and acellular capillaries and to avoid bias and ambiguities associated with manual analysis, automated techniques were established to reliably quantify pericytes and endothelial cells, as well as acellular capillaries in the mouse retina. Using these algorithms, DT-treated iDTR; M-Cre mice were shown to have a 7-15% decrease in pericytes compared to controls. Furthermore, there were twice as many acellular capillaries detected in the iDTR; M-Cre mice as compared to controls.

Using a mouse model of inducible mural cells loss, I have demonstrated a direct role for pericyte loss in the development of microangiopathies observed in DR without the confounding metabolic factors present in existing DR models. These results suggests that preventing or delaying pericyte dropout will avert or attenuate the retinal pathology associated with diabetes and highlight a potential for future novel therapies.

TABLE OF CONTENTS

CHAPTER 1

INTRODUCTION

CHAPTER 2

CHARACTERIZING AN INDUCIBLE MOUSE MODEL OF MURAL CELL DEATH

CHAPTER 3

ESTABLISHING A LONG TERM MOUSE MODEL OF INDUCIBLE MURAL CELL DEATH

CHAPTER 4

DISCUSSION

CHAPTER 5

MATERIALS AND METHODS

CHAPTER 6

MATERIALS AND METHODS: DEVELOPING AUTOMATED IMAGE ANALYSIS TECHNIQUES

REFERENCES

APPENDIX

ACKNOWLEDGEMENTS

First and foremost, I would like to sincerely thank my thesis advisor, Dr. Patricia D'Amore. Pat is not only a phenomenal mentor, but also truly a role model for women in science. Her guidance, candor, and passion have gone above and beyond in supporting me throughout my project, graduate school, and my many extracurricular interests. I would also like to thank Dr. Joseph Arboleda-Velasquez. If I could describe Joe in one word, it would be irreplaceable. Joe has a remarkable talent for mentoring and knew exactly when to lend guidance and when to allow independence in my project. Very soon, I know that "PI Joe" will continue Pat's legacy of great mentorship in his own lab. In addition, I would like to thank the members of "Team Notch," Dhanesh Amarnani, Vincent Primo, Alex James, and Mark Graham, for all of your help with my mice, genotyping, tissue collection, and bovine iParties. A special thank you to Dhanesh, my rock, who has been by my side throughout the project, helping with all of my mouse injections and live imaging. I would also extend a debt of gratitude to the Drs. Jinling Yang, Cindy Park-Windhol, and Allen Tseng for making me an honorary member of the "Asian Bay." The three of you have truly become my best friends, and I will forever miss "taco salad Mondays." I am very grateful to Drs. Magali Saint-Geniez, Leo Kim, and Eric Ng for all of their support, helpful suggestions, and experimental guidance. This thesis could not have been written without the editing and proofing of Christine Bagley. I cannot express how thankful I am for her generosity, time, and loving nature. In addition, I would like to thank all of the members of the D'Amore and Saint-Geniez labs for their countless help and support throughout my time in the lab. A huge thank you to my dissertation advisory committee members, Drs. Joyce Bischoff, Joanne Chan, and Rick Mitchell, for providing thoughtful guidance and direction throughout my thesis work.

I would like to thank my GSAS family, Deans Xiao-Li Meng, Margot Gill, Garth McCavana, Sheila Thomas, Russell Berg, and Stephanie Parsons, Ellen Fox, Susan Zawalich, and Dr. Jim Hogle. You all have been there supporting me from the beginning of my graduate career and throughout my days in the Graduate Student Council. A special thanks to Margot and Garth, who have been a guiding force in my personal and professional development throughout graduate school. My admiration and respect for you both is infinite and every growing. I would not be at Harvard without the support of Sheila Thomas. Sheila has been a mentor and friend for me before I even arrived at HMS. Your drive and commitment to diversity is inspiring.

I would like to thank my parents, Ronnie and Gwen Valdez, for their never-ending support. Thank you for being there for me always and your willingness to listen to me talk about flat mounts, “trypsin digests,” and the challenges that these techniques presented even though they sound more like a witch’s brew than science (cat eyelashes, rat whiskers, oh my!). Thank you to my sisters, Ashley and Kristi Valdez, for your love, support, and friendship. I would like to thank my husband, Clayton Mathews, for his encouragement, unwavering faith in me, love, and, most importantly, his patience. I could not have survived graduate school without you by my side.

Lastly, I would like to thank my group of friends, you know who you are, for making graduate school an amazing experience. We will always have Maine.

LIST OF ABBREVIATIONS

α-actin	alpha smooth muscle actin
Alk	activin receptor-like kinase
BBB	blood brain barrier
BM	basement membrane
BRB	blood retinal barrier
BRP	bovine retinal pericyte
C57BL/6	C57 black 6, wild-type mice
CADASIL	cerebral autosomal-dominant arteriopathy with subcortical infarcts and leukoencephalopathy
CNS	central nervous system
Ct	cycle threshold
CVD	cardiovascular disease
DMEM	Dulbecco's modified eagle medium
DR	diabetic retinopathy
DT	diphtheria toxin
DTR	diphtheria toxin receptor
EBM	subendothelial basement membrane
EC	endothelial cell
EF2	elongation factor-2
ELISA	enzyme-linked immunosorbent assay
FA	fluorescent angiography
FBS	fetal bovine serum

FDA	food and drug administration
GABA	gama-aminobutyric acid
GMP	guanosine monophosphate
GTP	guanosine triphosphate
H_2O	water
HB-EGF	heparin-binding epidermal growth factor-like growth factor
HPRT	hypoxanthine guanine phosphoribosyltransferase
ICAM-1	intercellular adhesion molecule-1
iDTR	Cre inducible diphtheria toxin receptor
IL-1β	interleukin-1-beta
IP	intraperitoneally
M-Cre	mural Cre (SMMHC CreER^{T2})
MMP	matrix metalloproteinase
mRNA	messenger ribonucleic acid
MSC	mesenchymal stem cell
MW	molecular weight
NF-κB	nuclear factor kappa B
NG2	neuron-glial 2
NO	nictric oxide
NOD	non-obese diabetic
NPDR	non-proliferative diabetic retinopathy
P	pericyte
PAS	periodic acid-Schiff

PBS	phosphate buffered saline
PCR	polymerase chain reaction
PDGF-B	platelet derived growth factor isoform B
PDGFRβ	platelet-derived growth factor receptor beta
PDR	proliferative diabetic retinopathy
PKC	protein kinase C
PRP	pan-retinal photocoagulation
px	pixel
qPCR	quantitative polymerase chain reaction
RGS-5	regulator of G protein signaling 5
RNA	ribonucleic acid
SMC	smooth muscle cell
SMMHC CreER^{T2}	smooth muscle myosin heavy chain Cre estrogen receptor-binding domain
STD	standard deviation
STZ	streptozotocin induced diabetes
TNFα	transforming growth factor-alpha
TGFβ	transforming growth factor-beta
TIE	Tyrosine kinase with immunoglobulin-like and EGF-like domains
TIMP	tissue inhibitor of metalloproteinases
Tmx	tamoxifen
TUNEL	terminal deoxynucleotidyl transferase dUTP nick end labeling
VCAM-1	vascular cell adherence molecule-1
VEGF	vascular endothelial growth factor

INDEX OF FIGURES

CHAPTER 1

INTRODUCTION

CHAPTER 2

CHARACTERIZING AN INDUCIBLE MOUSE MODEL OF MURAL CELL DEATH

CHAPTER 3

ESTABLISHING A LONG TERM MOUSE MODEL OF INDUCIBLE MURAL CELL DEATH

CHAPTER 6

MATERIALS AND METHODS: DEVELOPING AUTOMATED IMAGE ANALYSIS TECHNIQUES

APPENDIX

INDEX OF TABLES

CHAPTER 1

INTRODUCTION

CHAPTER 1

Introduction

PREFACE

In this chapter, Figure 1 has been adapted with permission from the 6th edition textbook, “Human Anatomy & Physiology,” by Elaine N. Marieb published in 2003 (page 718), the copyright of which is held by Pearson Education, Inc. Figures 2 and 3 have been adapted with permission from the article, “Fenestrated Subendothelial Basement Membranes in Human Retinal Capillaries,” by Edward C. Carlson in *Investigative Ophthalmology & Visual Science*, January 1989, Vol. 30, pages 1923-1932, the copyright of which is held by The Association for Research in Vision and Ophthalmology, Inc. Figure 4 has been adapted with permission from the article, “Pericytes: Developmental, Physiological, and Pathological Perspectives, Problems, and Promises,” by Annika Armulik, Guillem Genové, and Christer Betsholtz in *Developmental Cell*, August 2011, Vol. 21, pages 193-215, the copyright of which is held by Elsevier. Table 1 has been adapted with permission from the article, “Update on animal models of diabetic retinopathy: from molecular approaches to mice and higher mammals,” by Remya Robinson, Veluchamy Barathi, Shyam Chaurasia, Tien Wong, and Tim Kern in *Disease Models & Mechanisms*, July 2012, Vol. 5, pages 444-456, the copyright of which is held by The Company of Biologists, Ltd.

INTRODUCTION

Overview of the Vasculature

The cardiovascular system consists of two components: systemic circulation and pulmonary circulation. For the purposes of this introduction, I will focus on systemic circulation, the process by which oxygenated blood travels from the heart to the tissues and is returned to the heart deoxygenated. In the cardiac cycle, oxygenated blood flows from the left atrium via the aorta to the arteries into the arterioles and finally into the capillaries, where nutrients are transported to the peripheral tissues (Guyton 1987; Ross 1989; Marieb 2004). From the capillaries in peripheral tissues, deoxygenated blood then flows from the venules to the veins through the vena cava and finally to the right atrium.

Three major vessel types make up the vascular tree: arteries, veins, and capillaries. The arteries transport oxygenated blood away from the heart to the tissues under high pressure. Conversely, the veins carry deoxygenated blood from the tissues toward the heart under low pressure. Capillaries connect the arterioles and venules, which are part of the microvasculature that sprout from the arteries and veins, respectively. Furthermore, the capillaries are the site of transport of fluid, nutrients, gases, and other substances between the blood and surrounding tissues.

In addition to carrying oxygenated blood to the peripheral tissues, large arteries serve as a reservoir for high-pressure blood that is pulsated from the heart. Due to the elastic component of the medial layer of large arteries, they are able to stretch and store large volumes of blood from the heart. The large arteries then contract between heartbeats, allowing the blood to flow out. Small arteries have strong muscular walls, which permit powerful constriction when stimulated by factors such as levels of oxygen and carbon dioxide. Thus, the small arteries are the site of resistance and are able to control blood flow to the capillaries in peripheral tissues. Capillaries are the primary component of the vasculature; in the peripheral tissues, there are nearly 10 billion capillaries. Capillaries are highly specialized to meet the functional needs of the tissues that they vascularize (discussed in detail in Chapter 1 “Microvasculature”).

In addition to carrying deoxygenated blood back to the heart, the veins have many other important functions. Veins are considered blood reservoirs and are able to expand in order to store large volumes of blood. Due to the low blood pressure in veins, structural modifications in the veins are necessary to maintain that the rate of blood circulation to and from the heart is equivalent. One such modification is the venous valve, created by the tunica intima folds, which prevents reverse blood flow. Through the “venous pump,” veins drive blood forward through the vasculature. Further, veins help regulate cardiac output by limiting the amount of available blood for the heart to pump through the venous return.

Veins are approximately eight times more distensible than arteries. Therefore, they are capable of holding a much larger volume of blood, storing nearly 65% of the total blood volume in the body, whereas arteries contain only 15% of the total blood volume. Capillaries hold an even smaller portion (5%) of the total blood volume and maintain the systemic circulation’s critical function of material exchange between the blood and tissues.

Arteries are categorized as large, often referred to as elastic; medium or muscular; small, and arteriolar. Similarly, veins are categorized as large, medium, and venular. Arteries and veins are comprised of three layers: tunica intima, tunica media, and tunica adventitia. The tunica intima is the inner layer of the vessel and is comprised of endothelial cells (ECs). The tunica media is the middle layer of the vessel, composed of smooth muscle cells (SMCs), and the least defined and outermost layer of the vessel, the tunica adventitia, is composed of connective tissue.

In large arteries (diameter 1.5 cm), the tunica intima is formed by an endothelium lining with a basal lamina, an internal elastic membrane, and a subendothelial layer. The tunica media of the large arteries, the thickest layer, is comprised by elastic material with interceding layers of a SMCs, collagenous fibers, and extracellular matrix. The tunica adventitia, the outermost layer, is primarily composed of collagenous fibers, but also contains elastic fibers, fibroblasts, and macrophages. In large arteries, the tunica adventitia is fairly thin, and its width is less than half of the tunica media.

Whereas the tunica intima of medium arteries (diameter 6.0 mm) is similar to that of large arteries, it differs in that it has only a sparse subendothelial layer. The tunica media of medium arteries resembles that of large arteries, but has little elastic material present. The tunica adventitia of the medium artery is primarily composed of collagenous fibers like large arteries, however it is much thicker, nearly as thick as the tunica media. In addition, the tunica adventitia of medium arteries has a small external elastic lamina.

Though the tunica intima of the small artery (diameter 0.1-5 mm) has an internal elastic lamina, the arteriole (diameter 37.0 μm) does not always contain this lamina. The tunica media of the arteriole has one or two layers of SMCs, whereas small arteries can have up to eight layers of smooth muscle.

While the tunica intima, tunica media, and tunica adventitia layers are well characterized in the arteries, these layers are less defined in the veins. In the tunica intima of large veins (diameter 5.0 mm), the layers remain the same as in large arteries; however, it is difficult to determine whether the SMC border belongs to the tunica intima or tunica media. The layers of the tunica media of large veins remain similar to that of the large arteries with the addition of fibroblasts but are relatively thin by comparison. In large veins, the tunica adventitia is much thicker and contains bundles of SMCs. In comparison to large arteries, the tunica adventitia of large veins contains the same components, but does not include macrophages.

The composition of the tunica intima in medium veins is basically the same as medium arteries except that the internal elastic membrane, when present, is much thinner. Compared to medium arteries, the tunica media of medium veins is thinner, and SMCs are arranged circumferentially. In the medium veins, the tunica media is normally thinner than the tunica adventitia.

Microvasculature

The microvasculature is comprised of three components: arterioles, capillaries, and venules. Here, I will focus on capillaries, which are classified as either continuous or fenestrated. The most distinguishable characteristic of most continuous capillaries is the pinocytotic vesicles, which allow transepithelial transport of small molecules (Figure 1). Continuous capillaries are so called because of the continuous lining of ECs, which are connected by a variety of junctions including gap junctions, tight junctions, and adherens junctions. The endothelium of fenestrated capillaries have fenestrae or pores (approximately 80 to 100 nm diameter) (Figure 1). In some cases, these fenestra have a diaphragm that allows selective filtration of small molecules and proteins. Fenestrated capillaries are found in secretory and filtering organs such as the choroid plexus, choriocapillaris, and kidney, to name just a few.

In addition, there is a third type of capillary called a sinusoid. Sinusoidal capillaries, the largest of the three types of capillaries, are a specialized subset of the fenestrated capillaries and are distinguished by larger fenestrae (30-40 μm) without diaphragms (Figure 1). The larger fenestrae and the incomplete basal lamina in the sinusoid capillaries permit the passage of blood cells and serum proteins (Figure 1). Sinusoidal capillaries are found in the bone marrow, lymph nodes and adrenal glands. Finally, there is a subset of sinusoid capillaries, termed discontinuous sinusoidal capillaries, which lack tight junctions and are found in the liver and spleen.

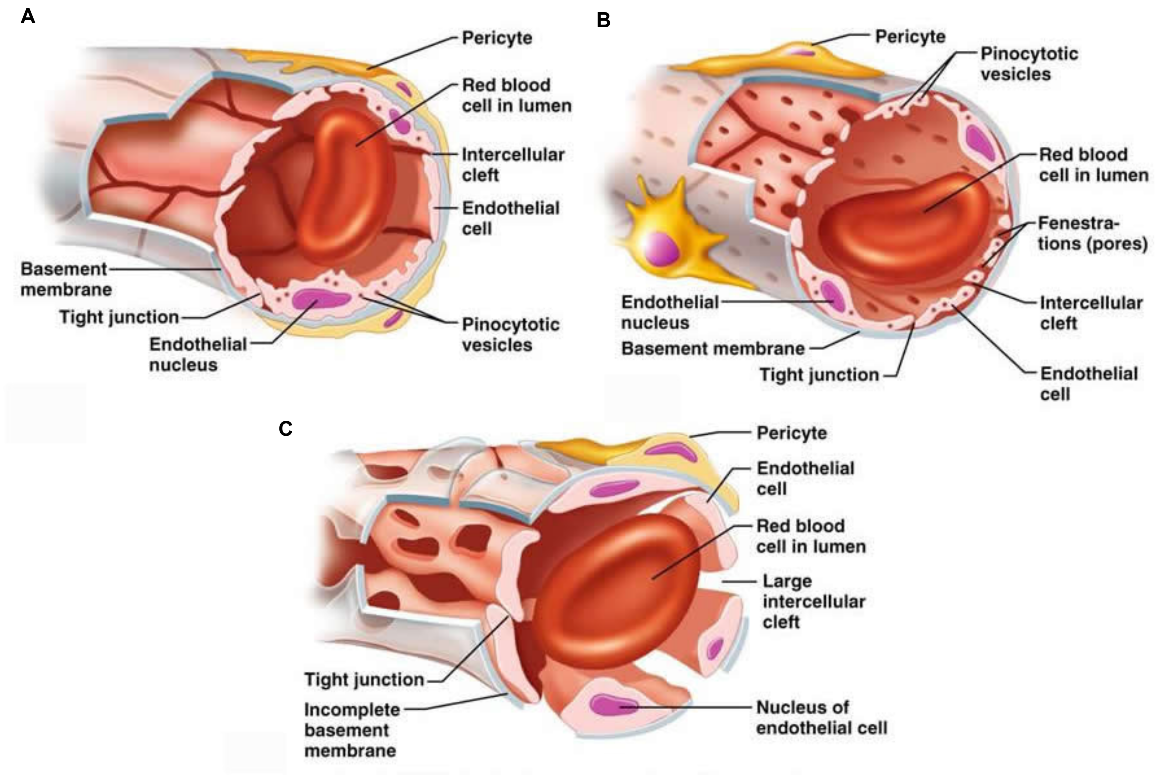

Figure 1. The Capillary.
A) Continuous capillary with continuous lining of ECs featuring tight junctions with few pinocytotic vesicles. B) Fenestrated capillary with pores (fenestrae). C) Sinusoid capillary with larger fenestrae and an incomplete basement membrane. (Adapted from Marieb 2004).

In 1885, Paul Ehrlich first demonstrated the existence of a blood brain barrier (BBB) when he injected dyes intravenously into the circulatory system of animals and found that they stained all organs except those in the central nervous system (CNS) (Ehrlich 1885). Ehrlich credited this phenomenon to a low affinity of the CNS for the dye (Ehrlich 1904). In 1913, Edwin Goldman, Ehrlich's student, injected trypan blue directly into the cerebrospinal fluid of animals and was only able to observe staining in brain cells, suggesting a barrier between the CNS and blood (Goldman 1913). The BBB is a filtering mechanism between the brain and the blood (Wislocke 1969; Pollay 1980).

Similar to the BBB, the blood retinal barrier (BRB) regulates permeability between the retina and the blood (Ashton 1965A and 1965B; Cuhna-Vaz 1976 and 1966). There were two initial reports on the existence of a BRB (Schnaudigel 1913; Palm 1947), as well as many early studies on the association of altered vascular permeability with retinal pathology (Cunha-Vaz 1966; Hanum 1938; Ballantyne 1946; Friedenwald 1950; Ashton 1951; Ashton, 1963). Yet, the ophthalmic field did not accept the existence of the BRB until 1965 (Cuhna-Vaz 1966 and 1976). Ashton and Cunha-Vaz injected histamine and colloidal carbon into animals and found labeling in many vessels of the eye including the iris, conjunctiva, and large vessels of the choroid but not in retinal and cerebral vessels, indicating the presence of a BRB similar to the BBB (Ashton 1965A).

The BBB and BRB share many features including extensive tight-junctions between ECs. The BBB and BRB allow the passage of necessary nutrients and gases while restricting passage of hydrophobic and potentially toxic molecules from the choroid to the brain and retina, respectively (Shakib 1966; Pollay 1980). Tight-junctions in the BBB and BRB differ from junctions in continuous capillaries in other organs, because they develop as a band, sealing any gaps between ECs (Shakib 1966; Cuhna-Vaz 1976; Pollay 1980).

The breakdown of the BRB can be examined by fluorescein angiography (FA) and vitreous fluorometery (Cuhna-Vaz 1967, 1975, 1976, and 2004). Using these techniques, clinicians can identify functional changes prior to the appearance of pathological events (Cuhna-Vaz 1976). Of note, an increase in permeability of the BRB is an early change in the pathogenesis of diabetic retinopathy (DR) (Ashton 1965A; Cuhna-Vaz 1967 and 1975; Norton 1967).

The Pericyte

Eberth and Rouget first observed the association of the perivascular cell with capillaries more than 140 years ago (Eberth 1871; Rouget 1873 and 1879). The pericyte has lengthy processes that stretch along the abluminal side of the capillary (Figure 2, Shepro 1993), the number and length of which differ among various microvascular beds. Secondary processes of pericytes, perpendicular to the primary processes, partially enclose the capillary (Figure 2, Shepro 1993). In 1923, Zimmerman coined the term “pericyte” for these perivascular cells (Zimmerman 1923); however the name for the pericyte, also referred to as a adventitial cell (Eberth 1871; Rouget 1873 and 1879), Rouget cell (Vimtrup 1922; Speiser 1968), intramural pericyte (Speiser 1968), mural cell (Kuwabara and Cogan 1963; Cogan and Kuwabara 1967), and pericapillary cell (Battig 1961), was debated throughout the 1960’s (Ashton 1966). The current definition of the pericyte, a cell embedded within the vascular basement membrane (BM), originated from electron microscopic analysis of capillaries (for a review, see Sims 1986).

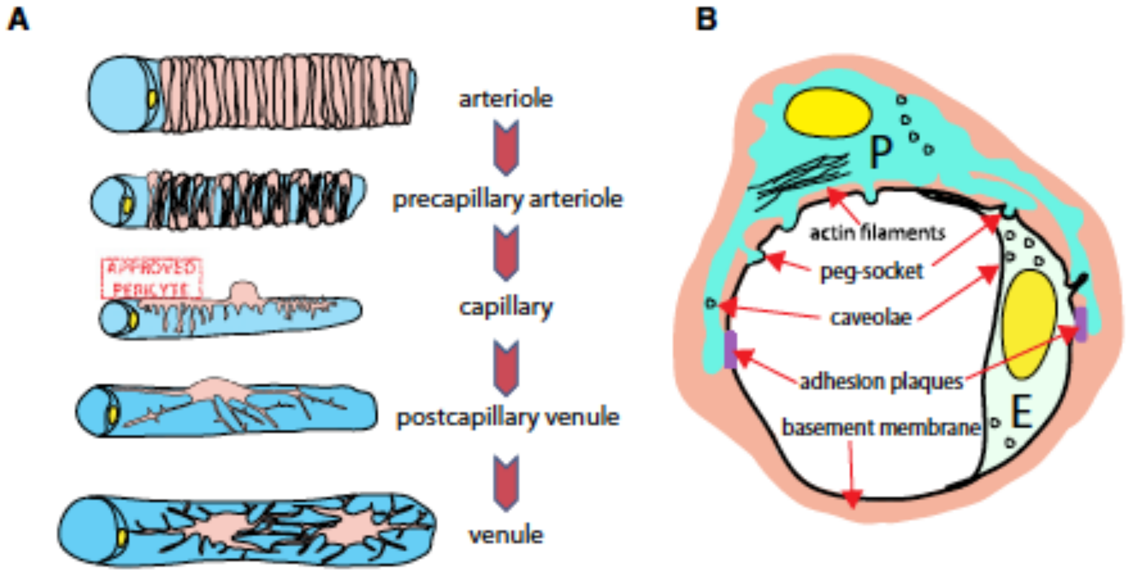

Figure 2. Pericyte Anatomy.
A) Mural cells in the microvasculature from arteriole to venule. Vascular SMCs circumferentially cover the arteriole and precapillary arteriole with few processes. Pericytes are present in the capillaries and have a rounded body with lengthy primary processes that are parallel to the vessel and secondary processes that are perpendicular to the vessel, enveloping the endothelium. Flattened mural cells wrap circularly around postcapillary venules with several thin processes, whereas the stellate shaped vascular SMCs with many processes in the venules do not. B) Pericyte-EC interactions in an ultrastructure schematic. Pericytes (P) and ECs (E) are separated by the BM, but still maintain physical contact through peg-and-socket arrangements and adhesion plaques. (Armulik 2011)

The BM is located on the abluminal side of the endothelium and is comprised of a protein-polysaccharide-rich layer and separates the EC from the pericyte. Interestingly, the subendothelial basement membrane (EBM) often has areas of discontinuity that allow the processes of ECs to directly contact the pericytes (arrows, Figure 3, Carlson 1989). The invagination of the processes of either ECs or pericytes into the membrane is called a peg-and-socket arrangement (Figure 4, Tilton 1979A; Cuevas 1984; Carlson 1989; Armulik 2005). This arrangement contains tight and gap junctions (Tilton 1979A; Cuevas 1984; Carlson 1989; Armulik 2005). ECs and pericytes can also interact through adhering plaques (Carlson 1989). Whereas, a majority of EC-pericyte interactions occur through peg-and-socket arrangements and adhering plaques, some ECs and pericytes communicate as a result of spatial proximity (~2 nm), which likely makes the exchange of diffusible factors (i.e. juxtacrine communications) more effective (Carlson 1989).

Pathological conditions are associated with changes in the BM. For example, in diabetes, the capillary BM dramatically thickens due to an increase in collagen type IV and laminin production (Ross 1989). Interestingly, there is a concomitant increase in permeability, though it is unclear if both changes occur in the same capillary.

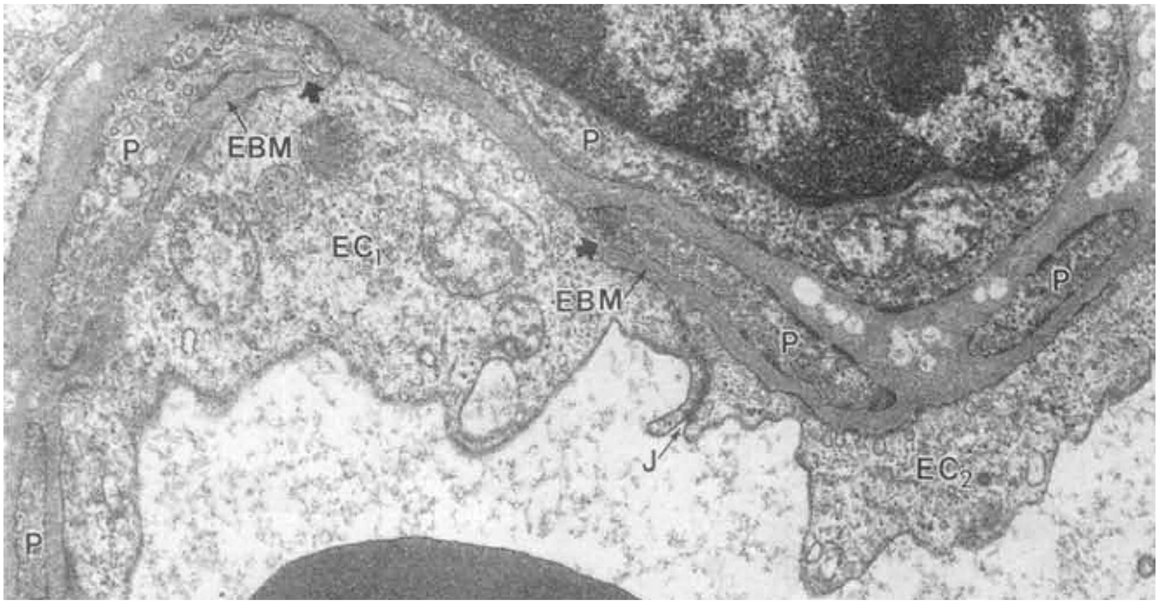

Figure 3. Pericyte-EC interactions.
Subendothelial basement membrane (EBM) discontinuities (arrows) allow EC processes to contact pericytes (P) in a human retinal capillary cross-section imaged by transmission electron microscopy. Intercellular junctions of neighboring ECs (J). Magnification x21,000. (Adapted from Carlson 1989).

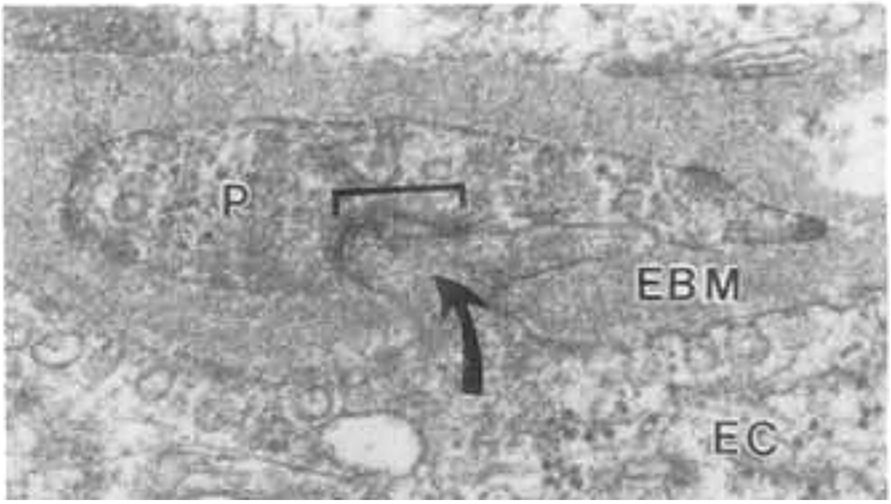

Figure 4. Peg-and-socket arrangement between pericyte and EC.
EC process (arrow) stretching through the subendothelial basement membrane (EBM) to interact with the pericyte (P), creating a peg-and-socket arrangement (bracket) in a human retinal capillary imaged by transmission electron microscopy. Magnification x41,000 (Adapted from Carlson 1989).

Pericyte abundance varies significantly by tissue. Capillaries of the CNS possess the highest EC to pericyte ratio of all tissues at a ratio of 1:1 in human retinas and a range of 5:1-3:1 in the human brain (Speiser 1968; Armulik 2011; Duh 2008). This contrasts with an EC to pericyte ratio is 10:1 in human cardiac muscle and lungs (Armulik 2011; Duh 2008; Shepro 1993). The pericyte density in human skeletal muscle is not agreed upon, as there are studies claiming as many as 100 ECs per pericyte and as few as 10 ECs per pericyte (Armulik 2011; Duh 2008; Shepro 1993; Tilton 1979B).

Currently, there are no specific molecular markers for pan-pericytes. Instead, a number of molecular markers are used to identify pericytes that vary on several factors including species, vessel type, developmental or angiogenic stage, tissue specificity, and pathology. Alpha-smooth muscle actin (α-actin), desmin, and regulator of G protein signaling 5 (RGS-5) are all intracellular protein markers for pericytes (Armulik 2005; Diaz-Flores 2009; Herman and D'Amore 1985; DeNofrio 1989; Fujimoto 1987; Nehls 1992; Bondjers 2003; Cho 2003). The cytoskeleton protein, α-actin, stains pericyte microfilament bundles, SMCs, myoepithelium, and myofibroblasts (Skalli 1989; Darby 1990; Armulik 2011). Desmin, a type III intermediate protein that labels pericytes, is also a marker for mature cardiac, skeletal, and SMCs (Nehls 1992; Bergers 2005; Armulik 2011). Although utilized less often than α-actin and desmin, the GTPase-activating protein, RGS-5, is also a marker for pericytes and vascular SMCs (Bonjers 2003; Cho 2003; Bergers 2005; Armulik 2011). Cell surface molecular markers for pericytes include neuron-glial 2 (NG2), platelet-derived growth factor receptor beta (PDGFRβ), and vascular cell adherence molecule-1 (VCAM-1) (Schlingemann 1990; Lindahl 1997; Carter 2001; Ozerdem 2001; Diaz-Flores 2009; Armulik 2011). In addition to being a marker for pericytes, the chondroitin sulfate proteoglycan, NG2, is also expressed in vascular SMCs, developing cartilage, muscle, bone, and other cell types (Schlingemann 1990; Ozerdem 2001; Huang 2010). The tyrosine-kinase receptor, PDGFRβ is expressed not only in pericytes, but also in developmental interstitial mesenchymal cells, myofibroblasts, smooth muscle, and some CNS neuronal cells (Lindahl 1997; Winkler 2010; Armulik 2011). Since VCAM-1 is expressed in both pericytes and ECs, it is not used as frequently as the other cell surface proteins markers (Carter 2001; Diaz-Flores 2009).

Prior to the development of transgenic mouse technology, studies to elucidate the functional role of the pericytes used in vitro systems. Methods to culture large vessel ECs were developed in the 1970's, while protocols to isolate microvascular ECs and pericytes were not developed until a decade later (Jaffe 1973; Gimbron 1974; Gitlin 1983).

Pericytes and ECs are in close proximity in vivo and their cell-cell interactions are important to many aspects of microvasculature development, function and stability. Insight into the nature and the role of cellular crosstalk between EC and pericytes has been obtained by coculturing the cells. A number of systems have been developed and are reviewed here because results obtained in these systems are relevant to the findings in this thesis.

The quickest and most straightforward method of examining pericyte-EC interactions is through direct contact two-dimensional coculture (Olridge and D'Amore 1987; Bryan and D'Amore 2008). For this purpose, the cells can be directly cultured in the same dish. Variables such as the effect of cell ratios can be examined using this system allowing cells to physically interact. Therefore, it is difficult to determine if observed effects are due to the cells contact and/or to diffusible molecules that might be released into the medium. To remove the variable of cell contact, pericytes and ECs can be cocultured using transwells to prevent direct contact. The under agarose assay is an alternate technique for studying pericyte-endothelial interactions without direct contact (Bryan and D'Amore 2008). In this assay, the cells are plated into wells created in agarose and the effect of one cell type on the other can be examined. Growth factors, neutralizing antisera or other agents can be added to the agarose to examine their effects on the cells' interactions.

Whereas two dimensional cocultures described above have been utilized to study basic pericyte-EC migration and proliferation, development of three dimensional coculture systems has allowed further elucidation of the interactions between pericytes in a model that is more physiologically relevant. Thus, culturing the cells on or in collagen or matrigel BM creates an environment more similar to what is found in vivo (Darland and D'Amore 2001; Bryan and D'Amore 2008). Under these conditions, pericytes and ECs are able to form vessels with EC forming the lumen and the pericytes abluminally associated. Such models have permitted investigation into more complex aspects of morphogenesis such as lumen formation, matrix production and vessel regression (Hirschi 1998; Bryan and D'Amore 2001).

Function of the pericyte

Whereas early studies hypothesized the functional role of pericytes, the isolation of bovine retinal pericytes (BRPs) for in vitro studies (described in detail in Chapter 1

"Pericytes," Gitlin and D'Amore 1983) created an avenue for conclusive experimental data illuminating pericyte function. Outlined below are the functional roles of the pericytes in capillary contractility, vessel stabilization, wound healing, and their potential as stem cells.

Contractility

Since their identification, it has been suggested that pericytes have contractile capacity and are involved in regulating capillary blood flow (Rouget 1873 and 1879; Vimtrup 1922; Zimmerman 1923; Dore 1923; Krogh 1929; Kuwabara and Cogan 1963; Cogan and Kuwabara 1967; Shepro 1993). The location and morphology of pericytes corroborate this idea, since pericyte processes envelope ECs (Shepro 1993). Additionally, pericytes express contractile proteins such as α-actin, tropomyosin, myosin, and calponin (Joyce 1984, 1985A, and 1985B; Herman and D'Amore 1985; DeNofrio 1989; Diaz-Flores 2009).

Several in vitro studies have demonstrated a contractile role for pericytes. In the silicone rubber assay, vasoactive agents are added to cultured BRPs and the silicone wrinkles when pericytes constrict (Harris 1980; Kelley 1987 and 1988; Hamilton 2010). For example, it was demonstrated that pericytes contract in the presence of particular biogenic amines found in blood plasma, such as histamine and serotonin (Kelley 1988). Also, using the silicone rubber assay, endothelin-1 and thromboxane A_2, EC-derived vasoconstriction agents, were shown to cause pericyte contraction, whereas prostaglandin I_2 and nitric oxide (NO), EC-derived vasodilators, were shown to cause pericyte relaxation (Dodge 1991; Haefiger 1994). In addition, angiotensin II caused pericyte contraction after pre-relaxation in the in vitro silicone rubber assay (Matsugi 1997). Adenosine, a potent vasodilator that accumulates in hypoxic and ischemic conditions, also causes pericyte relaxation in vitro (Matsugi 1997). Interestingly, pericyte contractility is inhibited by high glucose in the silicone rubber assay, which has implications for blood flow in early DR (Gillies and 1993).

Moreover, pericyte contractility has also been shown in vivo, in situ, and ex vivo. In a study of capillaries from rat hearts and hindlimb skeletal muscle, perfusion with angiotensin II, norepinephrine, or vasopressin, vasoconstriction agents, each demonstrated pericyte contractility in the hindlimb skeletal muscle (Tilton 1979B). Additionally, Peppiatt et al found that pericytes constrict in response to gamma-aminobutryic acid (GABA) antagonists in superfused rat retinas, and pericytes relax when treated with glutamate in superfused cerebral capillaries, demonstrating a role for neurotransmitters in pericyte tone (Peppiatt 2007).

A number of studies outline an important role for intercellular calcium levels in modulating pericyte contractility (Sakagami 1999, 2001A, and 2001B; Sugiyama 2005; Peppiatt 2007; Hamilton 2010). Using perforated-patch configuration of the patch–clamp technique, isolated rat retina capillaries were exposed to platelet-derived growth factor (PDGF)-BB, resulting in pericyte contraction and increased levels of calcium (Sakagami 2001B). Conversely, in chemically induced ischemic conditions, pericytes in isolated rat retinal capillaries were shown to relax and calcium levels decreased in the presence of PDGF-BB (Sakagami 2001B). Further, electrically stimulated isolated rat retinal capillary pericytes constrict, however when extracellular calcium was removed, they relax, suggesting a direct role of calcium in pericyte contractility (Peppiatt 2006).

Pericytes express contractile proteins and have been shown by many techniques (outlined above) to contract in the presence of vasoconstriction agents and relax in the presence of vasodilators. In addition, a link between calcium levels and pericyte contractility has been elucidated. The vasoactive molecules discussed above are derived from ECs, glial cells, neurons, and metabolic factors. While it is clear that the current data support a contractile role for pericytes, further elucidation of the mechanism by which these other cell types and metabolic factors provide stimulants to the pericytes for contraction is required.

Vessel Stability

Mechanistically, the association of pericytes with ECs leads to the deposition of the BM and inhibition of both EC and pericyte migration and proliferation (Olridge and D'Amore 1987; Sato and Rifkin 1989; Stratman 2009 and 2010), which are all hallmarks of vessel maturation. How pericytes contribute to vascular stability in adult vessels has begun to be elucidated. Relevant mechanisms may include pericyte regulation of EC-gene expression, pericyte BM deposition, and/or pericyte recruitment and integration into the vascular wall. Pericyte-EC interactions mediate several signaling pathways associated with vessel stability, including PDGF-B/PDGFRβ, TGFβ, and Angiopetin-1/TIE2.

Pericytes express PDGFRβ, the receptor for PDGF-B, a protein secreted by proliferating ECs (Armulik 2011). Mice with targeted disruption of *Pdgfrb* or *Pdgfb* developmentally lack pericytes, which leads to vascular dysfunction and embryonic lethality (Leveen 1994; Soriano 1994). In addition to pericyte loss, PDGF-B and PDGFRβ knockout models have abnormal EC ultrastructure and develop microangiopathies similar to those found in DR, including microaneurysms and leakage (Hellstrom 2001). During angiogenesis, PDGF-B is upregulated in tip cells causing pericytes to be drawn immediately to the developing angiogenic sprouts (Gerhardt 2002). Thus, PDGFRβ and PDGF-B are essential for the recruitment of pericytes during angiogenesis and vessel stability.

Although a majority of studies have focused on the developmental role of PDGFRβ and PDGF-B in pericytes, there have been recent reports on postnatal phenotypes. To generate postnatally viable animal models, PDGF-B cannot be deleted systemically. Therefore, PDGFB +/- mice and mice with an EC-specific conditional knockout of PDGF-B were created to study the effects of PDGF-B loss on pericytes (Enge 2002; Hammes 2002; Djarnegard 2003). In these models, pericyte loss occurs, but the degree of impact is variable (Enge 2002; Hammes 2002; Djarnegard 2003). PDGFB +/- mice were reported to have approximately 30% decrease in pericytes and a slight increase in acellular capillaries (Hammes 2002). Mice with EC-specific conditional knockout of PDGF-B exhibit microaneurysms and increased microvascular regression, when there is >50% pericyte coverage (Enge 2002; Djarnegard 2003). In addition, PDGF-B retention motif knockout mice displayed increased permeability when intravenously injected with molecular tracers and showed decreased CD71 expression, a known BBB marker, further elucidating a role for pericytes in barrier function (Armulik 2010). Loss of pericytes in PDGF-B mutants leads to a number of vascular dysfunctions, including acellular capillaries, microaneurysms, microvascular regression, and leakage, which are all symptomatic of vessel destabilization. Therefore, PDGF-B is necessary for vascular integrity.

Pericytes and ECs express transforming growth factor-β (TGFβ), as well as TGFβ receptors (Gaengel 2009). Thus, the elucidation of TGFβ signaling in either cell type is extremely complex (Gaengel 2009). To understand the broader role of TGFβ signaling, several knockout models of TGFβ/TGFβ receptors have been developed (*tgfb1*, *alk5*, *tgbr2, eng*, and *smad5*), most of which are embryonic lethal due to major abnormalities in the vasculature (Dickson 1995; Chang 1999; Yang 1999; Li 1999; Larsson 2001); half of the *tgfb1* knockout mice survive for approximately two weeks, while the other half are embryonic lethal (Dickson 1995). Mice deficient in TGFβ type I receptor, also referred to as Alk-5, and endoglin, a TGFβ binding protein, lack SMC investment and formation, respectively (Li 1999; Larsson 2001).

In addition, cell-cell interactions between pericytes and ECs are important for TGFβ signaling. For example, it has been demonstrated that pericyte-EC cocultures activate latent TGF-β1 and that contact between the cells is necessary (Antonelli-Orlidge 1989; Sato and Rifkin 1989). Distinct TGFβ type I receptors, activin receptor-like kinase (Alk)-1 and Alk-5, mediate TGF-β signaling (Gaengel 2009; Goumans 2002). In vitro studies showed that Alk-1 and Alk-5 have opposite effects on EC migration and proliferation (Goumans 2002). Further, in vivo studies targeting EC specific knockdown of Alk-5 have demonstrated a reduction in EC secretion of TGF-β1, which results in reduced signaling of TGFβ/Alk5 in pericytes (Carvalho 2004). Together, these data suggest an important and linked role for TGFβ signaling in pericytes and ECs.

Many reports have suggested the importance of angiopoietin-1/Tie2 signaling in pericyte-EC interactions and vascular development. EC express tie2, and angiopoietin-1 is produced by the pericytes (Sato 1995; Davis 1996; Sundberg 2002; Armulik 2005). *Ang1* and *tie2* knockout mice are pericyte deficient and suffer from cardiovascular failure at mid-gestation (Suri 1996; Patan 1998). Intravitreal injection of angiopoeitin-1 to a model in which retinal pericyte deficiency was induced with an anti-PDGFRβ antibody, was shown to rescue high-order architecture of the developing vasculature (Uemura 2002). Thus, angiopoeitin-1 in pericytes has a crucial role in vascular stability and maturation.

Pericytes as stem cells

The concept that pericytes are, in fact, mesenchymal stem cells (MSCs) has long been a topic of discussion and continues to be so today (Movat and Fernando 1964; Maxwell and Kruger 1965; Meyrick and Reid 1979; Shi 2003; Schwab and Gargett 2007; Zannetitino 2008; Corselli 2010). In an early investigation, pericytes were shown to differentiate into SMCs when cultured under hypoxic conditions (Meryick and Reid 1979). Evidence that pericytes share many markers with SMCs including the contractile proteins (α-actin, myosin, and cyclic GMP-dependent protein kinase) also suggests a conceivable role of pericytes as stem cells (Herman and D'Amore 1985; Joyce 1985A and 1985B; Sims 1986). In addition, it has also been shown that, in vitro, ECs induce multipotent mesenchymal 10T1/2 cells to differentiate into mural cells through PDGF-BB, which further corroborates the concept of stem cell-like properties in pericytes (Hirschi 1998; Hirschi 1999).

Pericytes have also been reported to differentiate into a number of cell types including phagocytes, adipocytes, SMCs, osteoblasts, granulocytes, and chondrocytes (Movat and Fernando 1964; Maxwell and Kruger 1965; Schwab and Gargett 2007; Corselli 2010;

Farrington-Rock 2004; Paquet-Fifield 2009; Mills 2013). For example, in a study by Farrington-Rock and colleagues, BRPs cultured as pellets in chondrogenic medium for three weeks expressed Sox9, aggrecan, and collagen II, which are chondrocyte markers, whereas ECs cultured under the same conditions did not (Farrington-Rock 2004). In addition, BRPs cultured in 20% rabbit serum for 2 weeks expressed peroxisome proliferator–activated receptor-γ2, an adipose marker. Further, when BRPs were harvested in diffusion chambers in nude mice for 56 days, mineralized cartilage and adipose-like cells (Farrington-Rock 2004). In another study, human endometrium stromal cells co-expressing CD146 and PDGFRβ, pericyte markers, were cultured with myogenic, adipogenic, osteogenic, and chondrogenic induction media for four weeks, and subsequently expressed markers of SMCs, osteoblasts, adipocytes, and chrondocytes, respectively (Schwab 2007). Taken together, these reports strongly implicate a functional role for pericytes as stem cells.

Wound healing

The role of the pericyte in wound healing was first noted in a wounding rabbit model in 1940 by Clark and Clark and later substantiated by Cliff in 1963 (Clark and Clark 1940; Cliff 1963). New capillaries sprout after injury occurs, and as the development of these new capillaries progress, pericytes begin to attach to the proliferating and maturing ECs (Cliff 1963; Crocker 1970). Subsequent studies showed that the cessation of EC proliferation was marked by the arrival of the pericyte, leading to the suggestion that pericytes have a regulatory role in capillary proliferation during wound healing (Crocker 1970).

A recent study demonstrated that the prevalence of MSCs increases with injury (Mills 2013). Conversely, many reports have treated wounding models with MSCs and demonstrated improved healing (Nakawaga 2005; Mansilla 2006; Wu 2007; Falanga 2007). MSCs are thus an obvious target for therapeutics in wound healing, but the isolation and purification of MSCs for human therapeutic use is complex and challenging. Hence, the use of pericytes in the place of MSCs may have potential.

Diabetic Retinopathy

Diabetes is a growing epidemic that affects 24.4 million people in the U.S. and 382 million people worldwide (International Diabetes Federation 2013). A chronic metabolic disease, diabetes is characterized by little to no insulin production by the pancreas (type I) or insulin resistance (type II) (International Diabetes Federation 2013; American Diabetes Association 2010). Ninety to ninety-five percent of diabetes cases in the US are type II (International Diabetes Federation 2013; American Diabetes Association 2010). Type II diabetics do not produce enough insulin, or their body does not recognize the insulin they do produce, resulting in a surplus of glucose (International Diabetes Federation 2013; American Diabetes Association 2010). Diabetic patients are hyperglycemic, and therefore have excess glucose in the bloodstream, which can damage blood vessels and nerves (International Diabetes Federation 2013; American Diabetes Association 2010).

Diabetics encounter many complications including macrovascular and microvascular diseases (Fowler 2008; Cade 2008; International Diabetes Federation 2013; American

Diabetes Association 2010). Cardiovascular disease (CVD) is the major cause of death in diabetics, who are four times more likely to develop CVD (Fowler 2008; Cade 2008). The microvascular complications include nephropathy, neuropathy, and diabetic retinopathy (DR) (Fowler 2008; Cade 2008). Nephropathy occurs in 35% of diabetic patients and eventually progresses to renal failure in these patients (Fowler 2008; Cade 2008; Tesfaye 2010). Neuropathy is seen in nearly half of all diabetic patients and often leads to lower limb amputations (Fowler 2008; Cade 2008; Yau 2012). DR is present to some extent in almost all diabetics 30 years after diagnosis and can lead to partial or total vision loss (Roy 2004; Cade 2008; Cheung 2010; Yau 2012).

DR is among the most common complication of both type 1 and type 2 diabetes, and a leading cause of permanent vision loss worldwide (Roy 2004; Cheung 2010; Yau 2012). There are two stages of DR: non-proliferative (NPDR) and proliferative (PDR). The early stage of DR, referred to as NPDR or background retinopathy, is characterized by morphological and functional abnormalities in glial and neuronal cells as well as degenerative changes in the choriocapillaris and retinal vessels (Cogan 1964; Gerhardt 2003; Antonetti 2012). These include microaneurysms, capillary swelling, and hemorrhaging (Cogan 1964; Gerhardt 2003; Antonetti 2012). As the disease progresses, vascular degeneration leads to ischemia, which induces the expression of vascular endothelial growth factor (VEGF) and retinal angiogenesis, a process referred to as PDR (Antonetti 2012; Taylor 1970; Sapieha 2010). PDR is associated with new vessel formation, fibroblast proliferation, and vitreous hemorrhaging, and both NPDR and PDR are associated with macular edema (Gerhardt 2003).

Clinical and experimental data provide strong support for the concept that the microvascular complications of DR are due in large part to hyperglycemia (The diabetes control and complications trial 2000). There is also mounting evidence that inflammation plays a key role in the pathophysiology of DR (Tang and Kern 2011). For example, in vitro studies have shown that high glucose causes increased expression of TNFα, TNFβ, interleukin (IL)-1β, nuclear factor (NF)-κB, intercellular adhesion molecule (ICAM)-1, and VEGF (Kowluru 2010).

In streptozotocin induced diabetic (STZ) and galactosemia mice, systemic inhibition of caspase-1 using minocycline decreased retina degeneration including production of acellular capillaries (Vincent and Mohr 2007); caspase-1 is the enzyme that generates mature IL-1β. In addition, diabetic (STZ-induced) mice were systemically treated with dehydroxymethylepoxyquinomicin, a NF-κB inhibitor, which decreased retinal leukostasis and ICAM-1 and VEGF expression compared to diabetic controls (Nagai 2007). Similarly, in ICAM-1 null mice with diabetes (STZ-induced) or hyperglycemia (galactosemia), hallmark characteristics of DR were decreased including pericyte loss, acellular capillaries, and leakage (Joussen 2004). Intravitreal injection of anti-$\text{VEGF}_{164(165)}$ aptamer in diabetic (STZ-induced) mice at short (three weeks) and long (two months) time points demonstrated significant decrease in retinal leukostasis and permeability (Ishida 2003). Further, it has been clearly demonstrated that hypoxia, leading to the upregulation of VEGF, is crucial for the transition from DR to PDR (Adamis 1994; Aiello 1994; Miller 1997; Joussen 2004; Antonetti 2006; Avery 2006; Mason 2006; Gologorsky 2012).

In 1961, Cogan first reported the loss of retinal microvascular pericytes, referred to as pericyte dropout, in NPDR (Cogan 1961) and pericyte dropout is the first morphological change observed in DR. Quantification of pericyte dropout in DR revealed a ratio of ECs to pericytes in normal (1:1) versus diabetic (4:1) retinal microvasculature (Speiser 1968). Pericyte dropout occurs temporally prior to the development of microangiopathies such as microaneurysms, acellular capillaries (Cogan 1961; Engerman 1989) vessel tortuosity, hyperpermeability, and capillary non-perfusion (Cogan and Kuwabara 1976; Klein 1984A and 1984B; Hammes 2002; Sasongko 2011).

Many reports using diabetic animal models support a link between pericyte dropout and microangiopathy, however in these studies causality is inconclusive due to the complexity of obese and hyperglycemic models (Robinson 2012). DR has been studied in several mouse models including STZ induced diabetes, non-obese diabetic (NOD), db/db, *Ins2*$^{\mathrm{Akita}}$ (Akita), Akimba, and the galactosemia model (Table 1, Robinson 2012). Although none of these models progress to PDR, they do develop some of the hallmarks of background or NPDR including microaneurysms, microvascular permeability and acellular capillaries (Table 1, Robinson 2012).

The goal of this work was to assess the precise role of the pericyte in retinal microangiopathy, wherein I hypothesized that pericyte loss is sufficient to cause microangiopathies in the adult microvasculature. To eliminate the variables encountered in the various models of diabetes, we have developed a mouse model of inducible mural cell loss. This model has allowed us to examine the effects of pericyte loss on the integrity and function of the adult retinal microvasculature.

Table 1. Mouse models of DR. Summary of retinal lesions found in mouse models of DR. (Adapted from Robinson 2012)

	Diabetic Retinopathy Mouse Model					
Retinal Lesions	STZ	db/db	NOD	Akita	Akimba	Galactosemia
Microaneurysms					+	+
Acellular capillaries	+	+		+		+
Pericyte loss	+	+				+
Venous bleeding					+	
Hemorrhages					+	
BM thickening		+				+
Tortuosity					+	
Retinal edema					+	
Retinal thinning	+			+		
Apoptosis of vascular cells	+		+			
Ganglion cell loss	+			+		
BRB breakdown		+				
Capillary dropout					+	

CHAPTER 2

CHARACTERIZING AN INDUCIBLE MOUSE MODEL OF MURAL CELL DEATH

AIM

To evaluate the role of pericyte loss in the adult retinal microvasculature using a mouse model of inducible mural cell dropout.

RATIONALE

Pericyte loss, commonly referred to as pericyte “drop-out,” was first described in human background, or non-proliferative, DR by Cogan in 1967 and is understood to be an early event in the development of DR (Cogan and Kuwabara 1967). The loss of pericytes precedes the development of other microangiopathies including microaneurysms, acellular capillaries (Cogan and Kuwabara 1961; Engerman 1989) vessel tortuosity, hyperpermeability, and capillary non-perfusion (Cogan and Kuwabara 1961; Klein 1984A and 1984B; Hammes 2002; Sasongko 2011). The temporal association between pericyte loss and microangiopathy is also supported by examination of several animal models of diabetes (Robinson 2012) where analysis of their causality is confounded by the effects of comorbidities and obesity commonly found in these models.

Similarly, in the PDGF-B/PDGFRβ knockout mice, the developmental absence of pericytes is associated with microaneurysms and embryonic lethality (Lindahl 1997; Armulik 2011). Mice with conditional ablation of PDGF-B in EC (Enge 2002), PDGF-B heterozygosity, or expressing PDGF-B hypomorphic mutants (Bell 2010; Armulik 2010) are all postnatally viable and show various degrees of pericyte deficiency and other microangiopathies. Yet, in each case, the postnatal phenotypes cannot be definitively distinguished from other developmental abnormalities. Thus, experimental demonstration of a link between pericyte loss and microvascular degeneration in the retina is lacking.

I aimed to develop a model that would allow investigation of the role of the pericyte in the development of retinal microangiopathies in non-diabetic mice. I accomplished this by using mice that would allow the direct induction of mural cell death in adult mice. This approach allowed me to examine the acute effects of pericyte loss on the integrity and function of the adult retinal microvasculature.

RESULTS

Mouse model of inducible mural cell loss

I first sought to establish a model of inducible mural cell death by breeding mice carrying a floxed allele of the iDTR, which has been shown to render mouse tissues susceptible to diphtheria toxin (DT) (Brochschnieder 2004; Buch 2005), with mice expressing tamoxifen-inducible Cre recombinase under the control of the SMMHC promoter (M-Cre), which would lead to mural cell specific death (Wirth 2008). After generating the iDTR; M-Cre mouse line, I established a timeline for induction of mural cell death. Since the goal is to examine the effect of pericyte loss in the adult, M-Cre and iDTR; M-Cre mice were injected intraperitoneally (IP) with tamoxifen (500 ng in 225 µl corn oil) at adult age (eight-weeks old). DT (1 µg in saline over two days) was administered eight- to 10-weeks after tamoxifen (Figure 5). This design allowed examination of the effects of DT-induced cell death in retinas from adult (16-18-weeks old) mice with spatial and temporal resolution (Figure 5).

To validate that the simian DTR is activated in the iDTR; M-Cre mice, vascularized tissues from untreated and tamoxifen treated iDTR; M-Cre mice were analyzed for the expression of DTR mRNA. As expected, DTR expression was detected by qPCR in the aorta and kidney of iDTR; M-Cre adult mice (10-weeks old mice, Figure 6) upon IP tamoxifen administration (Figure 5). Once it had been established that the DTR expression is induced in the presence of Cre, I wanted to validate that the M-Cre promoter was not leaky. To accomplish this, aorta-derived SMCs from iDTR; M-Cre mice were isolated and cultured then treated with vehicle (ethanol) or tamoxifen (1 μM in ethanol). Expression of the DTR was detected by qPCR in tamoxifen treated iDTR; M-Cre aorta-derived SMCs with a 4.5-fold increase compared to vehicle (Figure 7).

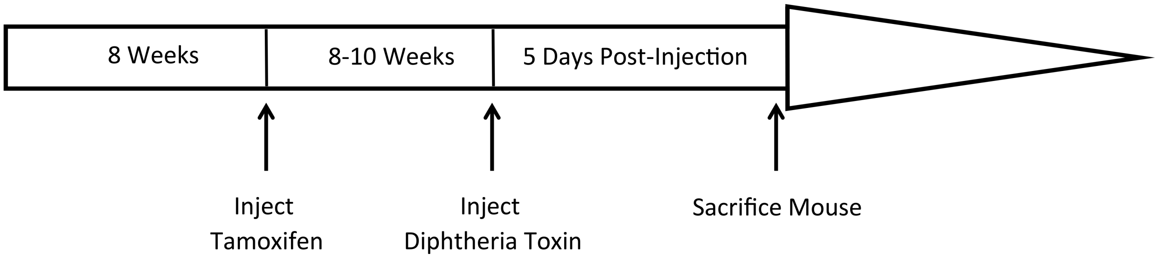

Figure 5. Generation of a mouse model of inducible mural cell loss.
Adult (eight-weeks old) M-Cre and iDTR; M-Cre mice were treated daily with tamoxifen (IP, 500 ng in 225 µl corn oil) for three days. Eight- to 10-weeks after tamoxifen treatment, mice were treated with DT (IP, 500 ng in 100 µl saline) for two consecutive days. Five days post-DT administration mice were euthanized and tissues were harvested for analysis.

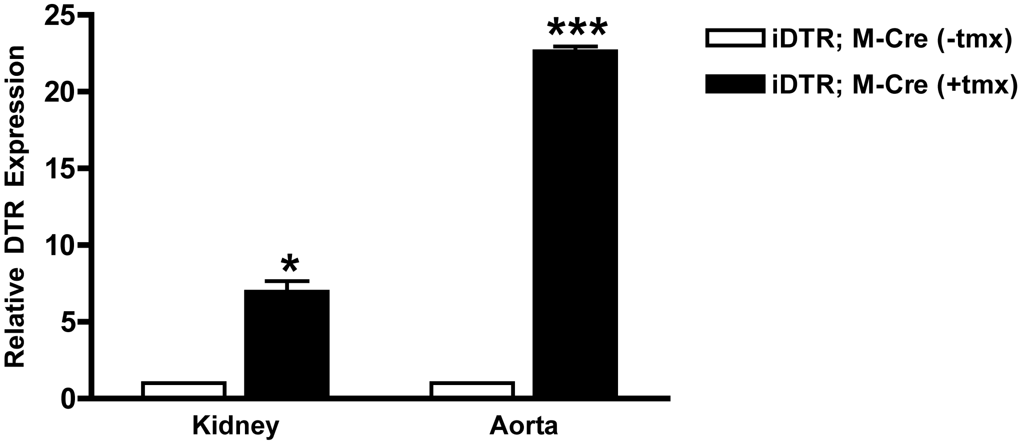

Figure 6. DTR expression in vascularized tissues from iDTR. M-Cre mice.
Tamoxifen was administered to eight-week-old iDTR. M-Cre mice; controls were mice of the same genotype that did not receive tamoxifen. Kidneys and aortas were collected from iDTR; M-Cre mice (10-weeks old) that had been treated with tamoxifen or control mice that had not been tamoxifen treated. mRNA was isolated by phenol chloroform extraction from whole tissues. Expression of the DTR was measured by quantitative PCR in the kidney and aorta. To calculate the fold-change using the standard 2-ΔΔCt formula, a Ct value of 35, corresponding to the lowest limit for detection, was used when signal was not detected for DTR. * $P < 0.05$, *** $P < 0.001$

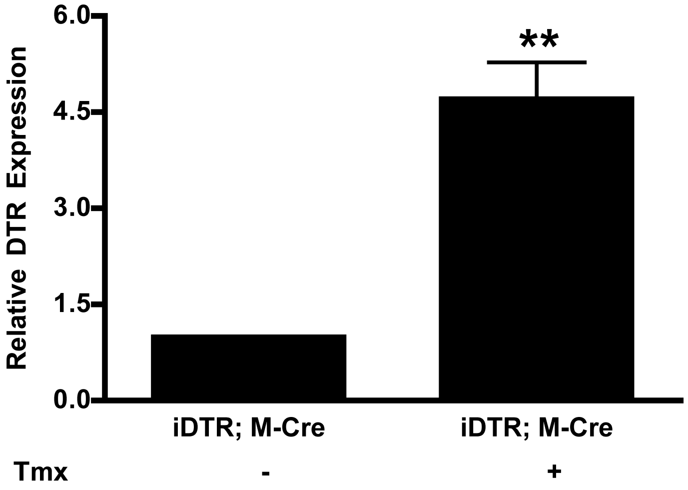

Figure 7. Expression of DTR in iDTR; M-Cre aorta-derived SMCs in vitro.
Aortas were collected from untreated iDTR; M-Cre mice (10-weeks old). Using collagenase II (175 units/ml) and dissection, the tunica adventitia of the aortas was removed. Aortas were cut lengthwise to expose the ECs, which were manually removed by scraping, and the remaining tunica media layer of the aorta was cultured overnight in 10% FBS in DMEM. A single cell suspension of aortic SMCs was created by further digesting the aorta with a collagenase II (175 units/ml) and elastase (0.5 mg/ml) mixture. iDTR; M-Cre aorta SMCs were treated with vehicle (ethanol) or tamoxifen (1 μM in ethanol) for 48 hours in 10% FBS DMEM. Total RNA was isolated using a RNeasy Kit (Qiagen). Expression of diphtheria toxin receptor (DTR) was measured by quantitative PCR. ** $P < 0.01$

The primary goal of this study is to establish a model of inducible mural cell dropout in a normal mouse. Thus, I wanted to validate that the treatments for induction in this mouse model did not influence major physiologic endpoints. To this end, blood was collected from M-Cre and iDTR; M-Cre mice by submandibular bleeding, and blood glucose levels were measured using a glucometer. There was no significant difference in blood glucose measurements post-tamoxifen or post-DT treatment (post-tamoxifen treatment: M-Cre – 170.0 ± 14.0 mg/dL, iDTR; M-Cre – 185.5 ± 28.6 mg/dL; post-DT treatment: M-Cre – 168.2 ± 14.8 mg/dL, iDTR; M-Cre – 176.7 ± 29.7 mg/dL, Figure 8A). Wild-type C57BL/6 male mice (nine- to 13-weeks old) have an average blood glucose 198 ± 13.6 mg/dL, and therefore the mice in this study are within normal range (Shonfeld). In addition, plasma insulin levels in iDTR; M-Cre, DT-treated M-Cre, and DT-treated iDTR; M-Cre mice were measured post-mortem by ELISA. No significant differences were observed in blood plasma insulin levels (DT-treated M-Cre – 0.788 ± 0.299 ng/ml, iDTR; M-Cre – 1.171 ± 0.848 ng/ml, DT-treated iDTR; M-Cre – 0.452 ± 0.050 ng/ml, Figure 8B).

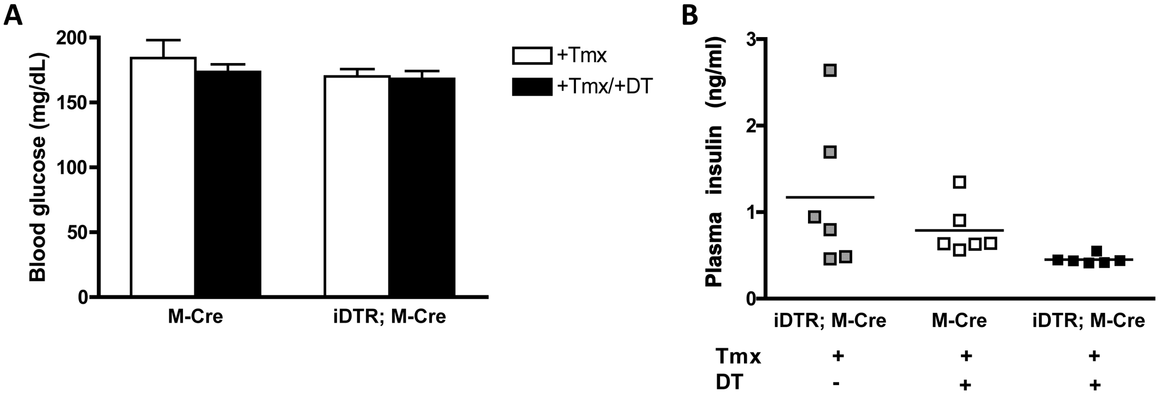

Figure 8. Glucose and insulin levels in iDTR; M-Cre mice.
(A) Blood was collected from M-Cre and iDTR; M-Cre mice (n=6) by submandibular bleeding and levels of blood glucose were measured using a glucometer. Administration of tamoxifen or DT did not influence blood glucose levels in M-Cre or iDTR; M-Cre mice. (B) Blood plasma was collected post-mortem from M-Cre and iDTR; M-Cre mice (n=6) and plasma insulin levels were measured by ELISA. Plasma insulin levels were not significantly different among any of the groups.

Tamoxifen treatment was associated with a significant increase (P<0.05) in body weight in iDTR; M-Cre mice, whereas DT treatment was associated with a significant decrease (P<0.05) in body weight compared to tamoxifen and/or DT treatment of M-Cre mouse, which had no effect on body weight (no treatment: M-Cre – 25.0 ± 4.73 g, iDTR; M-Cre – 24.5 ± 1.64 g; tamoxifen treatment: M-Cre – 28.7 ± 2.58 g, iDTR; M-Cre – 29.7 ± 1.63 g; DT treatment: M-Cre – 28.0 ± 1.67 g, iDTR; M-Cre – 25.8 ± 1.17 g, Figure 9A). Similarly, there was no difference in the weight of the kidney, brain, and heart (measured at sacrifice) among the groups (kidney: iDTR; M-Cre – 0.214 ± 0.021 mg, DT-treated M-Cre – 0.193 ± 0.015 mg, DT-treated iDTR; M-Cre – 0.164 ± 0.017 mg; brain: iDTR; M-Cre – 0.454 ± 0.017 mg, DT-treated M-Cre – 0.447 ± 0.021 mg, DT-treated iDTR; M-Cre – 0.450 ± 0.023 mg; heart: iDTR; M-Cre – 0.188 ± 0.024 mg, DT-treated M-Cre – 0.197 ± 0.059 mg, DT-treated iDTR; M-Cre – 0.169 ± 0.013 mg, Figure 9B). The weight of the liver was significantly different among the DT-treated iDTR; M-Cre mice and control groups (P<0.01) (liver: iDTR; M-Cre – 1.127 ± 0.140 mg, DT-treated M-Cre – 1.110 ± 0.197 mg, DT-treated iDTR; M-Cre – 0.756 ± 0.074 mg, Figure 9B), which is likely due to a decrease in glycogen observed in DT-treated iDTR; M-Cre mice (Supplemental Figure 3).

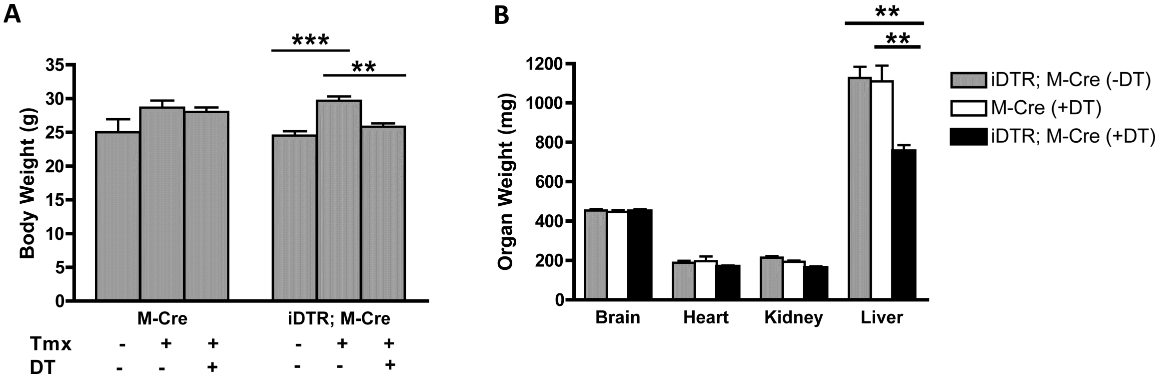

Figure 9. Measurements of physiological functions in iDTR; M-Cre mice.
(A) Body weights were measured in M-Cre mice (n=6) at eight-weeks of age (no treatment), 16-weeks of age (post-tamoxifen treatment), and 16-weeks plus 5 days (post-DT treatment). The weights of iDTR; M-Cre mice varied significantly between treatments. (B) Organ weights were measured in M-Cre (+DT), iDTR; M-Cre (-DT) and iDTR; M-Cre (+DT) mice (n=6) at 16-18-weeks of age. The livers of DT treated iDTR; M-Cre mice were significantly decreased. No differences were observed in the weights of brains, hearts, and kidneys among the three groups. $^{**}P < 0.01$, $^{***}P < 0.001$

Next, I sought to validate that DT treatment of iDTR; M-Cre mice that had been induced to express iDTR would lead to the death of mural cells (SMCs and pericytes). Whole retinal flat mounts were prepared and stained for alpha-smooth muscle actin (α-actin, green) to detect mural cells and terminal deoxynucleotidyl transferase dUTP nick end labeling (TUNEL, red) to detect fragmented DNA indicative of apoptotic cells. Consistent with the expression pattern expected from the SMMHC promoter-Cre driver, TUNEL-positivity was observed in vascular smooth muscle cells on retinal arteries (Figure 10A & B). TUNEL-positive cells were identified as pericytes on the basis of their localization and their co-staining with α-actin antibodies (Figure 10C). TUNEL-positive cells were located at microvessel bifurcations and along the abluminal surface of the microvasculature, positions characteristic of pericyte localization (Figure 10C & 11). Apoptotic cells were detected in retinal flat mounts from iDTR; M-Cre animals but were largely absent from mice lacking the iDTR transgene (Figure 11).

Following the demonstration of mural cell death in iDTR; M-Cre mice following the administration of DT, I sought to quantify the number of apoptotic cells present in the retina. Whole retinal flat mounts were prepared from DT-treated M-Cre and iDTR; M-Cre mice and stained for isolectin B4 (green) to detect ECs and TUNEL (red) to detect cell death. More than 40 TUNEL-positive mural vascular cells per retina were observed five days after the first DT injection (Figure 12); these were often seen near vessels lacking mural cell investment (Figures 10 & 11), indicating that cell death was a dynamic process (TUNEL-positive cells/retina: DT-treated M-Cre – 5.67 ± 1.53 vs. DT-treated iDTR; M-Cre – 43.20 ± 5.23; $P = 0.0018$; Figure 12).

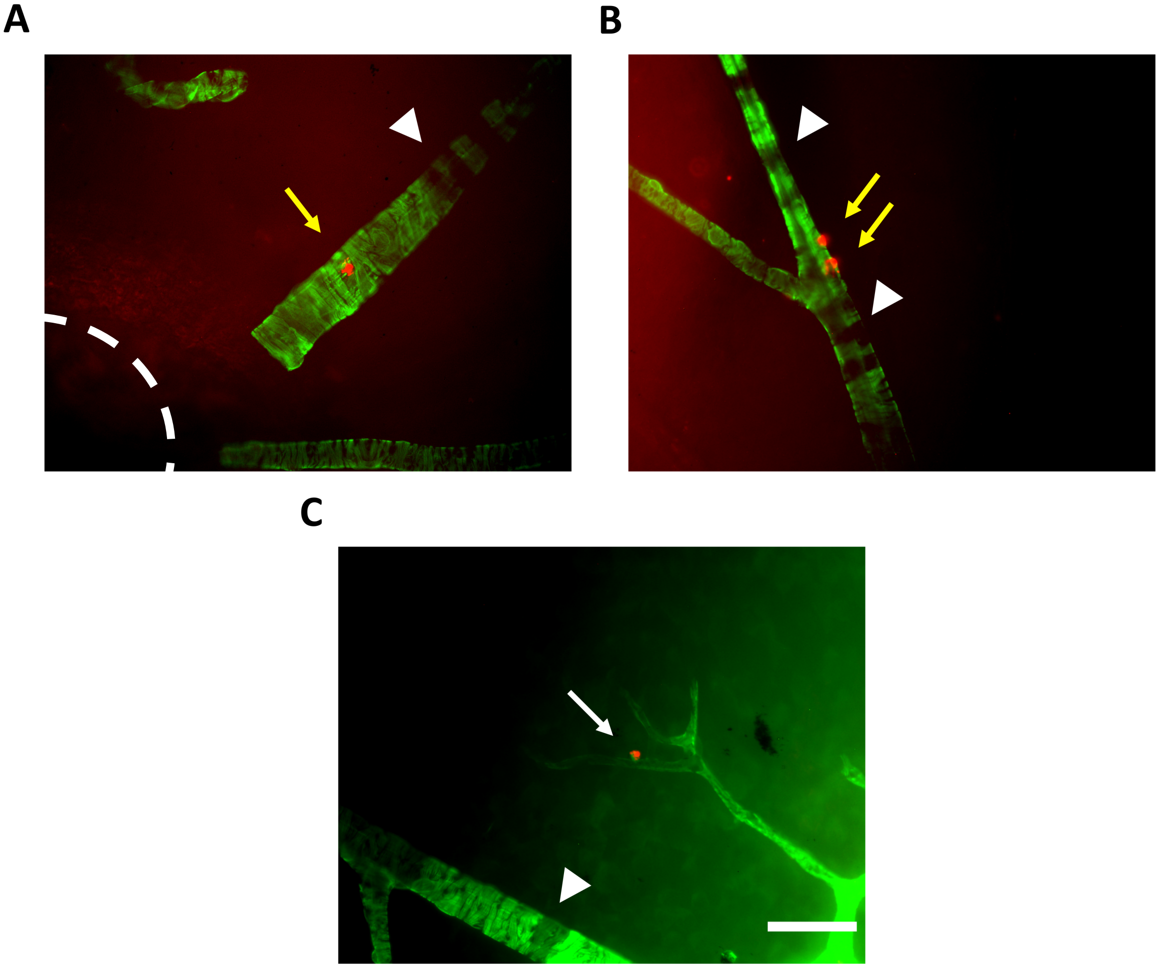

Figure 10. Mural cell apoptosis in an inducible mouse model of mural cell loss. Retinal flat mounts were stained for alpha smooth muscle actin (α-actin, green) to detect mural vascular cells (pericytes and smooth muscle cells) and for apoptotic cells using an in situ cell death detection kit (red). TUNEL-positive (A-B) SMCs (yellow arrows) and (C) pericytes (white arrow) as well as missing vascular smooth muscle cells (arrowheads) were observed in iDTR; M-Cre mice five days following DT injection. Dashed line represents location of optic nerve. Scale bar = 50 µm.

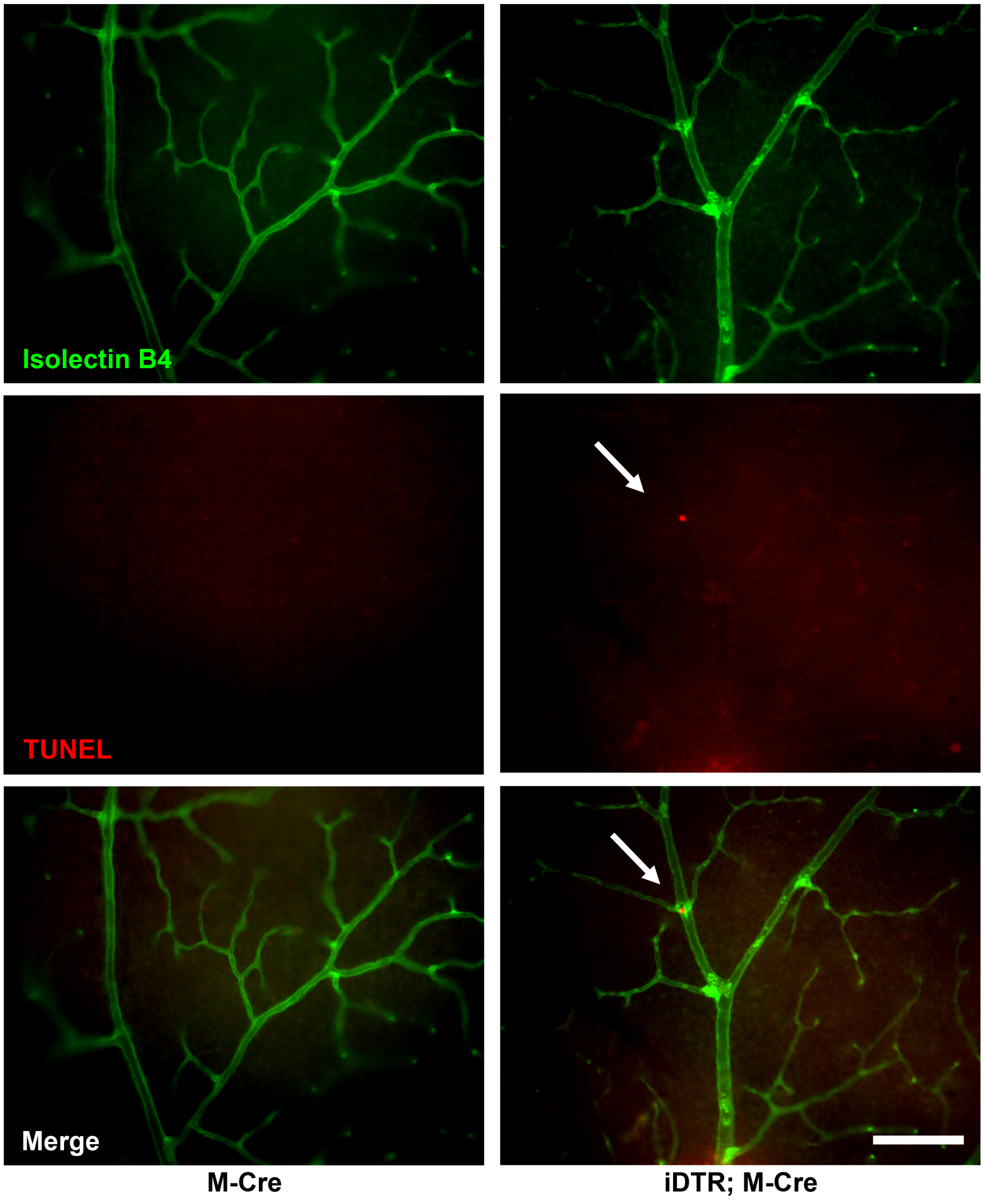

Figure 11. Characterization of inducible mouse model of mural cell loss.
Retinal flat mounts were stained for isolectin B4 (green) to detect ECs and with TUNEL (using an in situ cell death detection kit, red) to detect apoptotic cells. TUNEL-positive cells were observed in iDTR; M-Cre mice five days following DT injection (arrow). Scale bar = 100 µm.

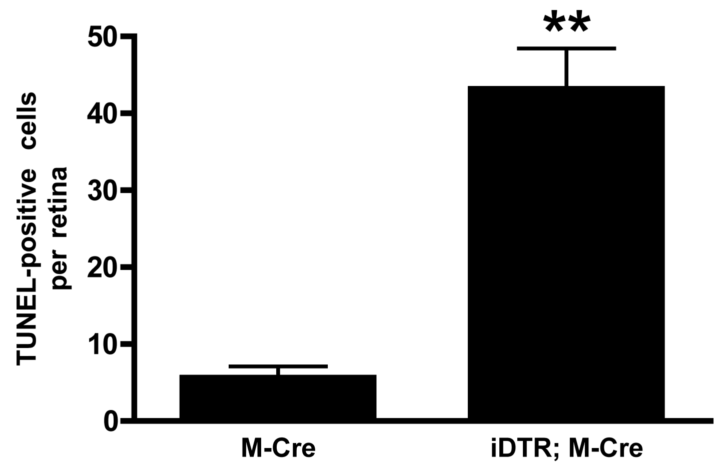

Figure 12. Quantification of apoptotic cells in an inducible mouse model of mural cell loss.

The number of apoptotic cells as quantified by counting the total number of TUNEL-positive nuclei in retinal flat mounts stained for isolectin B4 and with TUNEL from M-Cre (n=3) and iDTR; M-Cre (n=5) mice. Approximately 40 apoptotic cells per retina were observed in DT-treated iDTR; M-Cre mice and less than 6 apoptotic cells per retina were seen in DT-treated M-Cre. ** $P < 0.01$

Microangiopathy in mouse model of inducible mural cell death

I sought to determine the relationship between pericyte loss and hallmark characteristics of DR, such as microaneurysms and vascular leakage (Cogan and Kuwabara 1967; Klein 1984A and 1984B; Hammes 2002). To this end, whole retinal flat mounts were prepared from DT-treated M-Cre and iDTR; M-Cre mice and stained for isolectin B4 (green) to detect ECs and TUNEL (red). The total number of microaneurysms per retina was counted manually by visually assessing the fluorescent microscopy images. An average of three microaneurysms were observed per retina in iDTR; M-Cre mice, and these were often seen in capillaries in association with TUNEL-positive cells (microaneurysms/retina: DT-treated M-Cre – 0.33 ± 0.33 vs. DT-treated iDTR; M-Cre – 3.20 ± 0.49; P = 0.0063; Figure 13). This observation indicates that microaneurysms appear acutely after pericyte death, considering that DNA fragmentation is a late-stage event during apoptosis (Collins 1997). To determine if pericyte loss had an effect on vascular leakage, I perfused mice with 50 mg/ml fluorescein dextran ($2x10^6$ mw) in 4% paraformaldehyde in PBS prior to flat mounting; high molecular weight dextran should not escape an intact blood retinal barrier. An average of six hyperpermeable areas, identified as regions of fluorescein-dextran leakage, were observed per retina in iDTR; M-Cre mice, indicating breakage of the BRB (hyperpermeable areas/retina: DT-treated M-Cre – 0.66 ± 0.33 vs. DT-treated iDTR; M-Cre – 7.00 ± 1.87; P = 0.0363; Figure 14B). The number of leakage events was highly variable between mice but generally affected only the capillaries (Figure 14 and data not shown).

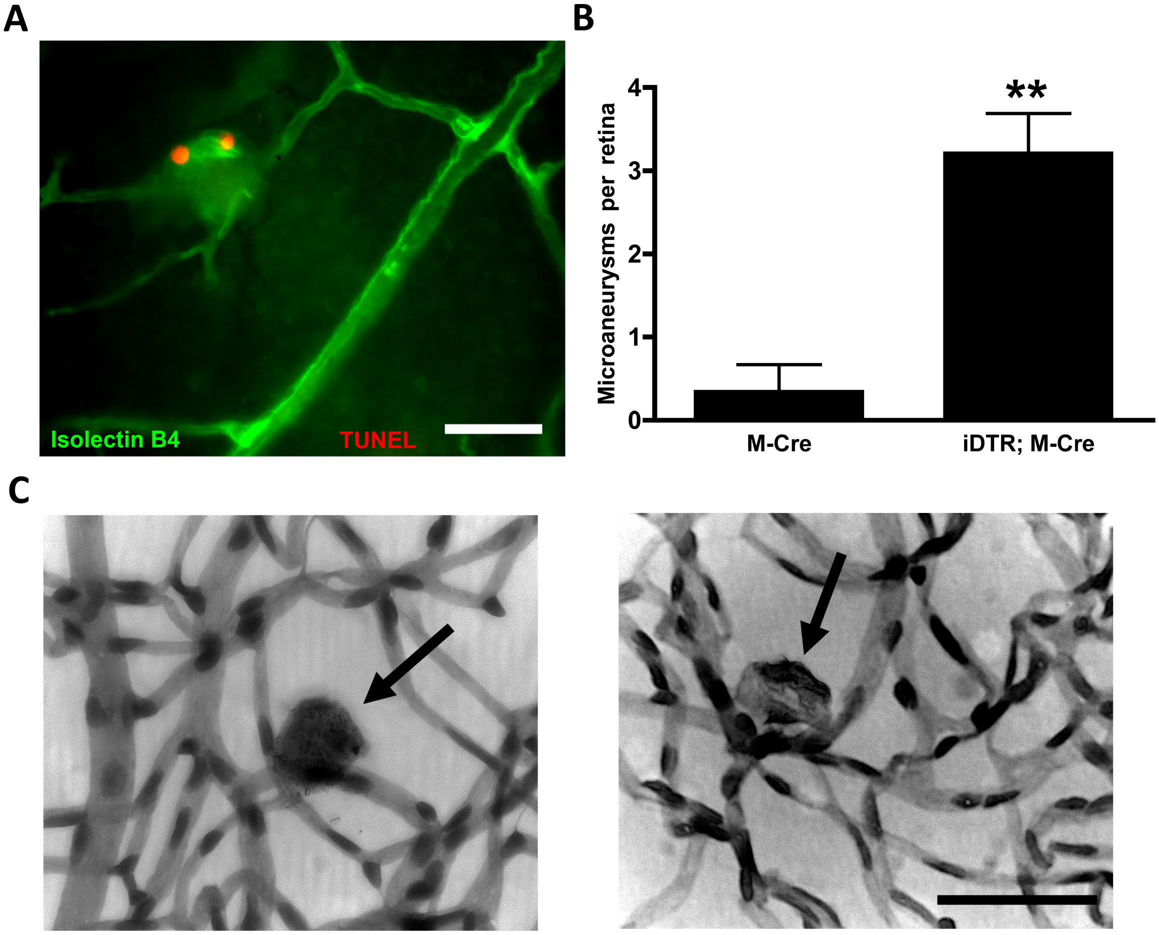

Figure 13. Pericyte loss in the retinal microvasculature is associated with the formation of microaneurysms.

(A) Microaneurysms were observed in retinal flat mounts from iDTR; M-Cre (+tamoxifen, +DT) mice labeled with isolectin-B4 to detect EC (green) and TUNEL (red). (B) Microaneurysms were quantified by assessing fluorescence microscopy images of M-Cre (+tamoxifen, +DT, n=3) and iDTR; M-Cre (+tamoxifen, +DT, n=5) mice. (C) Microaneurysms in retinal elastase digests stained for periodic acid-Schiff (PAS) and counterstained with hematoxylin from an iDTR; M-Cre (+tamoxifen, +DT) mouse. Scale bars = 50 µm. ** $P < 0.01$

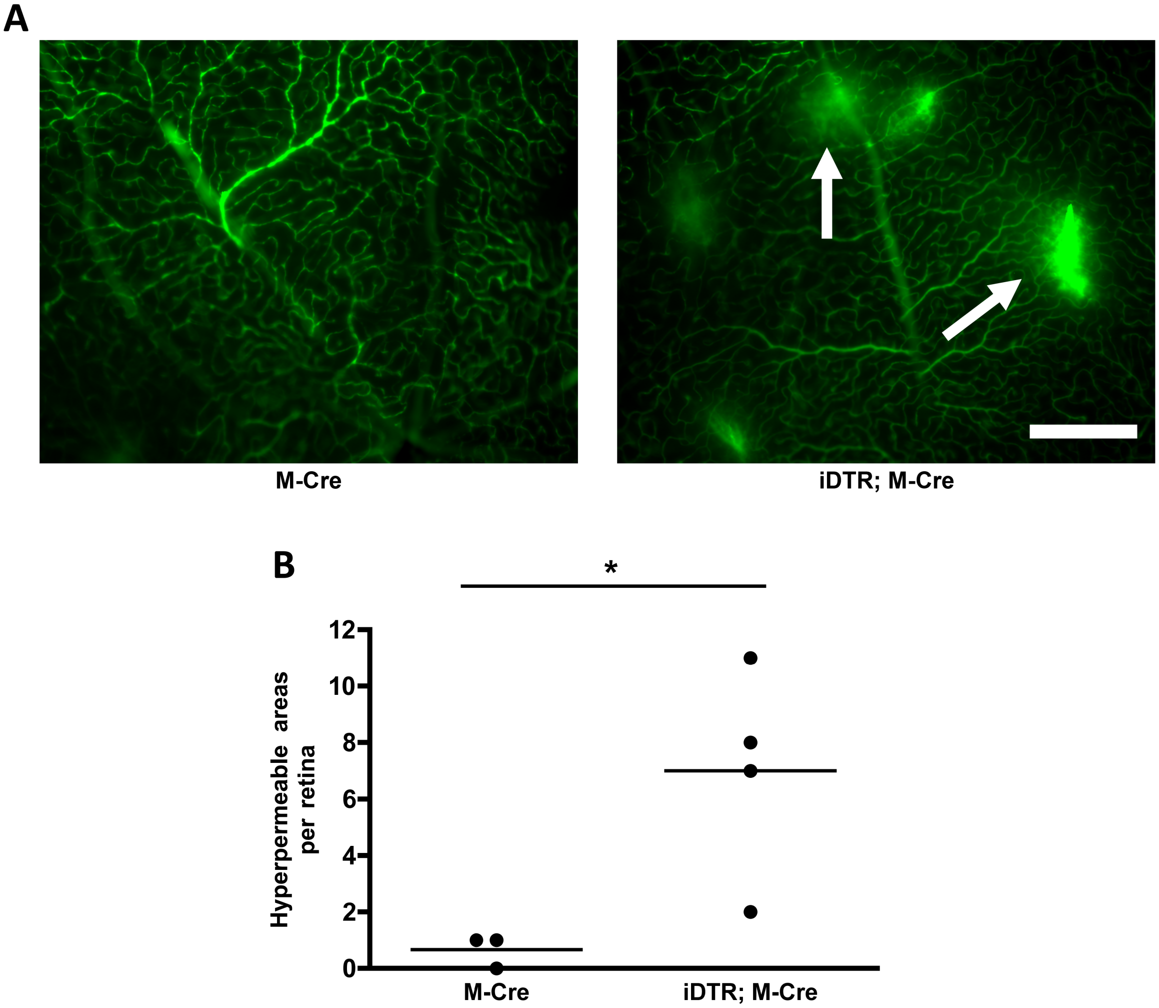

Figure 14. Increased microvascular permeability in retinal microvasculature of mice with inducible mural cell loss.

(A) DT-treated M-Cre (left panel) and iDTR; M-Cre (right panel) mice were perfused with 50 mg/ml fluorescein dextran (2×10^6 mw) prior to retina imaging using fluorescence microscopy. Areas of vascular leakage (arrows) were observed in DT-treated iDTR; M-Cre mice. (B) Hyperpermeable areas per retina were quantified in M-Cre (+tamoxifen, +DT, n=3) and iDTR; M-Cre (+tamoxifen, +DT, n=4) mice. Scale bar = 250 µm. * $P < 0.05$

Quantification of pericyte loss

TUNEL staining of retinal flat mounts yields a view of cell death occurring in a snapshot of time in the retinas of the mouse model of inducible mural cell loss. However, from the visualization of retinal flat mounts stained with α-actin and TUNEL (Figure 10), where there is already some mural cell loss (indicated by a lack of α-actin staining) and other mural cells are in the process of dying (indicated by TUNEL-positive cells), it is evident that the cell death process in this model is dynamic. Thus, I wanted to quantify the total loss of pericytes and ECs in the retinal microvasculature. The current standard in the field for pericyte and EC quantification is to isolate the retinal microvasculature by elastase digest and manually count the number of pericytes and ECs based on their size and morphology (Speiser 1968; Laver 1993; Kern and Engerman 1996; Hammes 1997; Zhang 2012). However, this standard is only applicable to rats, dogs, cats, primates, and humans and does not apply to mice, where distinguishing these cell types is less clear.

Therefore, in collaboration with Wimasis Image Analysis (www.wimasis.com), I established a methodology for quantifying pericytes and ECs in the retinal microvasculature of mice using automated image analysis (for full details see Chapter 6). To quantify pericytes and ECs in mice, the retinal vasculatures were isolated by elastase digest and then analyzed using automated image analysis (Figures 15, 16, 25 & 26). This analysis revealed that five days after DT administration approximately 7-15% of pericytes were lost from the retinal microvasculatures from DT-treated iDTR; M-Cre mice compared to the M-Cre and iDTR; M-Cre controls, respectively (pericytes/mm: DT-treated M-Cre – 8.647 ± 0.459, iDTR; M-Cre – 9.475 ± 0.490, DT-treated iDTR; M-Cre – 8.031 ± 0.302; Figure 16). This finding indicates that microangiopathy can be triggered by the loss of a relatively small proportion of pericytes (Figures 15 & 16). Interestingly, but perhaps not surprisingly, the number of endothelial cells was also reduced in DT-treated iDTR; M-Cre mice (8-9%, Figure 16), although this difference was not statistically significant, and no TUNEL-positive ECs were observed in the analysis.

In light of the decrease in both pericytes and ECs in the mouse model of inducible mural cell loss, I hypothesized that these mice might also display acellular capillaries. Acellular capillaries have been defined as capillaries lacking nuclei along their length with a minimum of one-fourth the width of a normal capillary (Kern and Engerman 2001; Zheng and Kern 2004; Zheng and Berkowitz 2007; Howell and Kern 2013); this definition which leaves room for a broad interpretation. Thus, in collaboration with Wimasis Image Analysis, I developed an automated image analysis system for identifying acellular capillaries in retinal microvasculatures. Image analysis automation was used to define acellular capillaries as those lacking nuclei in a length greater than the average internuclei distance and being a minimum of one-fourth the width of a normal capillary (for full details see Chapter 6) (Kern and Engerman 1996; Kern and Engerman 2001; Zheng and Kern 2004; Barber 2005; Zheng and Berkowitz 2007; Howell and Kern 2013). This analysis revealed that DT-treated iDTR; M-Cre mice had approximately twice as many acellular capillaries per millimeter of capillary length as the control groups (acellular capillaries/mm capillary length: DT-treated M-Cre – 0.400 ± 0.147, iDTR; M-Cre – 0.511 ± 0.114 DT-treated iDTR; M-Cre – 0.812 ± 0.062; $P<0.05$; Figures 17 & 18).

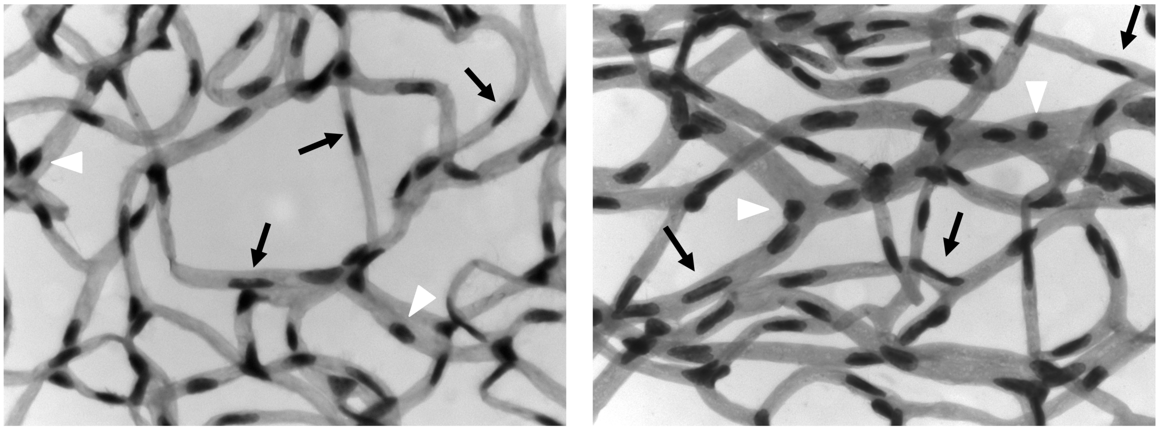

iDTR; M-Cre (-DT)

M-Cre (+DT)

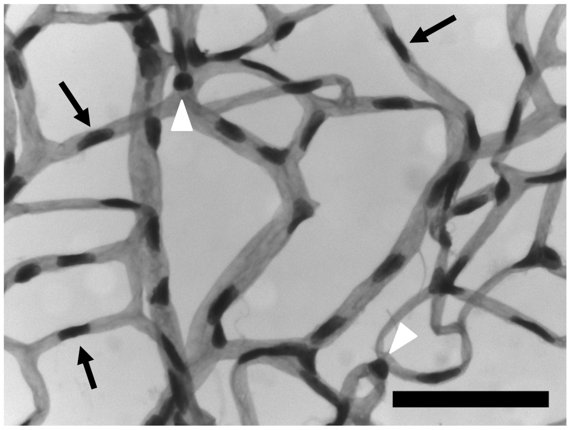

iDTR; M-Cre (+DT)

Figure 15. Retinal microvasculature of a mouse model of inducible mural cell loss. Vessels were digested from retinas using elastase and stained with periodic acid-Schiff (PAS) and hematoxylin. Elastase digested vasculature from iDTR; M-Cre (top left panel), DT-treated M-Cre (top right panel), and DT-treated iDTR; M-Cre (bottom panel) retinas showing pericytes (white arrowheads) and ECs (black arrows). Scale bars = 50 μm.

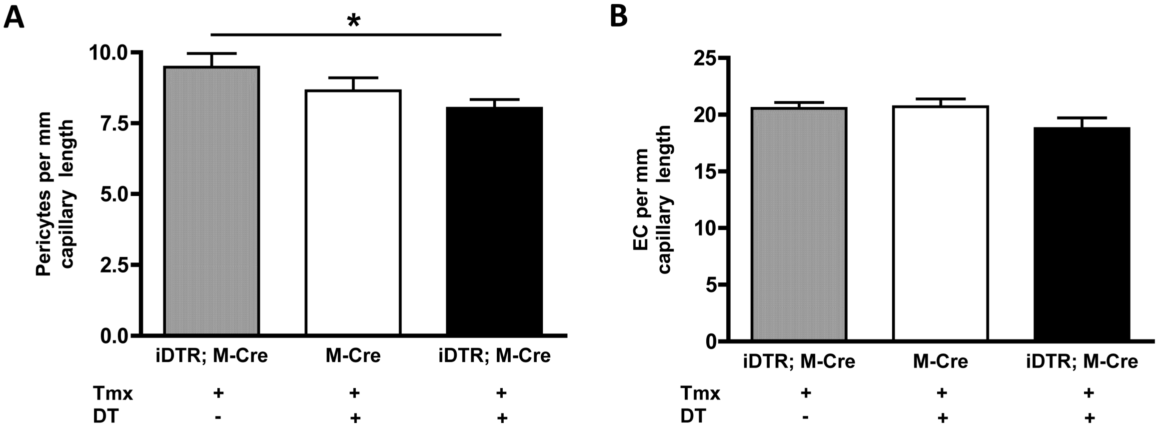

Figure 16. Loss of pericytes in retinal microvasculature of a model of inducible mural cell loss.

(A) The number of pericytes per mm capillary length and (B) the number of EC per mm capillary length were quantified using automated image analysis in 15 randomly selected images per retina in iDTR; M-Cre (+tamoxifen, no DT, n=8), M-Cre (+tamoxifen, +DT, n=7), and iDTR; M-Cre (+tamoxifen, +DT, n=8) mice. There was approximately 7-15% pericyte loss in DT-treated iDTR; M-Cre mice compared to control. * P=0.0251

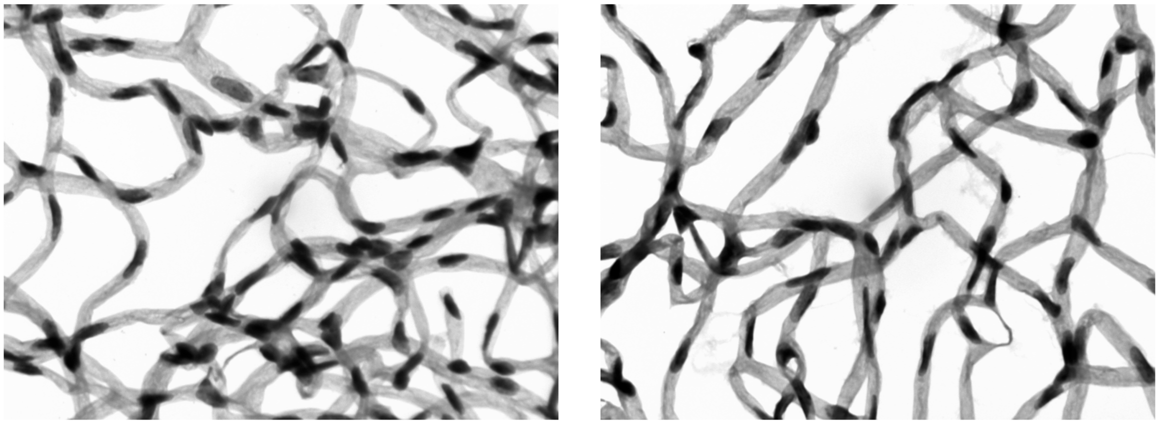

iDTR; M-Cre (-DT)

M-Cre (+DT)

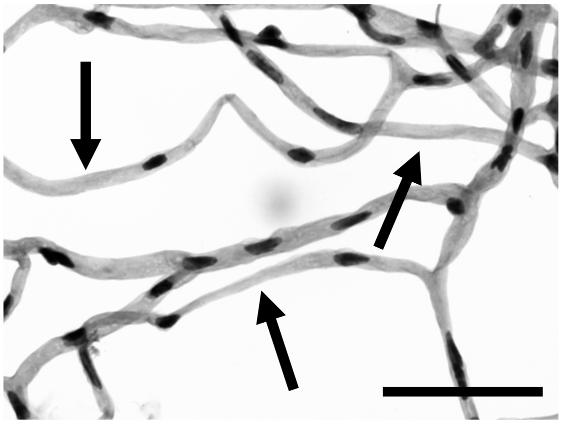

iDTR; M-Cre (+DT)

Figure 17. Retinal microvascular abnormalities in a model of inducible mural cell loss.

The retinal vasculatures were digested from iDTR; M-Cre (top left panel), DT-treated M-Cre (top right panel) and DT-induced iDTR; M-Cre (bottom panel) retinas and stained with periodic acid-Schiff (PAS) and hematoxylin. Acellular capillaries (bottom panel, arrows) were observed in elastase digests of retinal vessels from DT-treated iDTR; M Cre+ mice. Scale bars = 50 µm.

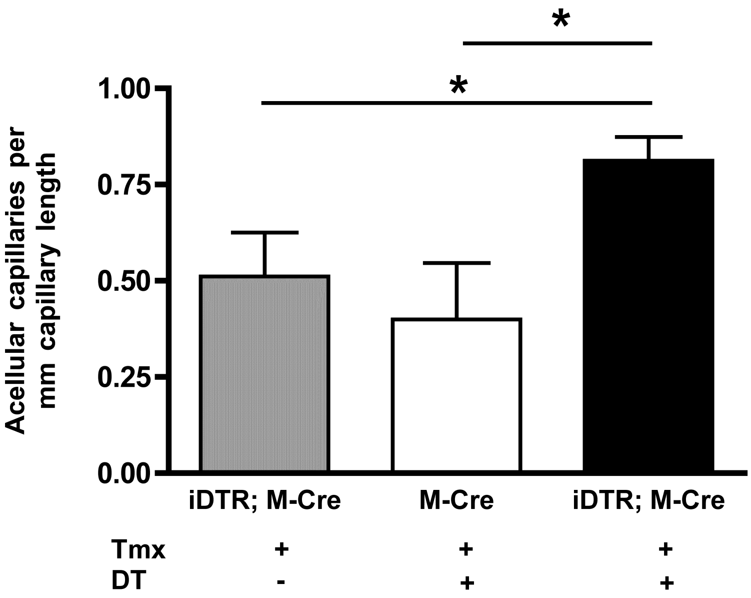

Figure 18. Quantification of acellular capillaries in an inducible model of mural cell loss.

The number of acellular capillaries per capillary length was evaluated in elastase digests of retinal microvasculatures using quantitative image analysis automation in 10 randomly selected images per retina in iDTR; M-Cre (+tamoxifen, no DT, n=8), M-Cre (+tamoxifen, +DT, n=7), and iDTR; M-Cre (+tamoxifen, +DT, n=8) mice. Approximately twice as many acellular capillaries were observed in DT-treated iDTR; M-Cre mice versus controls. * $P < 0.05$

CHAPTER 3

ESTABLISHING A LONG TERM MOUSE MODEL OF INDUCIBLE MURAL CELL DEATH

AIM

To establish a long-term adult mouse model of inducible mural cell loss in the retina.

RATIONALE

The mouse model of inducible mural cell loss described above uses systemic administration (IP) of tamoxifen and DT and allows for acute examination of the effects of pericyte loss on the retinal microvasculature (see Chapter 2). A limitation of this approach is that the model of inducible mural cell loss does not allow for analyses of the chronic effects of pericyte loss in vascular stability. About one week after DT injection, animals show signs of distress most likely caused by systemic effects of DT on non-vascular smooth muscle cells. Consistent with this interpretation, our mice did not show significant levels of mural cell loss from large vessels, as has been shown to occur in other mural cell death models (Clarke 2006). It would be of interest to analyze the long-term effects of pericyte cell loss on vascular stability and to determine to what extent late-stage DR is observed. Therefore, I sought to develop a model that would allow us to investigate the long-term effects of pericyte loss in retinal vascular stability in non-diabetic mice by locally inducing death of mural cells in adult mouse eyes.

RESULTS

Local adminstration of DT: a low dose pilot study

iDTR; M-Cre mice were established as described in Chapter 2. iDTR; M-Cre mice were injected IP with tamoxifen (500 ng in 225 μl corn oil) at adult age (eight-weeks old). To determine the dose of DT that would provide a gradual loss of mural cells, DT (0, 35 fg, or 350 fg in saline) was intravitreally injected six months after tamoxifen administration (eight-months old), as this was the age of the mice available for this pilot study (Figure 19). The beginning dose of DT (35 fg) was determined by taking the dose (1 μg DT) used in the systemic model of mural cell loss (see Chapter 2) and adjusting for the difference between the total mouse body volume (estimated as 20 ml) and the intravitreal space (7 μl). A higher (10X) dose of 350 fg DT was also included in this pilot series. Since Cre induction is permanent, there was no concern about the length of time between the administration of tamoxifen and DT.

I sought to validate that local administration of DT the iDTR; M-Cre mice would lead to death of mural cells (SMCs and pericytes). Whole retinal flat mounts were stained for isolectin B4 (green) to detect ECs and TUNEL (red) to detect cell death. Five days after DT injection, there was staining of non-vascular cells by isolectin B4; these are likely macrophages and reflect inflammation from the intravitreal injection of DT (Figure 20). In addition to binding ECs, isolectin b4 binds to cell membrane glycoconjugates containing terminal alpha-D-galactose, which are present in macrophages (Sorokin and Hoyt 1992). Thus, five days post-intravitreal injection of DT was too early for analysis due to inflammation.

Next, I examined the retinal vasculature at one-month post-intravitreal DT injection. Whole retinal flat mounts were prepared and stained for alpha-smooth muscle actin (α-actin, green) to detect mural cells and TUNEL (red) to detect cell death. Unlike the five-day time point, there was no evidence of an inflammatory response. However, there was also no evidence of the loss of mural cell investment at either dose of DT (Figure 21). Thus, it appears that the doses of DT used were not sufficient to induce mural cell death and higher doses of DT are necessary.

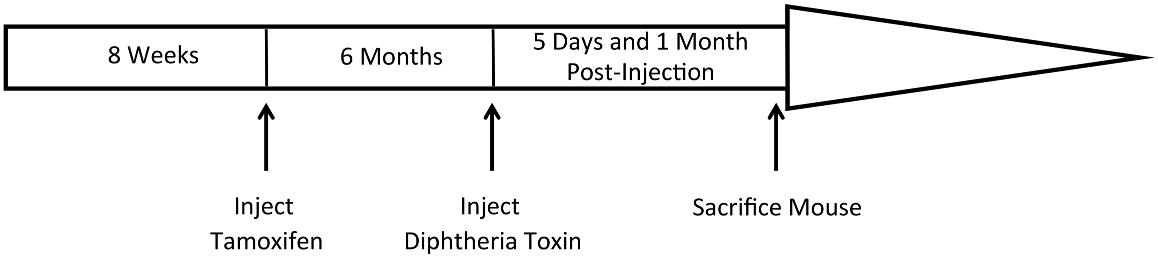

Figure 19. Pilot study timeline using local administration of low dose DT in iDTR; M-Cre mice.

iDTR; M-Cre mice were treated daily with tamoxifen (IP, 500 ng in 225 µl corn oil) for three days at eight-weeks of age. Six months after tamoxifen treatment, mice were intravitreally injected once with DT (0 fg, 35 fg, or 350 fg in saline). Five days and one month post-DT administration mice were euthanized and tissues were harvested for analysis.

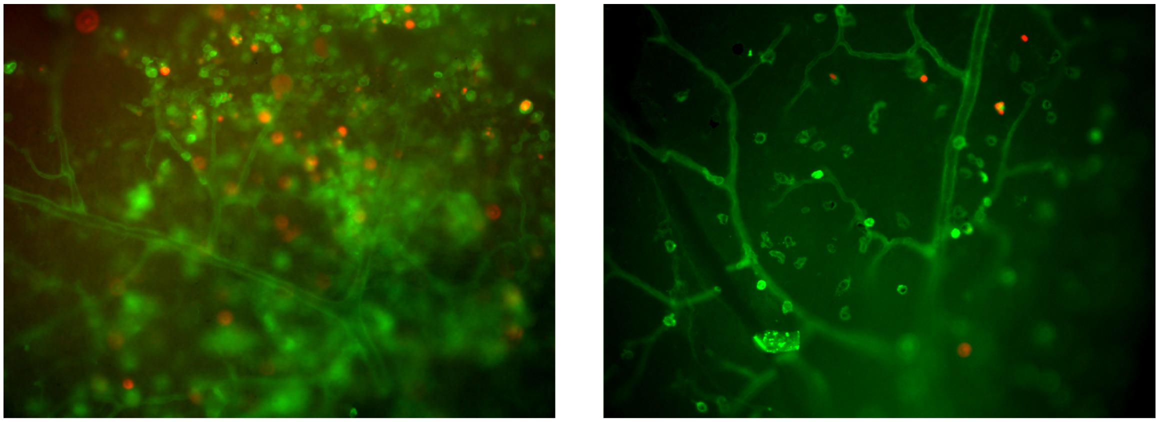

Saline **35 fg DT**

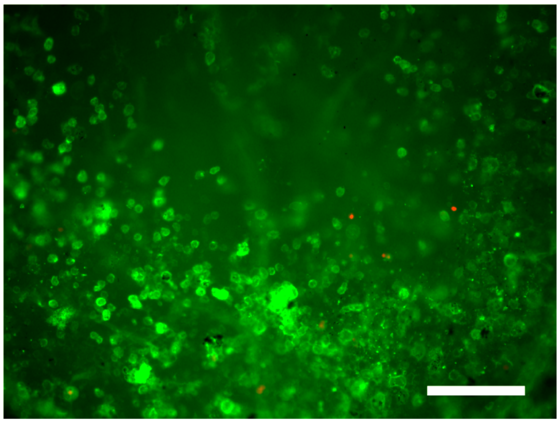

350 fg DT

Figure 20. Intravitreal injection of DT causes inflammation in the retina at five days post-injection.
Retinal flat mounts of iDTR; M-Cre mice intravitreally injected with saline (top left panel), 35 fg DT (top right panel), or 350 fg DT (bottom panel) were stained for isolectin B4 (green) to detect ECs and with TUNEL (red). Inflammation in the retina was evident five days after DT administration. Scale bar = 100 μm

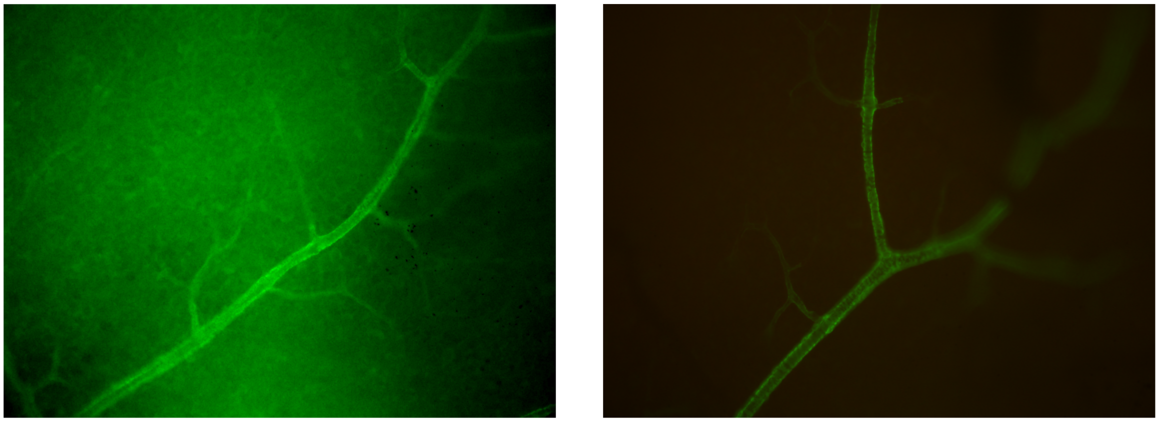

Saline

35 fg DT

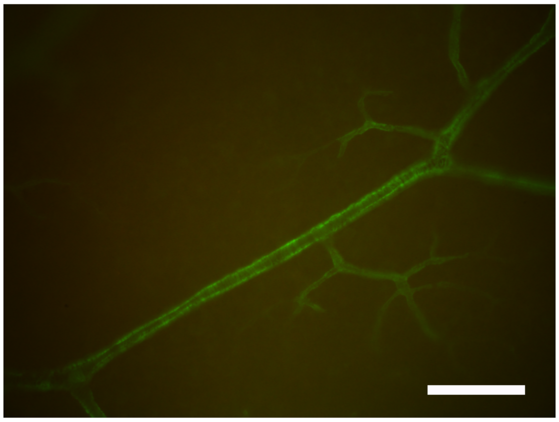

350 fg DT

Figure 21. Local administration of low dose DT does not cause mural cell loss in iDTR; M-Cre mice.

Retinal flat mounts of iDTR; M-Cre mice intravitreally injected with saline (left panel), 35 fg DT (middle panel), or 350 fg DT (right panel) were stained for smooth muscle actin (α-actin, green) to detect pericytes and with TUNEL (red). Loss of pericyte investment and microangiopathies were not observed. Scale bar = 100 μm.

Local adminstration of DT: a high dose pilot study

Results of the pilot study indicated that 350 ng DT in the iDTR; M-Cre mouse eye is not sufficient to cause mural cell death. So a second pilot study was undertaken using higher levels of DT. Adult (eight-weeks old) iDTR; M-Cre mice were IP injected with tamoxifen (500 ng in 225 μl corn oil) daily for three days and three months later DT (0 ng or 7 ng in saline) was intravitreally injected (Figure 22). This higher does was calculated using the dosage (1 μg DT) established in the systemic model of mural cell loss (see Chapter 2) and taking into account the total mouse blood volume estimated as 1 ml (versus body volume used in the first calculation) and the intravitreal space (7 μl).

Two weeks post-intravitreal injection, gross retinal vascular anatomy was examined using fundus photography. No overt changes in retinal vasculature were observed post-tamoxifen treatment (IP) (Figure 23A), however hemorrhages were observed after intravitreal injection in the presences and absence of DT (black arrows, Figure 23B). Fluorescent angiography (FA) revealed mild leakage in the vehicle- and DT-treated iDTR; M-Cre mice (Figure 24). Interestingly, intravitreal injection of DT in iDTR; M-Cre mice appears to be associated with decreased vessel width (Figure 24). In addition, fluorescein perfusion was delayed in DT-treated iDTR; M-Cre mice compared with vehicle-treated control (Figure 24). Also, vascular secondary branch perfusion was observed in vehicle-treated iDTR; M-Cre mice, but not in DT-treated iDTR; M-Cre mice (Figure 24).

The hemorrhages observed in this high dose (7 ng DT) pilot study may be indicative of damage caused by intravitreal injection. An additional challenge in intravitreally injecting adult mice is the possibility of puncturing the lens with the needle, which causes opacity and can lead to cataracts (data not shown). While the study presented here is a small pilot study (n=4 for each group), the data suggests that vascular changes may be occurring in the DT-treated iDTR; M-Cre mice. However, further analysis is required to determine the exact changes occurring after intravitreal injection of DT in iDTR; M-Cre mice and these studies are ongoing. Taken together, these data suggest that the intravitreal injection technique requires refinement and further development, but remains a viable option for establishing a long-term model of inducible mural cell loss.

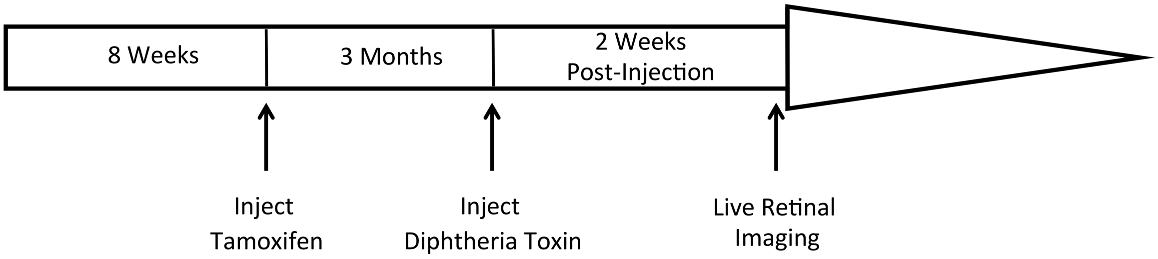

Figure 22. Pilot study timeline using local administration of high dose DT in iDTR; M-Cre mice.
iDTR; M-Cre mice were treated daily with tamoxifen (IP, 500 ng in 225 µl corn oil) for three days at eight-weeks of age. Three months after tamoxifen treatment, mice were intravitreally injected once with DT (0 ng or 7 ng in saline). Two weeks post-DT administration mice were analyzed for retinal vascular changes.

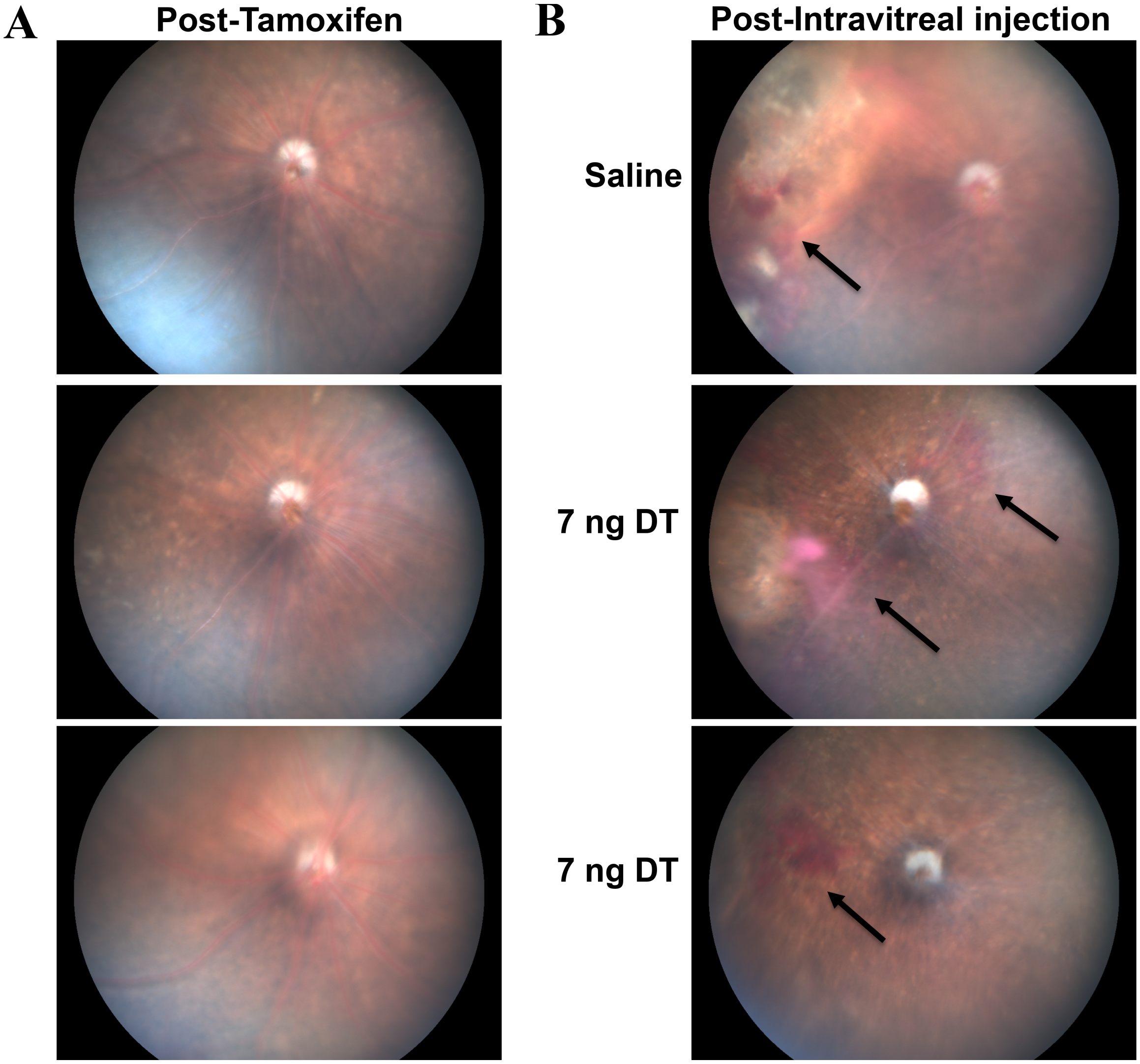

Figure 23. Live imaging in iDTR; M-Cre mice in high dose pilot study.
Fundus photography of retinal vasculature in adult iDTR; M-Cre mice A) post-tamoxifen treatment (IP) and B) two weeks post-intravitreal injection of DT (0 ng or 7 ng in saline). Hemorrhages (black arrows) occurred after intravitreal injection in the presence and absence of DT in iDTR; M-Cre mice. Mouse retinal vasculatures imaged post-tamoxifen treatment in A (left) were assessed again following intravitreal injection of vehicle or DT in B (right).

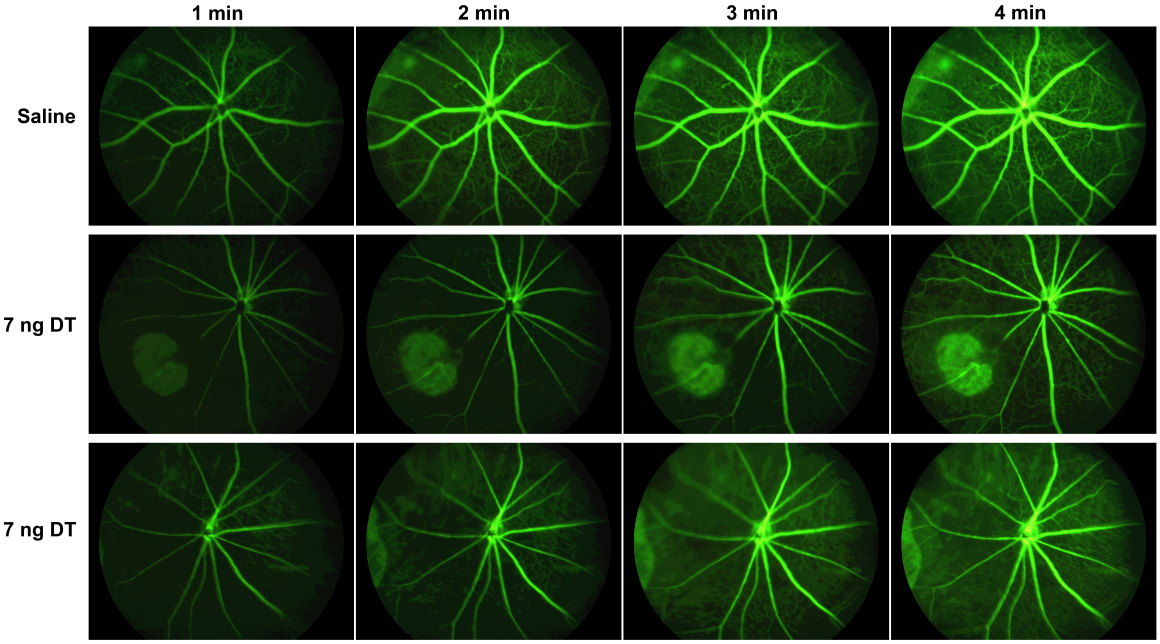

Figure 24. Vascular permeability changes in retinal microvasculature of mice with local induction of mural cell loss.
Vehicle-treated iDTR; M-Cre (first row) and DT-treated iDTR; M-Cre (second and third rows) mice were injected with 25% fluorescein sodium in saline (60 mg/kg mouse) prior to fundus photography. iDTR; M-Cre mice intravitreally treated with DT were observed to have thinner vessels (second and third rows) compared to vehicle-treated iDTR; M-Cre mice (first row). Intravitreally DT-treated iDTR; M-Cre mice had delayed fluorescein perfusion (second and third rows) compared to intravitreally injected vehicle controls (first row). Mouse retinal vasculatures evaluated in this experiment correspond with the same mouse eyes imaged in Figure 23.

CHAPTER 4

DISCUSSION

DISCUSSION

Developing a model of inducible mural cell loss

To directly examine the role of the pericyte in the pathogenesis of DR, it is essential to have a model that allows the investigation of pericyte loss in the adult retinal vasculature without the added complexity of diabetes, hyperglycemia, obesity, and/or obstructing a major signaling pathway. To accomplish this, mice carrying a floxed allele of the iDTR (Buch 2005; Brockschnieder 2004) were bred with mice expressing tamoxifen-inducible Cre recombinase under the control of the M-Cre promoter (Wirth 2008). Mice with induced expression of DTR are DT-sensitive because they express a simian DTR, a heparin-binding epidermal growth factor-like growth factor (HB-EGF) precursor (Buch 2005). In iDTR mice there is an upstream loxP-flanked STOP sequence that is deleted in the presence of Cre, thereby activating the expression of DTR (Buch 2005). In M-Cre (control) and iDTR; M-Cre (experimental) mice, the M-Cre promoter controls Cre recombinase that has a modified estrogen receptor-binding domain (CreER^{T2}) (Indra 1999; Wirth 2008). Cre-mediated recombination has been shown to occur exclusively in SMCs in SMMHC-CreER^{T2} (M-Cre) mice (Wirth 2008). Thus, upon M-Cre induction by tamoxifen, DTR expression is activated, rendering the mice DT sensitive. Subsequent administration of DT to these mice will lead to mural cell death.

In 1884, it was first discovered that *Corynebacteriym diphtheriae* causes diphtheria (Loeffler 1884). In the 1920's, the US had approximately 100,000-200,000 cases per year of diphtheria, of which 13,000-15,000 infected people died each year (Center for Disease Control 2012). Beginning in the 1930's, the wide use of vaccinations (typically diphtheria toxoid in combination with tetanus toxoid and pertussis vaccine) has virtually eradicated diphtheria from most developing countries (Center for Disease Control 2012).

Corynebacteriym diphtheriae produces DT, a single polypeptide chain made of 535 amino acids (~62 kDa) (Roux 1988; Pappenheimer 1977). DT is readily divided into two components (fragment A (DT-A) and fragment B (DT-B)) following separation of a single peptide and disulfide bond (Pappenheimer 1977). On the cell surface, DT-B binds to the DTR (HB-EGF precursor) and then internalized by the cell through receptor-mediated endocytosis (Saito 2001). Following translocation into the cytoplasm, DT-A inactivates elongation factor 2 (EF2) through catalysis, which results in protein synthesis inhibition and subsequent apoptosis in the target cell (Saito 2001; Buch 2005). Since murine (mouse) HB-EGF precursors do not bind DT-B, they are not DT sensitive (Saito 2001; Buch 2005). In the iDTR; M-Cre system employed for this study, mice express the simian (monkey) HB-EGF precursor (DTR), thus rendering them sensitive to DT (Buch 2005).

Whereas mouse models using the iDTR system with various Cre promoters have been demonstrated in the literature, none had employed the M-Cre promoter to induce mural cell death in mice. For example, using an oligodendrocyte-specific promoter (MOGi-Cre) with the iDTR system led to tremors, hind limb paralysis, and myelinated structure annihilation in the CNS, showing that DT can cross the BBB and access the CNS with systemic induction (IP) (Buch 2005). In addition, the iDTR system has been used to acutely ablate melanopsin-expressing retinal ganglion cells, which caused a deficiency in non-image forming visual functions, demonstrating that through systemic administration DT has access to the retinal space (Hatori 2008).

Therefore, to characterize iDTR; M-Cre mice, I had to first establish a timeline and dosage for induction of mural cell death. Numerous variables were examined including the use of active versus precursor tamoxifen, varied doses of tamoxifen and DT, and altering the time between DTR activation and administration of DT. In the final protocol that was used in the experiments presented in this thesis, adult (eight-weeks old) mice were IP injected on three consecutive days with tamoxifen to activate the DTR. Then, to induce mural cell death, DT was injected IP eight to ten weeks after tamoxifen administration. The effects of DT-induced mural cell death in adult mouse retinas (16-18-weeks old) were examined with particular attention to spatial and temporal resolution (Figure 5).

To ensure that the alterations that occur in the DT-treated iDTR; M-Cre do not influence major physiologic endpoints, blood glucose and plasma insulin levels were measured. Blood glucose measurements between the control and DT-treated iDTR; M-Cre mice did not vary with either treatment (tamoxifen or DT) (Figure 8A). Similarly, there was no significant difference in plasma insulin (collected post-mortem) levels among the groups (Figure 8B).

Limitations of the model

The iDTR; M-Cre mice began to show signs of deterioration eight days after the first DT injection. This decline in health is most likely the result of the fact that the promoter driving Cre would lead to the expression of iDTR in all smooth muscle (vascular and visceral) so that in addition to being expressed in by vascular SMCs, the iDTR would be expressed by nonvascular SMCs in organs such as the bladder and intestine. In support of this, iDTR; M-Cre mice displayed reduced body and liver weight following administration of DT (Figure 9). To avoid the complications that these issues might cause, I focused my investigation on a time point five days after the first DT injection, when iDTR; M-Cre mice were healthy and active.

Since DR develops over the course of decades, it would be worthwhile to determine to what extent late-stage DR, including components such a new vessel growth, is observed in mice with pericyte cell loss over time. In preliminary studies for creating a long-term model of mural cell loss, I administered DT (0, 35, 350 fg in saline) by intravitreal injection. In the initial pilot study, the dosage of DT was apparently too low as it did not cause mural cell death. However, a subsequent pilot study with intravitreal injection of a higher dose of DT (7 ng in saline), suggested that vascular changes may be occurring in iDTR; M-Cre (Figure 24). There are ongoing efforts to establish a long-term mouse model of mural cell death.

The M-Cre promoter drives expression of iDTR in mural cells, including both SMCs and pericytes. However, total ablation of mural cells is not observed and this was likely due to the mosaic effect of the M-Cre promoter. While this could be seen as a limitation of the model, it also has advantages, because it better approximates the time course of pericyte loss in DR, where mural cells are not lost simultaneously but rather die over the course of many years.

Models of pericyte deficit

Pericyte loss is an early pathological finding in DR and is temporally correlated with a number of other features of DR microangiopathy (Cogan 1967). PDGF-B and PDGFRβ null mice have been shown to have pericyte and/or SMC loss and develop microangiopathies associated with DR. However, as these models are generated by germ line deletions, they can only reveal the role of the mural cell in vascular development, rather than in pathology. Accordingly, approximately 25% of the PDGF-B mutants mice are embryonic lethal while a majority (~75%) die perinatally (Leveen 1994). Similarly, PDGFRβ -/- mice lack pericytes and SMC, are perinatal lethal, and display purpura, anemia, microaneurysms and thrombocytopenia (Soriano 1994).

During vessel maturation, pericytes associate with ECs, leading to the deposition of BM and inhibition of migration and proliferation in both cell types (Orlidge and D'Amore 1987; Sato and Rifkin 1989; Stratman 2009 and 2010). However, the role of pericytes in vascular stability in adult vessels has not been fully elucidated. Relevant mechanisms may include pericyte regulation of EC-gene expression including regulation of matrix metalloproteinases (MMPs). For example, changes in BBB-specific gene expression were reported in PDGF-B mutant adult mice ($Pdgfb^{\mathrm{Ret/Ret}}$ and $\mathrm{R26P}^{+/0}$) with pericyte deficiency, indicating a role for vessel stability EC-gene expression regulation by pericytes (Armulik 2010). Pericyte-derived tissue inhibitor of metalloproteinases (TIMP) -3, a known regulator of vascular stability, has been shown to block MMP-1 and -10 activity in EC-pericyte co-cultures (Saunders 2006). Thus, spatial and temporal regulation of EC-pericyte interactions is necessary for vascular stability.

Effects of diabetes on pericytes

Pericyte loss has long been associated with DR (Kuwabara and Cogan 1963). The association of hyperglycemia with pericyte loss has been most closely studied in animal models (galactosemia), which have been characterized by initial loss of pericytes followed by subsequent vascular damage, including microangiopathies observed in DR (Kern and Engerman 1996; Mizutani 1996). In vitro studies have shown that high glucose leads to pericyte apoptosis (Kowluru 2010; Geraldes 2013). In addition, pericyte apoptosis is not protected when BRPs are cultured in high glucose and returned to normal glucose environment (Kowluru 2010; Geraldes 2013). However, the mechanism by which pericyte loss occurs in the retina has not fully been elucidated.

A recent study implicates the protein kinase C (PKC) pathway in pericyte loss in high glucose environments. Pericyte loss is associated with PKCδ upregulation in hyperglycemic conditions in vitro, using BRPs cultured in high glucose, and in vivo, using STZ-induced diabetic mice (Geraldes 2013). Interestingly, diabetic PKCδ null mice (*Prkcd*$^{-/-}$) do not develop pericyte loss or subsequent microangiopathies associated with DR such as acellular capillaries and retinal permeability (Geraldes 2013). Thus, PKCδ plays an important and specific role in pericyte loss under hyperglycemic conditions such as those found in DR.

Increased levels of VEGF appear to play a role in permeability changes associated with DR, as anti-VEGF therapy has been shown to reduce macular edema and is currently approved by the FDA for its treatment (Massin 2010). Our laboratory has previously demonstrated the production of VEGF by a subset of retinal pericytes (Darland 2003). It is interesting to speculate that the observed increase in microvascular permeability in background DR may be due to glucose-induced increase in pericyte secretion of VEGF.

Models of DR

Some aspects of DR have been documented to develop in various mouse models of diabetes. Microaneurysms have been demonstrated in the retinas of mice fed high galactose for 21-months (galactosemia) (Kern 1996) and Akimba ($Ins2^{Akita}$ $VEGF^{+/-}$) mice displayed retinal microaneurysms as early as eight-weeks of age (Rakoczy 2010). However, both the galactosemia and Akimba mice are hyperglycemic making it impossible to identify the cause of the retinal microaneurysms. Saccular microaneurysms were clearly identified in the retina five days after the administration of DT in the model of inducible mural cell death, indicating that pericyte loss leads to the development of microaneurysms (Figure 13). The association of pericytes with ECs inhibits EC migration and proliferation (Olridge and D'Amore 1987; Antonelli-Olridge 1987; Sato and Rifkin 1989; Hirischi 1999). When pericytes are lost, as demonstrated in the model of inducible mural cell loss, ECs are no longer suppressed and are able to migrate and proliferate (Kuwarabara and Cogan 1963; Crocker 1970), leading to changes in BM composition and local dilation of the vessel, which forms microaneurysms.

Loss of pericytes also precedes the appearance of acellular capillaries in human DR (Cogan 1961; Engerman 1987) as well as in many mouse models of diabetes (STZ, galactosemia, db/db, $Ins2^{Akita}$) (Kern 1996; Barber 2005; Rakovcy 2010; Midena 1989; Schlingemann 1990; Ozerdem 2001). In iDTR; M-Cre mice treated with DT, long stretches of capillaries lacking pericytes and ECs were observed, whereas acellular capillaries were rarely noted in control mice (Figures 17 & 18). This observation supports the concept that mural cell loss leads to the formation of acellular capillaries. Pericyte-EC interactions are tightly regulated. Previous work in the D'Amore lab has shown that pericyte-derived VEGF is necessary for EC survival (Darland 2003). Taken together, this evidence suggests that loss of pericytes leads to localized EC death. When pericytes, and subsequently ECs, are lost in a sequential manner along a capillary, acellular capillaries develop.

Although macular edema is a common and vision-threatening complication of diabetes, its pathobiology remains unclear (Antonetti 2012). Ins2^{Akita} mice displayed increased vascular permeability after 12-weeks of hyperglycemia (Barber 2005) and the Akimba (Ins2^{Akita}VEGF$^{+/-}$) mice exhibited vascular leakage between eight and 16-weeks of age (Rakoczy 2010). I detected increased vascular permeability as evidenced by the leakage of fluorescein-dextran five days after DT treatment, indicating that pericyte loss leads to breakdown of the BRB (Figure 14). Loss of pericytes results in changes in EC phenotype, including loss of tight junction proteins, which results in EC migration and proliferation. In addition, pericyte loss can lead to EC death due to the lack of pericyte-derived VEGF (Darland 2003). Pericyte loss may also lead to changes in the BM composition, leading to increased permeability. These changes indicate that pericytes are necessary for maintaining the BRB.

In addition, vessel tortuosity was observed in iDTR; M-Cre mice treated with DT and was not only temporally but spatially associated with the absence of mural cells (Supplemental Figure 2, arrowheads). The Akimba mouse is the only diabetic mouse model for which retinal vessel tortuosity has been reported (Rakoczy 2010). While my results indicate that vessel tortuosity is due to mural cell loss, how the absence of pericytes leads to this phenotype is not obvious. The tortuosity may result from stretching and releasing motion of the vessels or a collapsing of the vessel. It may also be due to increased EC proliferation that would be expected to occur with pericyte loss. This model of inducible mural cell loss should be a helpful tool in elucidating the mechanism of this vessel abnormality.

The inducible model of mural cell loss that I have established displays a number of features that are characteristic of early stage or non-proliferative DR. Despite the severity of the phenotype (Figures 10-14), the burden of pericyte loss underlying microangiopathy in this model was relatively low (7-15%, Figure 16A).

Algorithm development and importance

Retinal pericyte and EC have been quantified in human retinal vasculature, as well as in several animal models using trypsin digests (Speiser 1968; Laver 1993; Kern and Engerman 1996; Hammes 1997; Zhang 2012). However, due to the difficulty of distinguishing between these two cell types in mice, retinal pericyte and EC counts have not been achieved in mouse models of DR. Since the model presented here depends on genetic manipulation, it was imperative that I develop a means to reliably quantify the individual vascular cells in the mouse retina. Therefore, working with Wimasis Imaging Analysis, I established an automated technique to quantify pericytes and ECs in elastase digests of mouse retinal vasculature (see Chapter 6).

Pericyte and EC were identified by size and morphology using an algorithm that employs aspect ratios and eccentricities. It has been shown that EC align in the direction of blood flow (Tkachenko 2013) and this feature leads to elongated nuclei so that ECs have a larger aspect ratio. On the other hand, pericytes are more round in shape than ECs, allowing eccentricity to be used to distinguish pericytes from ECs. Additional criteria were also incorporated to prevent false positives. For example, nuclei were excluded from the analysis if they were partially cut from view, overlapping with other nuclei, or on a vessel larger than a capillary (Figure 25).

Using these criteria, I created an automated methodology for quantifying pericytes and ECs in digests of the mouse retinal microvasculature. The algorithm, Wim_EC_Perycite_Count_Beta_1.02, is now available through Wimasis Imaging Analysis for other scientists to use in their analysis of mouse retinal microvasculature. In this regard it would be of interest to the field to know the pericyte:EC ratios in other models of that display pericyte loss such as PDGF-B and PDGFRβ null mice as well as diabetic mice, including as STZ-induced diabetes, db/db mice, and galactosemic mice.

In the discussion of DR, there is no specific definition of what constitutes an acellular capillary. Yet, in order to quantify acellular capillaries as an endpoint it is necessary to have specific criteria. I therefore partnered with Wimasis Imaging Analysis to develop an automated technique for classifying capillaries as acellular (see Chapter 6). We decided it was important to identify a minimum length of capillary that was cell free, but we needed to first ascertain the mean internuclei distance along the retinal capillaries in wild type mice. In the first iteration of the algorithm capillaries were considered to be acellular if they lacked nuclei along a length greater than two standard deviations above the mean internuclei distance. However, when this algorithm was tested, it was found to created a high number of false positives. I therefore conducted manual analysis and then iteratively used that data to create a model that accurately recognizes acellular capillaries. Additional parameters including a minimum width of one-fourth of a normal capillary and excluding vessels larger than capillaries were also applied to avoid false positives. The resulting algorithm, Wim_Acellular_Capillaries_Beta_1.03, is accessible for other labs to use in their analysis of acellular capillaries in mice. Again, this tool should be useful to quantify changes in other reported models of background DR, which to date have largely been reported in a qualitative fashion.

Current treatments of DR

The only way to prevent or delay the development of DR is hyperglycemic control. It is extremely challenging for diabetics to maintain normal glycemic ranges and often requires the use of many drug combinations, insulin injections, and/or a strict diet. When faced with the task of maintaining normoglycemia, diabetic patients often straddle the line between normal and either hyper- or hypo-glycemic blood glucose levels. In a six-year study, the Diabetes Control and Complications Trial Research Group tested the effects of intensive glucose control (three or more daily insulin injections with dosage based on blood glucose measurements made at least four times per day) versus conventional therapy (one or two daily insulin injections with self-monitoring of blood glucose daily) on DR progression in type I diabetics (The Diabetes Control and Complications Trial Research Group 1993). In patients with no signs of retinopathy at the start of the study, there was a 76% reduced risk of DR development in the intensive blood glucose control cohort (The Diabetes Control and Complications Trial Research Group 1993). In addition, patients with early DR in the intensive blood glucose control cohort had a 54% decreased risk of further DR development (The Diabetes Control and Complications Trial Research Group 1993).

Current therapies for PDR include pan-retinal photocoagulation (PRP), surgical removal of the vascular outgrowths, and more recently, anti-VEGF therapy (Jardeleza 2009; Newman 2010; Tonello 2008). PRP, the current gold standard for the treatment of PDR, involves the placement of laser burns throughout the retina. This treatment has been shown to reproducibly lead to the regression of new vessels, thereby reducing the risk of central vision loss (Tonello 2008). Interestingly, the mechanism whereby PRP controls the neovascularization is not understood. There is speculation that by destroying highly metabolic neural retinal tissue the need for oxygen is reduced, thus reducing the expression of hypoxia-induced VEGF. It has also been suggested that the laser injury thins the retina, allowing more diffusion from the underlying choriocapillaris. However, in the process of saving the patient’s central vision, PRP often causes loss of peripheral vision (Tonello 2008). Since anti-VEGF therapy is the only FDA-approved treatment of macular edema, which may appear at any stage of the disease, it is rarely used off-label in PDR as a surgical adjuvant because it has been shown to trigger retinal detachment (Massin 2010; Sohn 2012).

Nearly all of the current treatments of DR are focused on the late-stage of DR, PDR, when the disease has already progressed and may already be vision-threatening. Despite some progress in the treatment of DR, the understanding of the molecular and cellular mechanisms underlying the development of DR remains incomplete. Thus, it is essential that new therapeutics be developed to treat early stage or non-proliferative DR before the disease has advanced to vision loss.

Therapeutic potential

To identify more effective therapies, and perhaps more importantly preventative interventions, it is essential to identify molecular and cellular targets that initiate the cascade of events leading to DR. This model has allowed me to directly examine the role of pericyte loss in the development of diabetic microangiopathy and highlights the role of pericytes in instigating DR pathology in the retinal microvasculature. My results indicate that pericyte protection, rescue, or replacement may be a viable therapeutic target.

The mouse model of inducible mural cell loss could be used to pursue therapeutic treatment to rescue pericyte coverage in the adult. For example, intravitreal injection of pericyte recruiting proteins such as PDGF-B in the inducible model of mural cell loss may lead to restoration of pericytes. In a similar vein, new therapeutics that aim to recruit pericytes in patients with early DR could be tested in the inducible model of mural cell loss either acutely or long term to determine if they have pericyte restoring capabilities. Because the model of inducible mural cell loss can have dramatic effects acutely, this model could save a considerable amount of time in drug discovery compared to other models of DR, which require several months to a year to develop microangiopathies.

In addition, the inducible model of mural cell loss could be used to examine the viability of cell replacement therapy. For example, it has been demonstrated that intravitreal injection of healthy human endothelial progenitor cells ($CD34^+$ EPCs) are able to incorporate into the vasculature of diabetic mice (Caballaro 2007). Further, EPCs have been used in a number of clinical trials and have promising results in ischemic patients who display with improved perfusion following EPC administration (Tongers 2010). In addition, MSCs have been used as a multi-faceted approach to cell replacement therapy in diabetes aiming to improve cardiomyopathy, nephropathy, polyneuryopathy, and wound healing (Volarevic 2011). Thus, MSCs or progenitor cells differentiated into pericytes may provide a worthwhile mechanism for approaching cell replacement as a potential therapeutic in DR.

Future Directions

Limited by the effects of systemic mural cell loss, the version of the mouse model of inducible (IP) mural cell loss reported here allows for acute examination of the effects of pericyte loss on the retinal microvasculature (see Chapter 2). To determine the consequences of pericyte loss on vascular stability over time and to what extent late-stage DR might be observed, it would be interesting to analyze a long-term model of pericyte cell loss. In the work presented in this thesis, I completed an initial study to develop a longer-term model of mural cell loss. In these preliminary studies iDTR; M-Cre mice locally treated with DT were not observed to have mural cell loss.

I suspect that higher doses of DT than those used in the pilot study will be necessary to induce mural cell death via local administration. Although it is certainly possible that the DT administered intravitreally is not accessible to the pericytes, the fact that the pericytes are on the outside of the retinal capillaries and not shielded by the BRB reduce this possibility. Further, the success of intravitreal anti-VEGF therapies (ranging from 48-149 kDa), which is also presumably outside of the vasculature makes this less likely (Keane 2012).

If after reasonable efforts we find that intravitreal DT administration is not effective, another option would be to drive Cre expression with a promoter that is not expressed by nonvascular (visceral) muscle cell. Mice expressing Cre under the control of smooth muscle protein 22-alpha (SM22α) promoter, which is specific for vascular SMCs, could be crossed with the iDTR mice to create a model that can be systemically induced and would allow for long-term studies of mural cell death. It has been shown that systemic induction in iDTR; SM22α-Cre mice causes a 50-70% loss of vascular SMCs (Clarke 2006), but does not lead to lethality. Importantly, it has been reported that iDTR; SM22α-Cre mice maintain normal cellularity in their small intestine and bladder SMCs (Clarke 2006).

This model of inducible mural cell loss would allow examination of long-term effects of pericyte loss including effect on EC gene expression. Although gene expression studies could also be conducted in the model of acute pericyte loss that I have characterized in this thesis, the relatively low level of pericyte loss may lead to reduced signal (e.g. only a small percentage of the vasculature is effected). In contrast, loss of more pericytes in a longer-term model might be expected to affect more of the vasculature and make such array analysis more likely to succeed.

In addition, aorta-derived SMCs from untreated iDTR; M-Cre mice cocultured with ECs would provide an inducible in vitro system to study the consequence of pericyte loss on

EC gene expression patterns. In DR, there is EC dysfunction in response to hyperglycemic condition, which coincides with pericyte loss. Since the model of inducible mural cell loss is not hyperglycemic, it could be used to investigate the role of pericyte loss in EC dysfunction. Based on the tightly regulated cell-cell interactions between pericytes and ECs, I predict changes in genes regulating EC proliferation and migration as well as metabolic and barrier functions. Further, the capillary BM dramatically thickens in diabetes, potentially creating a barrier between pericytes and ECs. Some signaling pathways such as Notch, which requires direct cell-cell contact between pericytes and ECs, will be compromised. The model of inducible mural cell loss could be a valuable tool to dissect the various signaling pathways involved in normal EC-pericyte interactions.

Similarly, gene expression patterns could be examined in surrounding cells that are involved in vascular function, such as Müller cells and astrocytes, to determine the impact of pericyte loss on these cell types. Whereas it has been well established that astrocyte-EC interactions are important for BBB function (Goldstein 1988; Abbott 2006), it is unclear if there are similarly important interactions between glial cells and pericytes. Thus, the model of inducible mural cell loss could reveal whether a role exists for glial cell-pericyte interactions in BRB maintenance and vascular integrity.

The model of inducible mural cell loss develops hallmark characteristics of DR including microaneurysms and acellular capillaries, which are similar to the phenotypes (pericyte loss and acellular capillaries) observed in the STZ-induced diabetic model. Glial cells have been shown to be involved in DR. For example, following STZ-induction of diabetes, astrocyte gap junction proteins (connexin-26 and -43) are reduced in the adult retina resulting in significant astrocyte loss (Ly 2011). STZ-induced diabetes also leads to Müller cell activation in the adult retina (Ly 2011). While currently there are no data suggesting a link between pericyte loss and the changes in glial cell found in DR, using the model of inducible mural cell loss may give insight into these interactions.

While my studies have investigated the direct role of pericytes in microvascular stability in the absence of a diabetic milieu, there is potential to cross the iDTR; M-Cre mice with a diabetic mouse such as Akita or Akimba to determine if a more severe phenotype develops. Since the Akita and Akimba mice do not exhibit pericyte dropout, the loss of pericytes on a hyperglycemic background might be expected to lead to more dramatic phenotype, perhaps even mimicking late stage or proliferative DR. Alternatively, iDTR; M-Cre mice could be fed a high galactose diet with the aim of creating a more intense phenotype over a longer time course. While galactosemic mice do develop pericyte loss, this phenotype is only observed after a long time frame (many months).

In addition to providing a model for investigating the pathogenesis of DR, the inducible mural cell loss model may be useful as a tool to study other small vessel diseases marked by pericyte loss such as CADASIL (cerebral autosomal-dominant arteriopathy with subcortical infarcts and leukoencephalopathy), Alzheimer's disease (AD), and multiple sclerosis (MS). Associated with NOTCH3 mutations, CADASIL is a neurodegenerative disease characterized by ischemic stroke and loss of vascular SMCs and pericytes (Arboleda-Velasques 2008; Dziewulska 2012). A neurological disorder, AD is associated with amyloid β-peptide accumulation, tau pathology, BBB breakdown, neuronal loss and more recently, pericyte loss. Although the role of pericyte loss in AD is unclear, it is thought to be associated with the breakdown of the BBB (Zlokovic 2008). MS, an autoimmune disease affecting the CNS, has a range of symptoms including visual disturbances, coordination and balance issues, and permanent neurological complications (Zlokoviac 2008). In MS, ECs and pericytes express vascular cell adhesion molecule-1 (VCAM-1) and display T-cell adherence, suggesting a role for both cell types in the disease progression (Verbeek 1995). Since the role of pericyte loss in CADASIL, AD, and MS is unclear, the mural cell dropout model may serve as a unique and powerful tool to study their role in these pathologies.

Concluding remarks

Whereas pericyte-EC ratios in the retinal microvasculature of humans and animal models have been well studied, it has not been possible to conduct such analysis in mice due to the challenging nature of distinguishing the two cell types. In this work, I implemented a new technique to automate analysis of pericyte and EC quantification in mice. In addition, the criteria for classifying acellular capillaries have been ambiguous. Through the work in this thesis, I created a method to standardize acellular capillary quantification. Taken together, this work opens the door to continued understanding of the mechanism initiating the cascade of events leading to DR and a potential therapeutic for treating DR.

Since the early 1960’s, when Cogan, Toussaint, and Kuwabara observed that microaneurysms formed in diabetic patients were associated with pericyte loss (Kuwabara and Cogan 1963), it has been widely accepted that pericyte loss precedes microangiopathies and generally assumed that loss of pericytes trigger these events.

However, it has not been possible to demonstrate a direct causal role for pericyte loss in these pathologies. Using the mouse model of inducible mural cell loss, I characterized retinal vascular changes in the adult caused by pericyte loss including microaneurysms, acellular capillaries, and leakage. The work presented here demonstrates the direct role of pericytes in vascular stability and provides critical evidence to suggest pericytes as a potential therapeutic target.

CHAPTER 5

MATERIALS AND METHODS

MATERIALS AND METHODS

Mice

iDTR; M-Cre (experimental) and M-Cre (control) mice were generated by breeding Cre-inducible diphtheria toxin receptor (iDTR) transgenic mice (Buch 2005) with mice expressing tamoxifen-inducible Cre under the control of the smooth muscle myosin heavy chain promoter (SMMHC, M-Cre) (Indra 1999; Wirth 2008) (Stock numbers: 007900, 019079, Jackson Laboratory, Bar Harbor, ME). Both experimental and control mice (8-weeks old) were injected intraperitoneally (IP) daily for three days with tamoxifen (500 ng in 225 μl corn oil, Sigma-Aldrich, St. Louis, MO). Eight to 10 weeks after tamoxifen administration, mice were injected IP with diphtheria toxin (DT; 500 ng in 100 μl saline, Sigma-Aldrich) daily for two days. The corn oil used to dissolve tamoxifen was completely absorbed and did not interfere with the bioavailability of DT. As a negative control, some iDTR; M-Cre mice did not receive DT. Mice were euthanized for analysis five days after the first DT injection. Littermates were used for comparative analysis throughout. All animal protocols were approved by the Schepens Eye Research Institutional Animal Care and Use Committee.

Isolation and tamoxifen treatment of aorta-derived smooth muscle cells (SMCs)

Aorta-derived SMCs were collected as previously described (Rong 2003). Briefly, aortas collected from iDTR; M-Cre mice were digested for 10 minutes at 37°C using collagenase II (175 units/ml, Worthington Biochemical, Lakewood, NJ) and dissected to remove the tunica adventitia layer. The length of the aorta was cut and ECs were manually removed using a polyvinyl acetal surgical eye spear (Braintree Scientific Inc., Braintree, MA). The intact aorta tunica media layer was then cultured overnight in 10% FBS in Dulbecco's minimal essential medium (DMEM). The following day, a mixture of collagenase II (175 units/ml, Worthington Biochemical) and elastase type I (0.5 mg/ml, Sigma-Aldrich) was added and incubated at 37°C for 1 hour and 15 minutes to create a single cell suspension of aorta-derived SMCs. Aorta-derived SMCs were grown in 20% FBS DMEM for 48 hr and then maintained in 10%FBS DMEM. Cultured iDTR; M-Cre aorta-derived SMCs were treated with vehicle (ethanol) or tamoxifen (1 µM in ethanol) for 48 hours in 10% FBS DMEM.

RNA isolation and reverse transcription-PCR

Total RNA was isolated from mouse tissues using phenol-chloroform extraction (TRIzol, Life Technologies, Grand Island, NY) and from aorta-derived SMCs using an RNeasy kit (Qiagen, Valencia, CA). Reverse transcription was performed using iSCRIPT (BioRad, Hercules, CA). The primers used included:

Mouse *Hprt1*:

F- TCAGTCAACGGGGGACATAAA; R- GGGGCTGTACTGCTTAACCAG

Simian HB-EGF (DTR):

F- GCAGATCTGGACCTTTTGAGA; R- CCCGGAGCTCCTTCACATATT

qPCR was performed on a LightCycler 480II (Roche Diagnostics, Indianapolis, IN) using SYBR Green PCR Master Mix (Life Technologies). To calculate the fold-change using the standard 2-ΔΔCt formula, a Ct value of 35, corresponding to the lowest limit for detection, was used when signal was not detected for simian HB-EGF.

Biochemical measurements

Blood was drawn from mice by submandibular bleeding using a sterile splinter out (MEDIpoint, Mineola, NY) prior to treatment (eight weeks old), post-tamoxifen treatment (16 weeks old), and post-DT treatment (16 weeks plus five days old). Blood glucose was measured using an ACCU-CHEK Compact Plus Glucometer (Roche Diagnostics). Blood plasma was collected post-mortem from M-Cre (+DT), iDTR; M-Cre (-DT), and iDTR; M-Cre (+DT) mice and plasma insulin was measured by ELISA (ALPCO Diagnostics, Salem, NH).

Immunostaining

Flat-mounted retinas were permeabilized by incubation for 12 hr in PBlec (PBS minus salts, 0.1 mM $CaCl_2$, 0.1 mM $MgCl_2$, 0.1 mM $MnCl_2$) with 0.1% sodium citrate, 0.1% BSA, and 1% Triton-100X. Following permeabilization, retinas were washed with PBS and incubated overnight at 4°C with either *Griffonia simplicifolia* isolectin-B_4 conjugated to Alexa Fluor 488 (1:100, I21411, Life Technologies) to detect ECs, or with mAb anti-smooth muscle actin conjugated to FITC (1:100, F3777, Sigma-Aldrich) to detect pericytes and SMCs. The retinas were visualized using an Axioskop 2 Mot Plus microscope (Zeiss, used for imaging throughout unless noted). These images were used to assess the presence of microvascular abnormalities including microaneurysms.

TUNEL assay

Following overnight immunostaining as described above, retinas were washed with PBS, fixed for 10 minutes at room temperature with 4% paraformaldehyde, and washed again with PBS. TUNEL (Terminal deoxynucleotidyl transferase dUTP nick end labeling) was carried out using the In Situ Cell Death Detection TMR red kit (1215672910, Roche Diagnostics), following the manufacturer's guidelines. As positive and negative controls for each experiment, retinas from C57BL/6 mice were treated with DNase prior to TUNEL staining or were stained with only the TUNEL label solution without the terminal transferase, respectively. The retinas were then flat-mounted and TUNEL positive cells were visualized using fluorescence microscopy. The number of TUNEL positive cells per mouse retina was quantified in images that included every visible vessel in the retina.

Elastase digests

Eyes were fixed in 10% formalin for three days at 4ºC. Retinas were dissected from eyes and incubated in 0.15 M glycine in PBS overnight at 4ºC to remove excess formalin. The retinal vasculatures were then isolated using elastase digestion as described (Laver 1993; Zhang 2012). Briefly, retinas were incubated in elastase (324682, EMD Millipore, Billerica, MA) (40 unit/ml elastase in 100 mM sodium phosphate buffer, pH 6.5, containing 150 mM sodium chloride and 5 mM EDTA) for 1.5-2 hours at 37ºC. Retinas were placed in a petri dish filled with sterile filtered autoclaved H_2O and the vessels were cleaned by gently removing the neural retina using rat whisker brushes. Next, isolated vessels were mounted to a Superfrost Plus microscope slide (12-550-15, Fisher Scientific, Pittsburg, PA), dried overnight at room temperature, then stained with periodic acid-Schiff (PAS; Sigma-Aldrich) and counterstained with hematoxylin (Sigma-Aldrich). Elastase digests were imaged by light microscopy.

Morphometry

Isolated retinal networks were analyzed to determine the number of pericytes, ECs, and acellular capillaries. The total number of pericytes and ECs in 15 images and acellular capillaries in 10 images were quantified (magnification 700x). Fields examined were selected randomly (Supplemental Figure 4), excluding areas near the optic nerve and near the external border, and were analyzed using quantitative image analysis automation (Wimasis Imaging Analysis, Germany; described in detail in Chapter 6). ECs and pericytes were classified based on size and morphology using previously described morphological characteristics (Kuwabara and Cogan 1960; Cogan 1963; Speiser 1968). Acellular capillaries were defined as being a minimum of one-fourth the width of a normal capillary (Kern and Engerman 1993; Barber 2005) and displaying a nucleus-free length that was greater than the average internuclei distance calculated as 4(average + 2*standard deviation).

Fluorescein dextran perfusion

Mice were perfused with fluorescein dextran as previously described (Saint-Geinez 2008). Briefly, mice were deeply anesthetized using a mixture of ketamine (120 mg/kg IP) and xylazine (20 mg/kg IP) and perfused with 50 mg/ml fluorescein dextran ($2x10^6$ mw, FD2000S, Sigma-Aldrich) in 4% paraformaldehyde in PBS. Eyes were then collected and fixed overnight in 4% paraformaldehyde at 4ºC prior to whole mount preparation. Fluorescein dextran perfused whole retinal flat mounts were visualized using a Nikon Eclipse E800 (Nikon Corporation, Brighton, MI).

Intravitreal DT injections

Mice were anesthetized with a ketamine (120 mg/kg) and xylazine (20 mg/kg) mixture. One drop of 1% tropicamide (Bausch + Lomb, Rochester, NY) followed by one drop of 1% cyclopentolate hydrochloride (Altair Pharmaceuticals Inc., Aquebogue, NY) was applied to the cornea to dilate the pupils. GenTeal (Alcon Research Ltd., Sinking Spring, PA), an ocular lubricant, was applied as needed to keep eyes moist. Using a microsurgical microscope, a small incision was made behind the sclera near the cornea at the upper nasal limbus using the tip of a sharp 30-gauge needle. DT (0 fg, 35 fg, 350 fg, or 7 ng in saline) was injected into the vitreous using a 5 μl microinjection syringe with a 32G blunt end removable needle (87931, Hamilton Company, Reno, NV). Following intravitreal injection, eyes were treated with a triple antibiotic (Neo/Poly/Bac) Puralube ointment (Fera Pharmaceuticals, Locust Valley, NY).

Fundus photography

Mice were anesthetized with a mixture of ketamine (120 mg/kg) and xylazine (20 mg/kg). Pupils were dilated using one drop of 1% tropicamide (Bausch + Lomb) followed by one drop of 1% cyclopentolate hydrochloride (Altair Pharmaceuticals Inc.) applied to the cornea. Eyes were kept moist by applying the ocular lubricant Genteal (Alcon Research Ltd.) as needed. Both eyes were imaged using fundus photography (Micron III, Phoenix Research Labs, Pleasanton, CA).

Fluorescein angiography

Prior to fluorescein angiography (FA), mice were imaged using fundus photography as described above. Mice were then IP injected with 25% fluorescein sodium in saline (60 mg/kg mouse, NDC 46387-101-02, Alliance Inj LLC, El Paso, TX). Photographs using the Micron III (Phoenix Research Labs) were taken in the right eye of each mouse at regular time intervals (from 1 minute to 4 minutes post-IP injection).

CHAPTER 6

MATERIALS AND METHODS: DEVELOPING AUTOMATED IMAGE ANALYSIS TECHNIQUES

MATERIALS AND METHODS

Introduction

In 1960, Kuwabara and Cogan first described a technique, called trypsin digest, for isolating the retinal vasculature (Kuwabara and Cogan 1960). According to Kuwabara and Cogan, the ECs were described as, "…large, ellipsoid nuclei lying within the wall and oriented along the axis of the capillaries and small vessels, but oriented circumferentially in the arteries and veins" (Kuwabara and Cogan 1960). The pericytes were defined as, "…smaller, darker, and usually round nuclei situated on the outer portions of the wall" (Kuwabara and Cogan 1960). Later, it was noted that pericytes often protrude from the vessel wall (Cogan 1963). Since their discovery, trypsin digests have been instrumental in understanding morphological differences in retinal microvasculature between normal and pathologic situations.

Through the use of trypsin digests, it has been possible to quantify the presence of ECs, pericytes, ghost pericytes, microaneurysms, and acellular capillaries. Subsequently, an investigation by Speiser in 1968 demonstrated a dramatic change in the ratio of ECs to pericytes in the retina of normal (1:1) versus diabetic (4:1) patients (Speiser 1968). Similarly, trypsin digests have been studied to demonstrate the similarities between animal models and human disease. For example, an alteration in EC/pericyte ratio was observed in the retina of dog models (diabetic dogs (10:1) and galactosemia dogs (6.4:1)) compared to normal dogs (3.5:1) (Speiser 1968; Laver 1993; Kern and Engerman 1996; Hammes 1997; Zhang 2012). Thus, quantitative analyses of trypsin digests allow comparison among normal and diseased groups.

In 1993, Laver et al found that trypsin was not the active ingredient that digests away the neural retina (Laver 1993). Instead, their study exposed that elastase, a contaminant found in trypsin (215240, Difco, BD, Franklin Lakes, NJ), is the actual cause of digestion of the retinal neural tissue (Laver 1993). The use of elastase, rather than trypsin, has only recently begun to be introduced in the literature (Zhang 2012). Of note, the studies in this work were performed using elastase digests.

Automated image analysis for pericyte and EC quantification

Rationale

Quantification of pericytes and ECs using trypsin digests of retinal microvasculature has been well established in humans, dogs, and rats, but not for mice (Speiser 1968; Laver 1993; Kern and Engerman 1996; Hammes 1997; Zhang 2012). In a mouse model of DR, Tim Kern, a respected authority in animal models of diabetic retinopathy, stated, "Endothelial cell nuclei and pericyte nuclei were counted differentially in the midretina until approximately 1200 capillary cells per retina were counted; however, differentiation between these cell types was difficult, making the endothelial-pericyte ratio unreliable" (Kern and Engerman 1993). I therefore sought to establish an automated technique to quantify pericytes and ECs in mice.

Algorithm Development

Identification of pericytes and ECs in the automated system was based on size and morphology. Pericytes were defined as having nuclei round in shape most often found at vessel bifurcations or protruding from the vessels (blue, Figure 26B). ECs were defined as having elongated oval-shaped nuclei (green, Figure 26B). The roundness of the object or eccentricity was set between zero and one, where zero is a circle and one is a straight line. Eccentricity was used to differentiate ECs from pericytes since the latter are rounder. In the first version of the algorithm, 0.745 was used as a threshold, but this was raised to 0.860 in the final version of the algorithm. Further, the ratio between the maximum and minimum length of the object called an aspect ratio, was used in combination with eccentricity to distinguish pericytes from ECs. ECs have a bigger aspect ratio because they have elongated nuclei. The aspect ratio was initially set to 2.45, but early analyses revealed that this ratio was too high and incorrectly classified many ECs as pericytes. Thus, the aspect ratio was lowered to 1.97 to more effectively classify the two cell types. In the initial version, the algorithm underestimated the number of ECs (78%), but overestimated the number of pericytes (190%) based upon my manual analysis. The final version of the algorithm showed significant improvement indicated by detection of 116% of ECs and 93% of pericytes compared to my manual analysis. Given that manual analysis is biased and varied by individual, the degree of concordance between the final version of the algorithm and my manual analysis appeared satisfactory. The algorithm will consistently detect ECs and pericytes within the parameters set above without variation, while manual analysis will always fluctuate, especially among individuals. All the parameters discussed here were set using a classifier designed by Wimasis Imaging Analysis, which is proprietary and therefore not included.

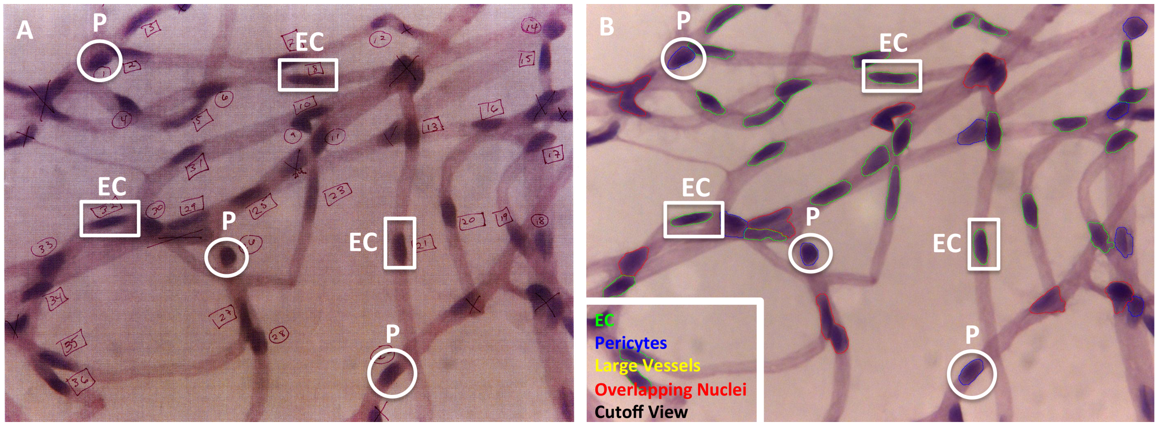

Figure 26. Automated image analysis for pericyte and EC counts.
Retinal microvasculatures were isolated by elastase digestion and stained with periodic acid-Schiff (PAS) and hematoxylin. Pericyte (P, circles) and EC (rectangles) quantification by A) manual analysis and B) automated image analysis.

Nuclei on the periphery of the image (cut off from view) were excluded, as it is not possible to determine the cell type without viewing the entire nuclei. Also excluded were nuclei that were overlapping, as it was not feasible to reliably distinguish the morphology of each individual nuclei (red, Figure 27B). As a threshold between singular nuclei and overlapping nuclei, the maximum area was set to 3100 px. Additionally, the solidity, which is the surface area of the nuclei divided by the convex hull, was set to a minimum of 85% to discard overlapping nuclei. Further, to avoid false positives, the minimum area was set to 1000 px, which prevented debris from being detected as a nucleus.

Since the analysis is focused on the retinal microvasculature, only capillary nuclei were quantified. By selectively quantifying capillaries, quantification was restricted to pericytes and SMCs were excluded from the analysis, such as nuclei of cells in large vessels (yellow, Figure 27B). Large vessels were defined according to a minimum length (750 px) and a minimum width (100 px). Nuclei with more than 50% of their surface on a large vessel were not included in the analysis. Since there are multiple vessel crossings and determination of their origin is challenging, an algorithm of minimum angle variation was applied to assign each branch to its precursor vessel. Capillary length (in mm) was also required to standardize pericyte and EC counts among the groups.

The final algorithm for automated image analysis of pericyte and EC quantification in mouse elastase digests (discussed above) was developed in collaboration with Wimasis Imaging Analysis and can be identified as, “Wim_EC_Perycite_Count_Beta_1.02.”

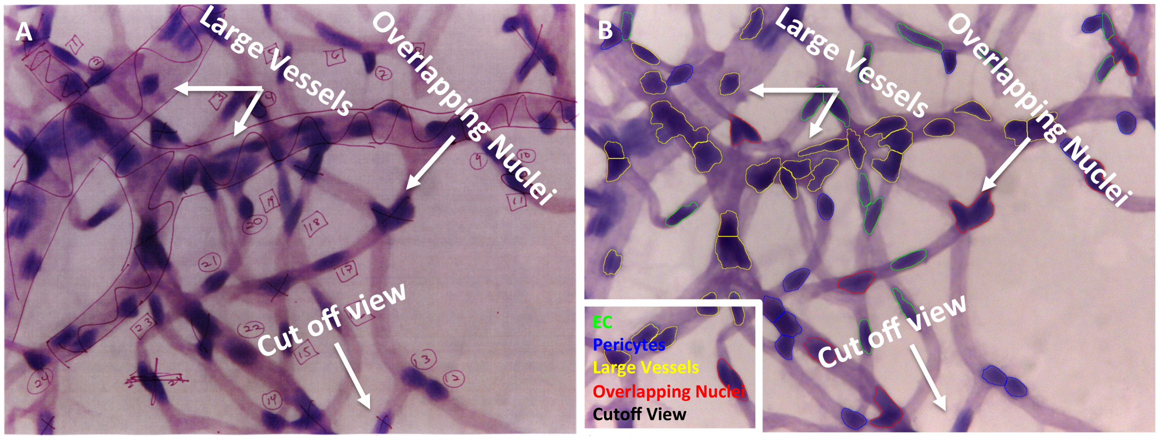

Figure 27. Automated image analysis parameters for pericyte and EC counts. Retinal vessels digested by elastase and stained with periodic acid-Schiff (PAS) and hematoxylin. A) Manual analysis showing exclusion factors for developing an algorithm to quantify pericytes and ECs. B) Automated image analysis of same image showing nuclei excluded in large vessels (yellow), in overlapping areas (red), or cut off from view.

Automated image analysis for quantification of acellular capillaries

Rationale

In a study of a DR mouse model, Tim Kern defined acellular capillaries as, "…basement membrane tubes lacking cell nuclei and maintaining at least one-fourth the normal capillary caliber over their length" (Kern and Engerman 1993). Because this definition does not specify a minimum length of vessel lacking nuclei, there currently is no standard. Therefore, I established an automated technique to quantify acellular capillaries in mice.

Algorithm Development

The specifications included in the initial algorithm framework to quantify acellular capillaries were that acellular capillaries do not have nuclei and must be a minimum of one-fourth the width of a normal capillary. Analysis using these parameters identified an excessive number of acellular capillaries in both control and experimental mice. Therefore, further criteria were included to capture and accurately represent the data.

For the second round of development, it was judged to be essential to standardize the minimum length of an acellular capillary. Thus, a capillary is considered to be acellular if it lacks nuclei along a length greater than two standard deviations above the mean internuclei distance; with internuclei distance defined as the distance between nuclei along the same capillary. Hence, prior to determining if a capillary is acellular, it is necessary to measure the internuclei distance in the retinal microvasculature using the Euclidean distance formula among the controls and iDTR; M-Cre mice (10 images per animal, n=4 animals per group) to ascertain the mean. Once the mean internuclei distance in the retinal microvasculature from the controls and iDTR; M-Cre mice was established, the standard deviation was calculated and the length of two standard deviations above the mean internuclei distance was determined. The following equation was used to identify acellular capillaries (MinInternucliDist):

$$\text{MinInternucleiDist} = \text{meanInternucleiDistance} + 2*\text{stdInternucleiDistance}$$

Using these parameters, the algorithm determined which vessels contained no nuclei in a distance equal to MinInternucleiDist. However, a new challenge arose at this stage of development. Although some capillaries clearly appeared to be acellular by visual analysis, they were misclassified as cellular by the algorithm because of the proximity of nuclei from adjacent vessels. To address this issue, Wimasis Imaging Analysis iteratively fit my manual analysis into the algorithm (Figure 28) and produced the following final equation to identify acellular capillaries:

$$\text{MinInternucleiDist} = 4*(\text{meanInternucleiDistance} + 2*\text{stdInternucleiDistance})$$

One caveat of using this algorithm for quantifying acellular capillaries is that the internuclei distance varies depending on the number of images and the genotype/phenotype of the animals used. Consequently, it was necessary to identify which animal genotype would be used for calculating the mean internuclei distance. To minimize any bias that might be introduced by using one control over the other, both of the controls and the experimental mice (iDTR; M-Cre, DT-treated M-Cre, and DT-treated iDTR; M-Cre) were used to calculate the mean internuclei distance. Using all three groups yielded the largest internuclei distance and therefore the most stringent conditions for defining acellular capillaries.

The other criteria for identification of acellular capillaries is that they be a minimum of one-fourth the width of a normal capillary. For this measurement to be conducted it was necessary to establish the width of a normal capillary. To this end, the algorithm measured the width of all capillaries with normal internuclei distance. If a capillary with an internuclei distance outside the normal range was detected, but did not meet the criteria of being at least one-fourth the width of a normal capillary, the capillary was not categorized as an acellular capillary. Vessels larger than capillaries were not considered in this analysis. For both cellular and acellular capillary lengths, the results are expressed in mm.

The final algorithm for automated image analysis of acellular capillary quantification in mouse elastase digests (discussed above) was developed in collaboration with Wimasis Imaging Analysis and can be identified as, “Wim_Acellular_Capillaries_Beta_1.03.”

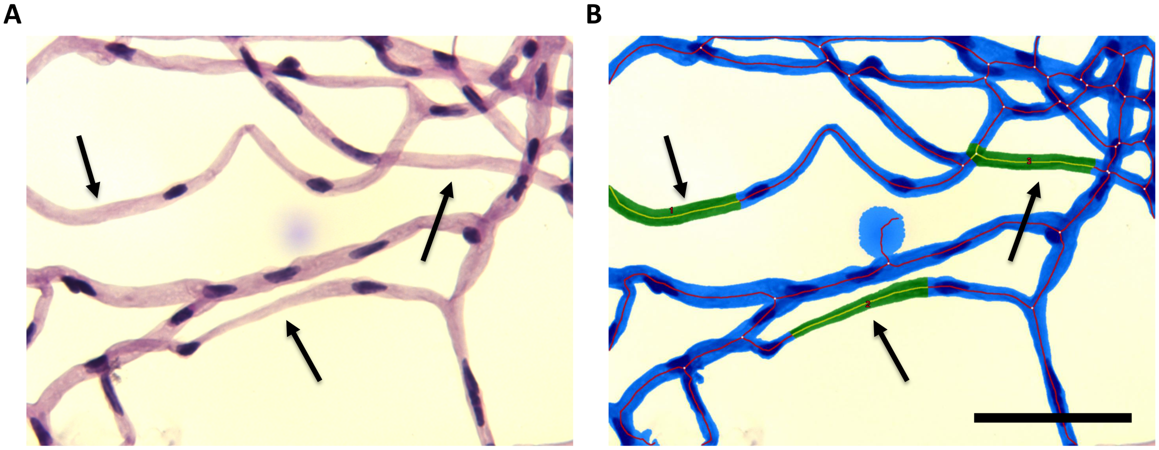

Figure 28. Automated image analysis for acellular capillary quantification.
Vessels digested from retinas using elastase and stained with periodic acid-Schiff (PAS) and hematoxylin. (A) Manual detection of acellular capillaries (black arrows). (B) For algorithm development, acellular capillaries (green, black arrows) were defined as a capillary length greater than or equal to 4(average internuclei distance + 2STD) lacking nuclei and a minimum width of one-fourth that of a regular capillary. Scale bar = 100 µm.

REFERENCES

Abbott, N.J., Ronnback, L, Hansson, E. Astrocyte-endothelial interactions at the blood-brain barrier. (2006) Nature Reviews Neuroscience. **7**, 41-53.

Adamis, A.P., Miller, J.W., Bernal, M.T., D'Amico, D.J., Folkman, J., Yeo, T.K., Yeo, K.T. Increased vascular endothelial growth factor levels in the vitreous of eyes with proliferative diabetic retinopathy. (1994) American journal of ophthalmology. **118**, 445-450.

Aiello, L.P., Avery, R.L., Arrigg, P.G., Keyt, B.A., Jampel, H.D., Shah, S.T., Pasquale, L.R., Thieme, H., Iwamoto, M.A., Park, J.E., et al. Vascular endothelial growth factor in ocular fluid of patients with diabetic retinopathy and other retinal disorders. (1994) The New England journal of medicine. **331**, 1480-1487.

American Diabetes Association. Diagnosis and Classification of Diabetes Mellitus. (2010) Diabetes Care. **33**, S62-S69.

Antonelli-Orlidge, A., Saunders, K.B., Smith, S.R., D’Amore, P.A. An activated form of transforming growth factor beta is produced by cocultures of endothelial cells and pericytes. (1989) PNAS. **86**, 4544-4548.

Antonetti, D.A., Barber, A.J., Bronson, S.K., Freeman, W.M., Gardner, T.W., Jefferson, L.S., Kester, M., Kimball, S.R., Krady, J.K., LaNoue, K.F., Norbury, C.C., Quinn, P.G., Sandirasegarane, L., Simpson, I.A. Diabetic retinopathy: seeing beyond glucose-induced microvascular disease. (2006) Diabetes. **55**, 2401-2411.

Antonetti, D.A., Klein, R., Gardner, T.W. Diabetic retinopathy. (2012) The New England journal of medicine. **366**, 1227-1239.

Arboleda-Velasquez, J.F., Zhou, Z., Shin, H.K., Louvi, A., Kim, H.H., Savitz, S.I., Liao, J.K, Salomone, S., Ayata, C., Moskowitz, M.A., Artavanis-Tsakonaas, S. Linking Notch signaling to ischemic stroke. (2008) PNAS. **105**, 4856-4861.

Armulik, A., Abramsson, A., Betsholtz, C. Endothelial/pericyte interactions. (2005) Circ Res. **97**, 512-523.

Armulik, A., Genove, G., Betsholtz, C. Pericytes: developmental, physiological, and pathological perspectives, problems, and promises. (2011) Developmental cell. **21**, 193-215.

Armulik, A., Genove, G., Mae, M., Nisancioglu, M.H., Wallgard, E., Niaudet, C., He, L., Norlin, J., Lindblom, P., Strittmatter, K., Johansson, B.R., Betsholtz, C. Pericytes regulate the blood-brain barrier. (2010) Nature. **468**, 557-561.

Ashton and Cunha-Vaz. Effect of histamine on the permeability of the ocular vessels. (1965A) Archives of Ophthalmology. **73** 211-223.

Ashton N. Bowman lecture. The blood-retinal barrier and vaso-glial relationships in retinal disease. (1965B) Trans. Ophthal. Soci. U.K. **85** 199-230

Ashton, N. and de Oliveira, F. Nomenclature of pericytes. Intramural and extramural. (1966) Brit. J. Opthal. **50**, 119-123.

Ashton, N. Retinal micro-aneurysms in the non-diabetic subject. (1951). Brit J Ophthal. **35**, 189.

Ashton, N. Studies of the retinal capillaries in relation to diabetic and other retinopathies. (1963) Brit J Ophthal. **47**, 521-538.

Avery, R.L. Regression of retinal and iris neovascularization after intravitreal bevacizumab (Avastin) treatment. (2006) Retina. **26,** 352-354.

Ballantyne, A. J. The State of the Retina in Diabetes Mellitus (1946) Trans Ophthal Soc UK **66**, 503-542

Barber, A.J., Antonetti, D.A., Kern, T.S., Reiter, C.E., Soans, R.S., Krady, J.K., Levison, S.W., Gardner, T.W., Bronson, S.K. The Ins2Akita mouse as a model of early retinal complications in diabetes. (2005) Investigative ophthalmology & visual science. **46**, 2210-2218.

Battig, CG and Low, FN. The Ultrastructure of Human Cardiac Muscle and its Associated Tissue Space. (1961) American Journal of Anatomy. **108**, 199-229.

Bell, R.D., Winkler, E.A., Sagare, A.P., Singh, I., LaRue, B., Deane, R., Zlokovic, B.V. Pericytes control key neurovascular functions and neuronal phenotype in the adult brain and during brain aging. (2010) Neuron. **68**, 409-427.

Bensley, RR. and Vimtrup, BJ. On the nature of the rouget cells of capillaries. (1928) The Anatomical Record. **39**, 37-55.

Bergers, G., Song, S. The role of pericytes in blood-vessel formation and maintenance. (2005). Neruo-Oncology. **7**, 452-464.

Bjarnegard, M., Ene, M., Norlin, J., Gustafsdottir, S., Fredriksson, S., Abramsson, A., Takemoto, M., Gustafsson,E., Fassler, R., Betsholtz, C. Endothelium-specific ablation of PDGFB leads to pericyte loss and gloerular, cardiac and placental abnormalities. (2003) Development and disease. **131**, 1847-1857.

Bondjers, C, Kalen, M, Hellstrom, M, Scheidl, SJ, Abramsson, A, Renner, O, Lindahl, P, Cho, H., Kehrl, J, and Betsholtz, C. Transcription profiling of platelet-derived growth factor-B-deficient mouse embryos identifies RGS5 as a novel marker for pericytes and vascular smooth muscle cells. (2003) American J of Pathology. **162**, 721-729.

Bryan, B. and D'Amore, PA. Pericyte isolation and use of endothelial/pericyte coculture models. (2008) Methods in Enzymology. **443**, 315-331.

Buch, T., Heppner, F.L., Tertilt, C., Heinen, T.J., Kremer, M., Wunderlich, F.T., Jung, S., Waisman, A. A Cre-inducible diphtheria toxin receptor mediates cell lineage ablation after toxin administration. (2005) Nature methods. **2,** 419-426.

Caballero, S., Sengupta, N., Afzal, A., Chang, K.H., Calzi, S.L., Guberski, D.L., Kern, T.S., Grant, M.B. Ischemic vascular damage can by repaired by healthy, but not diabetic, endothelial progenitor cells. (2007) Diabetes. **56**, 960-967.

Cade, W.T. Diabetes-related microvascular and macrovascular diseases in the physical therapy setting. (2008) Physical Therapy. **88**, 1322-1335.

Carlson, EC. Fenestrated subendothelial basement membranes in human retinal capillaries. (1989) Investigative Ophthalmology and Visual Science. **30**, 1923-1932.

Carter, RA and Wicks, IP. Vascular Cell Adhesion Molecule 1 (CD106) A Multifaceted Regulator of Joint Inflammation (2001) Arthritis and Rheumatism. **44**, 985-994.

Carvalho, R.L, Jonker, L., Goumans, M.J., Larsson, J., Bouwman, P., Karlsson, S., Dijke, P.T., Arther, H.M., Mummery, C.L. Defective paracrine signaling by TGF beta in yolk sac vasculature of endoglin mutin mice: a paradigm for hereditary haemorrrhagic telangiectasia. (2004) Development. **131**, 6237-6247.

Center for Disease Control. Diphtheria. Epidemiology and prevention of vaccine-preventable diseases. (May 2012). The Pink Book: Course Textbook.
Chang, H., Huylebroeck, D., Verschueren, K., Guo, Q., Matzuk, M.M., Zwijsen, A. Smad5 knockout mice die at mid-gestation due to multiple embryonic and extraembryonic defects. (1999) Development. **126**, 1631–1642.

Cheung, N., Mitchell, P., Wong, T.Y. Diabetic retinopathy. (2010) Lancet. **376**, 124-136.

Cho, H, Kozasa, T, Bondjers, C, Betsholtz, C, and Kehrl, JH. Pericyte-specific expression of Rgs5: implications for PDGF and EDG receptor signaling during vascularmaturation. (2003) FASEB J. **17**, 440-442.

Clark, E. R. and Clark, Eleanor L. Microscopic observations on the extra-endothelial cells of living mammalian blood vessels. (1940) Amer. J. Anat. **66**, 1-49.

Clarke, M.C.H., Figg, N., Maguire, J.J., Davenport, A.P., Goddard, M., Littlewood, T.D., Bennett, M.R., Apoptosis of vascular smooth muscle cells induces features of plaque vulnerability in atherosclerosis. (2006) Nature Medicine. **12**, 1075-1080.

Cliff, W.J. Observations on healing tissue: a combined light and electron microscopic investigation. (1963) Trans R. Soc. Lond. Ser. B. **246**, 305-325.

Cogan, D.F. Retinal Vascular Patterns. VI. Mural cells of the retinal capillaries. (1963) Arch Ophthal. **69**, 114-124.

Cogan, D.G. and Kuwabara, T. The Mural Cell in Perspective. (1967) Arch Ophthal **78**, 133-139.

Cogan, D.G. Diabetic Retinopathy. (1964) The New England journal of medicine **270**, 787-788.

Cogan, D.G., Toussaint, D., Kuwabara, T. Retinal vascular patterns. IV. Diabetic retinopathy. (1961) Archives of ophthalmology. **66**, 366-378.

Corselli, M., Chen, C.W., Crisan, M., Lazzari, L., Peault, B. Perivascular ancestors of adult multipotent stem cells. (2010) Arterioscler Thromb Vasc Biol. **30**, 1104-1109.

Crocker, D.J., Murad, T.M., Geer, J.C. Role of the pericyte in wound healing. An ultrastructural study. (1970) Experimental and molecular pathology. **13**, 51-65.

Cuevas, P., Gutierrez-Diaz, J.A., Reimers, D., Dujovny, M., Dias, F.G., Ausman, J.I. (1984). "Pericyte endothelial gap junctions in human cerebral capillaries." Anat. Embryol. **170**: 155-159.

Cunha-Vaz, J.C. The blood–retinal barriers system. Basic concepts and clinical evaluation. (2004) Exp Eye Research. **78**, 715-721.

Cunha-Vaz, J.G. and Murice, D.M. The active transport of fluorescein by the retinal vessels and the retina. (1967) J. Physiol. **191**, 467-486

Cunha-Vaz, J.G., Campos, AJ, Figo, GM. Early breakdown of the blood-retinal barrier in diabetes. (1975) Brit. J. Ophthal **59**, 649.

Cunha-Vaz, Shakib, Ashton. Studies on the permeability of the blood-retinal barrier. I. On the existence, development, and site of a blood-retinal barrier. (1966) British Journal of Ophthalmology. **50**, 441

Cunha-Vaz. Studies on the permeability of the blood-retinal barrier. III. Breakdown of the blood-retinal barrier by circulatory disturbances. A topographical study of the vascular tree. (1966) British Journal of Ophthalmology **50**, 505

Cunha-Vaz. The Blood-retinal barriers. (1976) Documenta Ophthalmologica **41**, 287-327.

Darby, I, Dkalli, O, Gabbiani, G. Alpha-smooth muscle actin is transiently expressed during experimental wound healing. (1990). Laboratory Investigation. **63**, 21-29.

Darland, D.C. and D'Amore, P.A. TGF beta is required for the formation of capillary-like structures in three-dimensional cocultures of 10T1/2 and endothelial cells. (2001) Angiogenesis. **4**, 11-20.

Davis, G.E., Senger, D.R. Extracellular matrix mediates a molecular balance between vascular morphogenesis and regression. (2008) Current opinion in hematology. **15**,197-203.

Davis, S., Aldrich, T.H., Jones, P.F., Acheson, A., Compton, D.L., Jain, V, Ryan, T.E., Bruno, J., Radziejewski, R., Maisonpierre, P.C., Yancopoulos, G.D. Isolation of angiopoietin-2, a ligand for the TIE2 receptor, by secretion-trap expression cloning. (1996) **87**, 1161-1169.

DeNofrio, D, Hoock, TC, Herman, IM. Functional sorting of actin isoforms in microvascular pericytes. (1989) J. Cell Biology. **109**, 191-202.

Diaz-Flores, L., Gutierrez, R., Madrid, JF, Varla, H, Valladares, F, Acosta, E, Martin-Vasallo, P, Diaz-Flores Jr, L. Pericytes. Morphofunction, interactions and pathology in a quiescent and activated mesenchymal cell niche. (2009) Histol Histopathol **24**, 909-969.

Dickson, M.C., Martin, J.S., Cousins, F.M., Kulkarni, A.B., Karlsson, S., Akhurst, R.J. Defective haematopoiesis and vasculogenesis in transforming growth factor-beta 1 knock out mice. (1995) Development. **121**, 1845–1854.

Dodge, A.B., Hechtman, H.B., Shepro, D. Microvascular Endothelial-derived Autacoids Regulate Pericyte Contractility. (1991) Cell Motility and the Cytoskeleton. **18**, 180-188.

Duh, E. (2008). Diabetic Retinopathy. Humana Press. Retrieved 26 February 2014, from <http://www.myilibrary.com?ID=185103>

Dziewulska, D. and Lewandowska, E. Pericytes as a new target for pathological processes in CADASIL. (2012) Neuropathology. **32**, 515-521.

Eberth, CJ. In: Handbuch der Lehre von den Geweben des Menschen und der Theire. Leipzig. (1871)

Ehrlich, P. Das Sauerstoffbedürfnis des Organismus- Eine farbenanalytische Studie, (1885) Berlin.

Ehrlich, P. Ueber die beziehungen von chemischer constitution, verteilung und pharmakologischer wirkung. (1904) Gesammelte Arbeiten zur Immunitaetsforschung, Hirschwald, Berlin. pp 574.

Elemente in der Gefisswand der Blutcnpillaren. (1922) Zeitschr. f. Anat. u. Entwickelungsg, Bd. 65, S. 150-184.

Enge, M., Bjarnegard, M., Gerhardt, H., Gustafsson, E., Kalen, M., Asker, N., Hammes, H.P., Shani, M., Fassler, R., Betsholtz, C. Endothelium-specific platelet-derived growth factor-B ablation mimics diabetic retinopathy. (2002) The EMBO journal. **21**, 4307-4316.

Engerman, R.L. Pathogenesis of diabetic retinopathy. (1989) Diabetes. **38**, 1203-1206.

Falanga, V., Iwamoto, S., Chartier, M., Yufit, T., Butmarc, J., Kouttab, N., Shrayer, D., Carson, P. Autologous bone marrow-derived cultured mesenchymal stem cells delivered in a fibrin spray accelerate healing in murine and human cutaneous wounds. (2007) Tissue Eng. **13**, 1299-2312.

Farrington-Rock, C., Crofts, N.J., Dhoerty, M.J., Ashton, B.A., Criffin-Jones, C., Canfield, A.E. Chondrogenic and adipogenic potential of microvascular pericytes. (2004) Circulation. **110**, 2226-2232.

Flammer, Konieczka, Bruno, Virdis, Flammer, Taddei. The eye and the heart. (2013) European Heart Journal. **34** 1270-1278.

Fowler, M.J. Microvascular and macrovascular complications of diabetes. (2008) Clincial diabetes. **26**, 77-82.

Friedenwald JS. Diabetic Retinopathy. American J Ophthalmology. (1950) **33**, 1187-99.

Fujimoto, T, and Singer, SJ. Immunocytochemical studies of desmin and vimentin in pericapillary cells of chicken. (1987) J. Hitochem and Cyochem. **35**,1105-1115.

Gaengel, K., Genove, G., Armulik, A., Betsholtz, C. Endothelial-mural cell signaling in vascular development and angiogenesis. (2009) Arterioscler Thromb Vasc Biol. **29**, 630-638.

Geraldes, P., Hiraoka-Yamamoto, J., Matsumoto, M., Clermont, A., Leitges, M., Marette, A., Aiello, L., Kern, T.S., King, G.L. Activation of PKCδ and SHP1 by hyperglycemia causes vascular cell apoptosis and diabetic retinopathy. (2013) Nature Medcine. **15**, 1298-1306.

Gerhardt, H., and Betsholtz, C. Endothelial-Pericyte interactions in angiogenesis. (2003) Cell Tissue Res. **314**, 15-23.

Gillies, M.C., Su, R. High glucose inhibits retinal capillary pericyte contractility in vitro. (1993) IOVS. **34**, 3396-3401.

Gimbron, MA, Cotran, RS, Folkman, J. Human vascular endothelial cells in culture: Growth and DNA synthesis. (1974) J Cell Biol. **60**, 673-684l.

Gitlin, JD and D'Amore, PA. Culture of retinal capillary cells using selective growth media. (1983) Microvascular research. **26**, 74-80.

Goldman, G.E. Vitalfärbung am Zentralnervensystem. (1913) Abh. Preuss. Akd. Wiss. **1**, 1-60.

Goldstein, G.W. Endothelial cell-astrocyte interactions. A cellular model of the blood-brain barrier. (1988) Ann N Y Acad Sci. **529**, 31-39.

Gologorsky, D., Thanos, A., Vavvas, D. Therapeutic interventions against inflammatory and angiogenic mediators in proliferative diabetic retinopathy. (2012) Mediators of inflammation **2012**, 629452.

Goumans, M.J., Valdimarsdottir, G., Itoh, S., Rosendahl, A., Sideras, P., and Dijke, P.T. Balancing the activation state of the endothelium via two distinct TGF-β type I receptors. (2002) EMBO Journal. **21**, 1743-1753.

Guyton, A.C. (1987) O'Keefe, K. and Zawodny, L. (Eds.) Human Physiology and Mechanisms of Disease. Philadelphia, PA: W.B. Saunders Company.

Haefiger, I.O., Zschauer, A., Anderson, D.R. Relaxation of Retinal Pericyte Contractile Tone Through the Nitric Oxide-Cyclic Guanosine Monophosphate Pathway. (1994) IOVS. **35**, 991-997.

Hamilton, N.B., Attwell, D., Hall, C.N. Pericyte-mediated regulation of capillary diameter: a component of neurovascular coupling in health and disease. (2010) Frontiers in Neuroenergetics. **2**, 1-14.

Hammes, H.P., Lin, J., Renner, O., Shani, M., Lundqvist, A., Betsholtz, C., Brownlee, M., Deutsch, U. Pericytes and the pathogenesis of diabetic retinopathy. (2002) Diabetes **51**, 3107-3112.

Hammes, H.P., Martin, S., Federlin, K., Geisen, K., Brownlee, M. Aminoguanidine treatment inhibits development of diabetic retinopathy. (1991) PNAS. **88**, 11555-11558.

Hanum, Steen. Diabetic retinitis; clinical studies of 195 cases of retinal changes in diabetics. (1938) Diss. E. Munksgaard,.

Harris, A., Wild, P., Stopak, D. Silicone Rubber Substrata: A New Wrinkle in the Study of Cell Location. (1980) Science. **208**177-179.

Hatori, M., Le, H., Vollmers, C., Keding, S.H., Tanaka, N., Schmedt, C., Jegla, T., Panda, S. Inducible ablation of melanopsin-expressing retinal ganglion cells reveals their central role in non-image forming visual responses. (2008) Plos One. **3**, e24651.

Hatori, M., Le, H., Vollmers, C., Keding, S.R., Tanaka, N., Schmedt, C., Jegla, T., Panda, S. Inducible Ablation of melanopsin-expressing retinal ganglion cells reveals their central role in non-image forming visual responses. (2008) Plos One. **3**, e2451

Hellström, M., Gerhardt, H., Kalén, M., Li, X., Eriksson, U., Wolburg, H. and Betsholtz, C. (2001). Lack of pericytes leads to endothelial hyperplasia and abnormal vascular morphogenesis. J. Cell Biol. 153, 543-553.

Hellström, M., Lindahl, K.M., Abramsson, A., Betsholtz, C. Role of PDGF-B and PDGFR-beta in recruitment of vascular smooth muscle cells and pericytes during embryonic blood vessel formation in the mouse. (1999) Development. **126**, 3047-3055.

Herman, IM, and D'Amore, PA. Microvascular pericytes contain muscle and nonmuscle actins. (1985) J. Cell Biology. **101**, 43-52.

Hirshi, K.K., Rohovsky, D'Amore, P.A. PDGF, TGF-B, and heterotpic cell-cell interactions mediate endothelial cell-induced recruitment of 10T1/2 cells and their differentiation into smooth muscle fate. J. Cell Biology. **141**, 805-814.

Huang, FJ, You, WK, Bonaldo, P, Seyfried, TN, Pasquale, EB, Stallcup, WB. Pericyte deficiencies lead to aberrant tumor vascularizaton in the brain of the NG2 null mouse. (2010) Developmental Biology. **344**, 1035-1046.

Indra, A.K., Warot, X., Brocard, J., Bornert, J.M., Xiao, J.H., Chambon, P., Metzger, D. Temporally-controlled site-specific mutagenesis in the basal layer of the epidermis: comparison of the recombinase activity of the tamoxifen-inducible Cre-ER(T) and Cre-ER(T2) recombinases. (1999) Nucleic acids research. **27**, 4324-4327.

International Diabetes Federation. (2013) IDF Diabetes Atlas, 6th edn. Brussels, Belgium: International Diabetes Federation. http://www.idf.org/diabetesatlas

Ishida, S., Usui, R., Yamashiro, K., Kaji, Y., Ahmed, E., Carrasquillo, K.G., Amano, S., Hida, T., Oguchi, Y., Adamis, A.P. VEGF164 is proinflammatory in the diabetic retina. (2003) IOVS **44**, 2155-2162.

Jaffe, EA, Nachman, RL, Becker, CG, Minick, CR. Culture of human endothelial cells derived from umbilical veins. (1973) J Clin Invest. **52,** 2745-2756.

Jardeleza, M.S., Miller, J.W. Review of anti-VEGF therapy in proliferative diabetic retinopathy. (2009) Seminars in ophthalmology. **24**, 87-92.

Joussen AM, Poulaki V, Le ML, Koizumi K, Esser C, Janicki H, Schraermeyer U, Kociok N, Fauser S, Kirchhof B, Kern TS, Adamis AP: A central role for inflammation in the pathogenesis of diabetic retinopathy. (2004) The FASEB journal. **18**, 1450-1452.

Joussen, A.M., Poulaki, V., Le, M.L., Koizumi, K., Esser, C., Janicki, H., Schraermeyer, U., Kociok, N., Fauser, S., Kirchhof, B., Kern, T.S., Adamis, A.P. A central role for inflammation in the pathogenesis of diabetic retinopathy. (2004) The FASEB Journal. **12**, 1450-1452.

Joyce, N.C., DeCamilli, P., Boyles, J. Pericytes, like vascular smooth muscle cells, are immunocytochemically positive for cyclic GMP-dependent protein kinase. (1984) Microvascular research. **28**, 206-219.

Joyce, N.C., Haire, M.F., Palade, G.E. Contractile proteins in pericytes. II. Immunocytochemical evidence for the presence of two isomyosins in graded concentrations. (1985). J. Cell Biology. **100**, 1387-1395.

Joyce, N.C., Haire, M.F., Palade, G.E. Contractile proteins in pericytes. I. Immunoperoxidase localization of tropomyosin. (1985) J. Cell Biology. **100**, 1379-1386.

Keane, P.A. and Sadda, S.R. Development of anti-VEGF therapiesfor intraocular use: a guide for clinicians. (2012) Journal of Ophthalmology. **2012**, 483034.

Kelley, C., D'Amore, P., Hechtman, H.B., Shepro, D. Microvascular Pericyte Contractility In Vitro: Comparison with Other Cells of the Vascular Wall. (1987) J. Cell Biology. **104**, 483-490.

Kelley, C., D'Amore, P., Hechtman, H.B., Shepro, D. Vasoactive hormones and cAMP affect pericyte contraction and stress fibres in vitro. (1988) J. Muscle Research and Cell Motility. **9**, 184-194.

Kern, T.S. and Engerman, R.L. A mouse model of diabetic retinopathy. (1993). Arch Ophthalmol. **114**, 986-990.

Kern, T.S. and Engerman, R.L. Capillary lesions develop in retina rather than cerebral cortex in diabetes and experimental galactosemia. (1996) Arch. Ophthalmology. **114**, 306-310.

Klein, R., Klein, B.E., Moss, S.E., Davis, M.D., DeMets, D.L. The Wisconsin epidemiologic study of diabetic retinopathy. III. Prevalence and risk of diabetic retinopathy when age at diagnosis is 30 or more years. (1984A) Archives of ophthalmology. **102**, 527-532.

Klein, R., Klein, B.E., Moss, S.E., Davis, M.D., DeMets, D.L. The Wisconsin epidemiologic study of diabetic retinopathy. II. Prevalence and risk of diabetic retinopathy when age at diagnosis is less than 30 years. (1984B) Archives of ophthalmology **102**, 520-526.

Kowluru, R.A., Zhong, Q., Kanwar, M. Metabolic memory and diabetic retinopathy: Role of inflammatory mediators in retinal pericytes. (2010) Experimental Eye Research. **90**, 617-623.

Kuwabara and Cogan. Retinal Vascular Patterns. VI. Mural Cells of the Retinal Capillaries. (1963) **69**, 114-124.

Kuwabara, T. and Cogan, D.G. Studies of retinal vascular patterns. Part I. Normal Vasculature. (1960) Arch in Ophthal. **74**, 124-131.

Larsson, J., Goumans, M.J., Sjo¨strand, L.J., van Rooijen, M.A., Ward D, Leve´en, P., Xu, X., ten Dijke, P., Mummery, C.L., Karlsson, S. Abnormal angiogenesis but intact hematopoietic potential in TGF-beta type I receptor-deficient mice. (2001) EMBO J. **20**, 1663–1673.

Laterra J, Keep R, Betz LA, et al. Blood—Cerebrospinal Fluid Barrier. In: Siegel GJ, Agranoff BW, Albers RW, et al., editors. Basic Neurochemistry: Molecular, Cellular and Medical Aspects. 6th edition. Philadelphia: Lippincott-Raven; 1999. Available from: http://www.ncbi.nlm.nih.gov/books/NBK27998/

Laver, N.M., Robison, W.G., Jr., Pfeffer, B.A. Novel procedures for isolating intact retinal vascular beds from diabetic humans and animal models. (1993) Investigative ophthalmology & visual science. **34**, 2097-2104.

Leveen, P., Pekny, M., Gebre-Medhin, S., Swolin, B., Larsson, E., and Betsholtz, C. Mice deficient for PDGF B show renal, cardiovascular, and hematological abnormalities. (1994) Genes Dev. **8**, 1875-1887.

Li, D.Y., Sorensen, L.K., Brooke, B.S., Urness, L.D., Davis, E.C., Taylor, D.G., Boak, B.B., Wendel, D.P. Defective angiogenesis in mice lacking endoglin. (1999). Science. **284**, 1534-1537.

Liew, Wang. Retinal vascular signs: a window to the heart? Rev Esp Cardiol (2011) **64** 515-521.

Lindahl, P., Johansson, B.R., Leveen, P., Betsholtz, C. Pericyte loss and microaneurysm formation in PDGF-B-deficient mice. (1997) Science. **277**, 242-245.

Loeffler, F. Mitt. Gesundheitamte (1884) Aus dem Kaiserl **2**, 421-499.

Ly, A., Yee, P., Vessey, K.A., Phipps, J.A., Jobling, A.I, Fletcher, E.L. Early inner retinal astrocyte dysfunction during diates and development of hypoxia, retinal stress, and neuronal functional loss. (2011) IOVS. **52**, 9316-0326.

Mansilla, E., Martin, G.H., Drago, H., Sturla, F., Salas, E., Gardiner, C., Bossi, S., Lamonega, R., Guzman, A., Nunez, A., et al. Bloodstream cells phenotypically identical to human mesenchymal bone marrow stem cells circulate in large amounts under the influence of acute large skin damage: new evidence for their use in regenerative medicine. (2006) Transplant Proc. **38**, 29-36.

Marieb, E.N. (2004) Human anatomy and physiology. San Francisco, CA: Pearson Education, Inc.

Mason, J.O., Nixon, P.A., White, M.F. Intravitreal injection of bevacizumab (Avastin) as adjunctive treatment of proliferative diabetic retinopathy. (2006) American journal of ophthalmology **142**, 685-688.

Massin, P., Bandello, F., Garweg, J.G., Hansen, L.L., Harding, S.P., Larsen, M., Mitchell, P., Sharp, D., Wolf-Schnurrbusch, U.E., Gekkieva, .M, Weichselberger, A., Wolf, S. Safety and efficacy of ranibizumab in diabetic macular edema (RESOLVE Study): a 12-month, randomized, controlled, double-masked, multicenter phase II study. (2010) Diabetes care. **33**, 2399-2405.

Matsugi, R., Chen, Q., and Anderson, D.R. Adenosine-induced relaxation of cultured bovine retinal pericytes. (1997) IOVS. **38**, 2695-2701.

Maxwell, D.S., and Kruger, L. Small blood vessels and the origin of phagocytes in the rat cerebral cortex following heavy particle irradiation. (1965) Experimental neurology. **12**, 33-54.

Meyrick, B., and Reid, L. Hypoxia and incorporation of 3H-thymidine by cells of the rat pulmonary arteries and alveolar wall. (1979) Am J pathol. **96**, 51-70.

Miller, J.W., Adamis, A.P., Aiello, L.P. Vascular endothelial growth factor in ocular neovascularization and proliferative diabetic retinopathy. (1997) Diabetes/metabolism reviews. **13**, 37-50.

Mills, S.J., Cowin, A.J., Kaur, P. Pericytes, mesenchymal stem cells and the wound healing process. (2013) Cells. **2**, 621-634.

Mitzutani, M., Kern, T.S., Lorenzi, M. Accelerated death of retinal microvascular cells in human and experimental diabetic retinopathy. (1996) Journal of Clinical Investigation. **97**, 2883-2890.

Movat, H.Z., Fernando, N.V.P. The fine structure of the terminal vascular ved. IV. The venules and their perivascular cells (pericytes, adventitial cells). (1964) Experimetnal and molecular pathology. **3**, 98-114.

Nagai, N., Izumi-Nagai, K., Oike, Y., Koto, T., Satofuka, S., Ozawa, Y., Yamashiro, K., Inoue, M., Tsubota, K., Umezawa, K, Ishida, S. Suppression of diabetes-induced retinal inflammation by blocking the angiotensin II type 1 receptor or its downstream nuclear factor-kB pathway. (2007) IOVS. **48**, 4342-4350.

Nakagawa, H., Akita, S., Fukui, M., Fujii, T., Akino, K. Human mesenchymal stem cells successfully improve skin-substitute wound healing. (2005) Br. J. Dermatol. **153**, 29-36.

Nehls, V., Denzer, K., Drenckhahn, D. Pericyte involvement in capillary sprouting. (1992) Cell Tissue Res. **270**, 469-474.

Newman, D.K. Surgical management of the late complications of proliferative diabetic retinopathy. (2010) Eye **24**, 441-449.

Nilausen, K. The vasoformative tissue in the foetal retina with particular reference to the histochemical demonstration of tis alkaline phosphatase activity. (1958) Acta Ophthal. **36**, 65-69.

Norton, E.W. and Gutman, F. (1967) Kimura, S. and Caygill, W. (eds.) Fluorescein angiography of the retina in diabetes mellitus. Vascular complications of diabetes mellitus: with special emphasis in microangiopathy of the eye. Mosby, St. Louis, MO.

Olridge, A. and D'Amore, P.A. Inhibition of capillary endothelial cell growth by pericytes and smooth muscle cells. (1987) J. Cell Biology. **105**, 1455-1462.

Oshima, M., Oshima, H., Taketo, M.M. TGF-beta receptor type II deficiency results in defects of yolk sac hematopoiesis and vasculogenesis. (1996) Dev Biol. **179**, 297–302.

Ozerdem, U, Grako, KA, Dahlin-Huppe, K, Monosov, E, Stallcup, WB. NG2 proteoglycan is expressed exclusively by mural cells during vascular morphogenesis. (2001) Developmental dynamics. **222**, 218-227.

Palm, E. On the occurrence in the retina of conditions corresponding to the blood-brain barrier. (1947) Acta Ophthalmology **25**, 29-35.

Pappernheimer, A.M. Diphtheria toxin. (1977) Ann Rev Biochem. **46**, 69-94.

Paquet-Fifield, S., Schluter, H., Li, A., Aitken, T., Gangartirkar, P., Blashki, D., Koelmeyer, R., Pouliot, N., Palatsides, M., Ellis, S., et al. A role for pericytes as microenvironmental regulators of human skin tissue regeneration. (2009) J Clin Invest. **119**, 2795-2806.

Patan, S. TIE1 and TIE2 receptor tyrosine kinases inversely regulate embryonic angiogenesis by the mechanism of intussusceptive microvascular growth. (1998) Microvascular Research. **56**, 1-21.

Peppiatt, C.M., Howarth, C., Mobbs, P., Attwell, D. Bidirectional control of CNS capillary diameter by pericytes. (2007) Nature. **443**, 700-704.

Pollay, M., Roberts, PA. Blood-Brain Barrier: A definition of normal and altered function. (1980) Neurosurgery. **6**, 675-685.

Robinson, R., Barathi, V.A., Chaurasia, S.S., Wong, T.Y., Kern, T.S. Update on animal models of diabetic retinopathy, from molecular approaches to mice and higher mammals. (2012) Disease models & mechanisms. **5**, 444-456.

Rong, J.X., Shapiro, M., Trogan, E., Fisher, E.A. Transdifferentiation of mouse aortic smooth muscle cells to macrophage-like state after cholesterol loading. (2003) PNAS. **100**, 13531-13536.

Ross, M.H, Reith, E.J., Romrell, L.J. (1989) Histology – A text and atlas. Baltimore, MD: Williams & Wilkins.

Rouget, C. Memoire sur le developpement, la structure et les proprieties physiologiques des capillaries sanguins et lymphatiques. Arch Physiol Normale Pathol (1873) **5**, 603-661.

Rouget, C. Sur la contractilite des capillaires sanguins. CR (1879) Acad Sci. **88**, 916-918.

Roux, E. and Yersin, A. Contribution a l'etude de la diphtheria. (1888) Ann Inst Pasteur **2**, 629-661.

Roy, M.S., Klein, R., O'Colmain, B.J., Klein, B.E., Moss, S.E., Kempen, J.H. The prevalence of diabetic retinopathy among adult type 1 diabetic persons in the United States. (2004) Archives of ophthalmology. **12,** 546-551.

Sagare, A.P., Bell, R.D., Zhao, Z., Ma, Q., Winkler, E.A., Ramanathan, A., Zlokovic, B.V. Pericyte loss influences Alzheimer-like neurodegeneration in mice. (2013) Nature Communication. **4**, 2932.

Saint-Geniez, M., Maharaj, A.S., Walshe, T.E., Tucker, B.A., Sekiyama, E., Kurihara, T., Darland, D.C., Young, M.J., D'Amore, P.A. Endogenous VEGF is required for visual function, evidence for a survival role on muller cells and photoreceptors. (2008) PloS one. **3**, e3554.

Sakagami, K. Kawamura, H., Wu, D.M., Puro, D.G. Nitric oxide/cGMP-induced inhibition of calcium and choloride currents in retinal pericytes. (2001A) Microvascular Research. **62**, 196-203.

Sakagami, K., Kodama, T., Puro, D.G. PDGF-induced coupling of function with metabolism in microvascular pericytes of the retina. (2001B) IOVS. **42**, 1929-1944.

Sakagami, K., Wu, D.M., Puro, D.G. Physiology of rat retinal pericytes: modulation of ion channel activity by serum-derived molecules. (1999) J. Physiology. **521**, 637-650.

Sapieha, P., Hamel, D., Shao, Z., Rivera, J.C., Zaniolo, K., Joyal, J.S., Chemtob, S. Proliferative retinopathies: angiogenesis that blinds. (2010) The international journal of biochemistry & cell biology. **42**, 5-12.

Sasongko MB, Wong TY, Nguyen TT, Cheung CY, Shaw JE, Wang JJ. Retinal vascular tortuosity in persons with diabetes and diabetic retinopathy. (2011) Diabetologia. **54,** 2409-2416.

Sato, T.N., Tozawa, Y., Deutsh, U., Wolburg-Buchholz, K., Fujiwara, Y., Gendron-Maguire, M., Dridley, T., Wolburg, H., Risau, W., Qin, Y. Distinct roles of the receptor tyrosine kinases Tie-1 and Tie-2 in blood vessel formation. (1995) Nature. **376**, 70-74.

Sato, Y., and Rifkin, D.B. Inhibition of endothelial cell movement by pericytes and smooth muscle cells: activation of a latent transofrming growth factor-β1-like molecule by plasmin during co-culture. (1989) J. Cell Biology. **109**, 309-315.

Saunders, W.B., Bohnsack, B.L., Faske, J.B., Anthis, N.J., Bayless, K.J., Hirschi, K.K., Davis, G.E. Coregulation of vascular tube stabilization by endothelial cell TIMP-2 and pericyte TIMP-3. (2006) The Journal of cell biology. **175**, 179-191.

Schlingemann, RO, Rietveld, FJR, de Wall, RMW, Ferrone, S, Ruiter, DJ. Expression of the high molecular weight melanoma-associated antigen by pericytes during angiogenesis in tumors and in healing wounds. (1990)American J of Pathology. **136**, 1392-1405.

Schnaudiegel. Die Vitalfarbung mit Trypanblau am Auge. (1913) Graefes Arch Ophthalmol. **86**, 93-97.

Schonfeld G. Strain survey of liver and plasma lipids and blood glucose levels in 11 inbred strains of mice. MPD:32301. Mouse Phenome Database web site, The Jackson Laboratory, Bar Harbor, Maine USA. http://phenome.jax.org, Apr, 2014.

Schwab, K.E., Gargett, C.E. Co-expression of two perivascular cell markers isolates mesenchymal stem-like cells from human endometrium. (2007) Hum Reprod. **22**, 2903-2911.

Shakib, M. and Cunha-Vaz, J.G. Studies of the permeability of the blood-retinal barrier. IV. Role of the junctional complexes of the retinal vessels on the permeability of the blood-retinal barrier. (1966) Exp. Eye Res. **5**, 229-234.

Shepro, D. and Morel, NM, Pericyte physiology. (1993) FASEB J. **7**, 1031-1038.

Shi, S., Gronthos, S. Perivascular niche of postnatal mesenchymal stem cells in human bone marrow and dental pulp. (2003) J Bone Miner Res. **18**, 696-704.

Sims, DE. The Pericyte – A Review. (1986) Tissue and Cell. **18**, 153-174.

Skalli, O, Pelte, MF, Peclet, MC, Gabbiani, G, Gugliotta, P, Bussolati, G, Ravoazzola, M, Orci, L. Alpha-smooth muscle actin, a differentiation marker of smooth muscle cells, is present in microfilamentous bundles of pericytes. (1989) J Histochem Cyochem. **37**, 315.

Sohn, E.H., He, S., Kim, L.A., Salehi-Had, H., Javaheri, M., Spee, C., Dustin, L., Hinton, D.R., Eliott, D.. Angiofibrotic response to vascular endothelial growth factor inhibition in diabetic retinal detachment: report no. 1. (2012) Archives of ophthalmology. **130**, 1127-1134.

Soriano, P. Abnormal kidney development and hematological disorders in PDGF beta-receptor mutant mice. (1994) Genes dev. **15**, 1888-1896.

Sorokin, S.P. and Hoyt, R.F. Macrophage development: I. Rationale for using Griffonia simplicifolia isolectin B4 as a marker for the line. (1992) Anat Rec. **232**, 520-526.

Speiser, P., Gittelsohn, A.M., Patz, A. Studies on diabetic retinopathy. 3. Influence of diabetes on intramural pericytes. (1968) Archives of ophthalmology. **80**, 332-337.

Speiser, P., Gittelsohn, AM, Patz, A. Studies on diabetic retinopathy. III. Influence of diabetes on intramural cells. (1968). Arch. Opthal. **80**, 332-337.

Stratman, A.N., Malotte, K.M., Mahan, R.D., Davis, M.J., Davis, G.E. Pericyte recruitment during vasculogenic tube assembly stimulates endothelial basement membrane matrix formation. (2009) Blood. **114**, 5091-5101.

Stratman, A.N., Schwindt, A.E., Malotte, K.M., Davis, G.E. Endothelial-derived PDGF-BB and HB-EGF coordinately regulate pericyte recruitment during vasculogenic tube assembly and stabilization. (2010) Blood. **116**, 4720-4730.

Sugiyama, T., Kawamura, H., Yamanishi, S., Kobayashi, M., Katsumura, K, Puro, D.G. Regulation of P2X7-induced pore formation and cell death in pericyte-containing retinal microvessels. (2005). Am. J. Physiol. Cell Physiol. **288**, C568-C576.

Sundberg, C., Kowanetz, M., Brown, L.F., Detmar, M., Dvorak, H.F. Stable expression of angiopoietin-1 and other markers by cultured pericytes: phenotypic similarities to a subpopulation of cells in maturing vessels during later stages of angiogenesis in vivo. (2002) Laboratory Investigation. **82**, 387-401.

Suri, C., Jones, P.F., Patan, S., Bartunkova, S., Maisonpierre, P.C., Davis, S., Sato, T.N., Yancopoulos, G.D. Requisite role of angiopoeitin-1, a ligand for the TIE2 receptor during embryonic angiogenesis. (1996) Cell. **87**, 1171-1180.

Tang, J. and Kern, T.S. Inflammation in diabetic retinopathy. (2011) Progress in Retinal and Eye Research. **30**, 343-358.

Taylor, E,. Dobree, J.H. Proliferative diabetic retinopathy. Site and size of initial lesions. (1970) The British journal of ophthalmology **54**, 11-18.

Tesfaye, S., Boulton, A.J.M, Dyck, P.J., Freeman, R., Horowitz, M., Kempler, P., Lauria, G., Malik, R.A., Spallone, V., Vinik, A., Bernardi, L., Valensi, P. Diabetic neuropathies. update on definitions, diagnostic criteria, estimation of severity, and treatments. (2010). Diabetes Care, **33**, 2285-2293.

The Diabetes Control and Complications Trial Research Group. The effect of intensive treatment of diabetes on the development and progression of long-term complications in insulin-dependent diabetes mellitus. (1993) New England Journal of Medicine. **329**, 977-986.

The Diabetes Control and Complications Trial/Epidemiology of Diabetes Interventions and Complications Research Group. Retinopathy and nephropathy in patients with type 1 diabetes four years after a trial of intensive therapy. (2000) The New England journal of medicine. **342**, 381-389.

Tilton, R.G., Kilo, C., Williamson, J.R., Murch, D.W. Differences in pericyte contractile function in rat cardia and skeletal muscle microvasculatures. (1979A) Microvascular research. **18**, 336-352.

Tilton, RG, Kilo, C, and Willimason, JR. Pericyte-endothelial relationships in cardiac and skeletal muscle capillaries. (1979B) Microvasc. Res. **18**, 325-335.

Tkachenko, E., Gutierrez, E., Saikin, S.K., Fogelstrand, p., Kim, C., Groisman, A., Ginseberg, M.H. The nucleus of endothelial cell as a sensor of blood flow direction. (2013) Biology Open. **2**, 1007-1012.

Tonello, M., Costa, R.A., Almeida, F.P., Barbosa, J.C., Scott, I.U., Jorge, R. Panretinal photocoagulation versus PRP plus intravitreal bevacizumab for high-risk proliferative diabetic retinopathy (IBeHi study).(2008) Acta ophthalmologica. **86**, 385-389.

Tongers, J., Roncalli, J.G., Losordo, D.W. Role of endothelial progenitor cells during ischemia-induced vasculogenesis and collater formation. (2010) Microvasc. Res. **79**, 200-206.

Uemura, A., Ogawa, M., Hirashima, M., Fujiwara, T., Koyama, S., Takagi, H., Honda, Y., Wiegand, S.J., Yancopoulos, G.D., Nishikawa, S.I. Recombinant angiopoietin-1 restores high-order architecture of growing blood vessels in mice. (2002) J. Clin. Invest. **110**, 1619.

Valarevic, V., Arsenijevic, N., Lukic, M.L., Stojkovic, M. Concise review: mesenchymal stem cell treatment of the complications of diabetes mellitus. (2011) Stem Cells. **29**, 5-10.

Verbeek, M.M., Westphal, J.R., Ruiter, D.J., de Waal, R.M. T lymphocyte adhesion to human brain pericytes is mediated via very late antigen-4/vascular cell adhesion molecule-1 interactions. (1995) Journal of Immunology. **154**, 5876-5884.

Vimtrup, BJ. Beitrage zur Anatomie der Capillaren. 1. Ueber contractile Elemente in der Gefisswand der Blutcnpillaren. (1922) Zeitschr. f. Anat. u. Entwickelungsg, Bd. 65, S. 150-184.

Vincent, J.A. and Mohr, S. Inhibition of caspase-1/interleukin-1b signaling prevents degeneration of retinal capillaries in diabetes and galactosemia. (2007) Diabetes. **56**, 224-230.

Winkler, EA, Bell, RD, Zlokovic, BV. Pericyte-specific expression of PDGF beta receptor in mouse models with normal and deficient PDGF beta receptor signaling. (2010) Molecular Neurodegeneration. **5**, 32.

Wirth, A., Benyo, Z., Lukasova, M., Leutgeb, B., Wettschureck, N., Gorbey, S., Orsy, P., Horvath, B., Maser-Gluth, C., Greiner, E., Lemmer, B., Schutz, G., Gutkind, J.S., Offermanns, S. G12-G13-LARG-mediated signaling in vascular smooth muscle is required for salt-induced hypertension. (2008) Nature medicine. **14**, 64-68.

Wislocke, G.B. and Dempsey, E.W. The chemical cytology of the choroid plexus and blood-brain barrier of the rhesus monkey (Macaca Mulatta). (1969) J. Comp. Neurol. **88**, 319-426.

Wu, Y., Chen, L., Scott, P.G., Tredget, E.E. Mesenchymal stem cells enhance wound healing through differentiation and angiogenesis. (2007) Stem Cells. **25**, 1648-2659.

Yang, X., Castilla, L.H., Xu, X., Li, C., Gotay, J., Weinstein, M., Liu, P.P., Deng, C.X. Angiogenesis defects and mesenchymal apoptosis in mice lacking SMAD5. (1999) Development. **126**, 1571–1580.

Yau J.W., Rogers S.L., Kawasaki R., Lamoureux E.L., Kowalski J.W., Bek T., Chen S.J., Dekker J.M., Fletcher A., Grauslund J., Haffner S., Hamman R.F., Ikram M.K., Kayama T., Klein B.E., Klein R., Krishnaiah S., Mayurasakorn K., O'Hare J.P., Orchard T.J., Porta M., Rema M., Roy M.S., Sharma T., Shaw J., Taylor H.,Tielsch J.M., Varma R., Wang J.J., Wang N., West S., Xu L., Yasuda M., Zhang X., Mitchell P., Wong T.Y. Meta-Analysis for Eye Disease (META-EYE) Study Group. Global prevalence and major risk factors of diabetic retinopathy. (2012) Diabetes Care. **3**, 556-564.

Zannettino, A.C., Paton, S., Khor, A.A., Itescu, F., Gimble, J.M. Multpotential human adipose-derived stromal stem cells exhibit a perivascular phenotype in vitro and in vivo. (2008) J Cell Physiol. **214**, 413-421.

Zhang, Q., Guy, K., Pagadala, J., Jiang, Y., Walker, R.J., Liu, L., Soderland, C., Kern, T.S., Ferry, R., He, H., Yates, C.R., Miller, D.D., and Steinle, J.J. Compound 49b prevents diabetes-induced apoptosis through increased IGFBP-3 levels. (2012) Ophthalmology and Visual Science. **53**, 3004-3013.

Zimmerman, K. Der Peinere Bau der Blutcapillaren. A Anat Entwicklungsgesch. (1923) **68**, 29-109.

Zlokovic, B.W. The blood-brain barrier in health and chronic neurodegenerative disorders. (2008) Neuron. **57**, 178-201.

APPENDIX

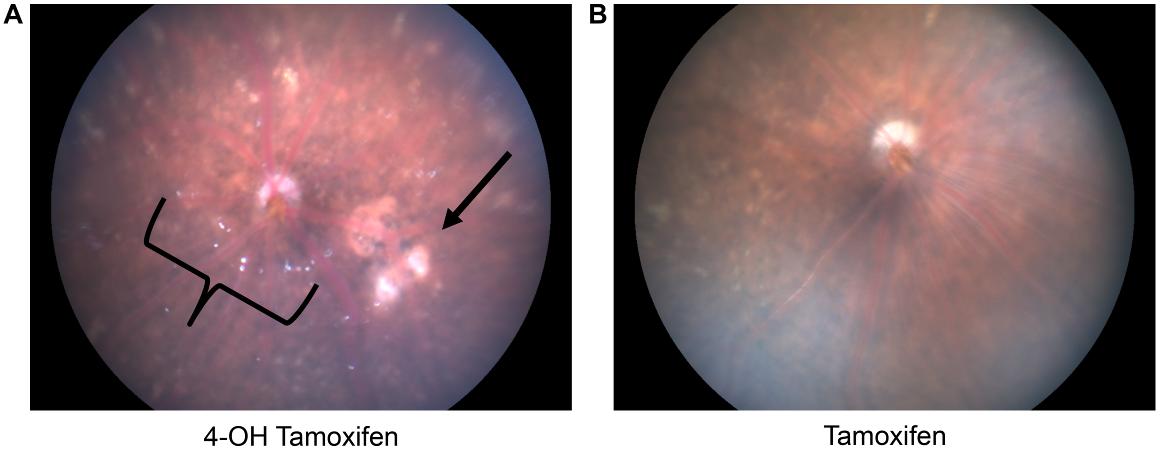

Supplemental Figure 1. 4-OH tamoxifen toxicity in the retina of iDTR; M-Cre mice. Fundus photography of iDTR; M-Cre mice eight- to 10-weeks post-IP injection with A) the active drug, 4-OH tamoxifen (500 ng in 225 µl corn oil) daily for five days or B) the precursor drug, tamoxifen, (500 ng in 225 µl corn oil) daily for three days. 4-OH tamoxifen showed signs of tamoxifen toxicity, as seen by tamoxifen crystal deposits (bracket) and retinal damage (arrow).

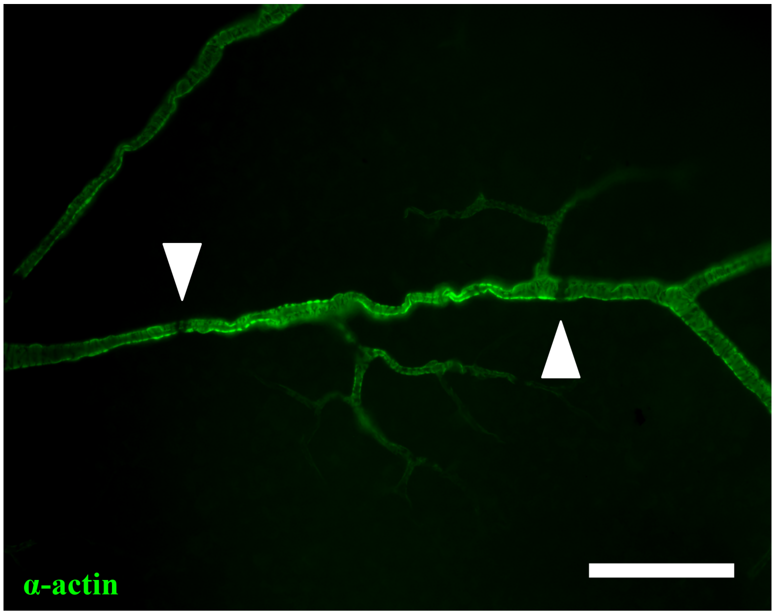

Supplemental Figure 2. Mural cell loss is associated with tortuosity in iDTR; M-Cre mice.
Retinal flat mounts were stained for alpha smooth muscle actin (α-actin, green) to detect mural vascular cells (pericytes and smooth muscle cells). Areas with mural cell loss (arrowheads) were associated with vessel tortuosity in systemically (IP) DT-treated iDTR; M-Cre mice. Scale bar = 100 μm.

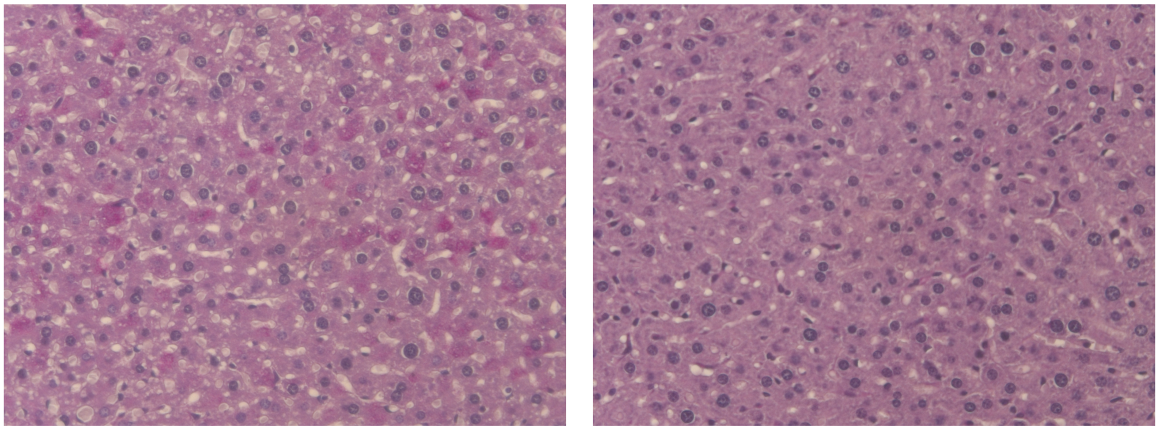

iDTR; M-Cre (-DT) **M-Cre (+DT)**

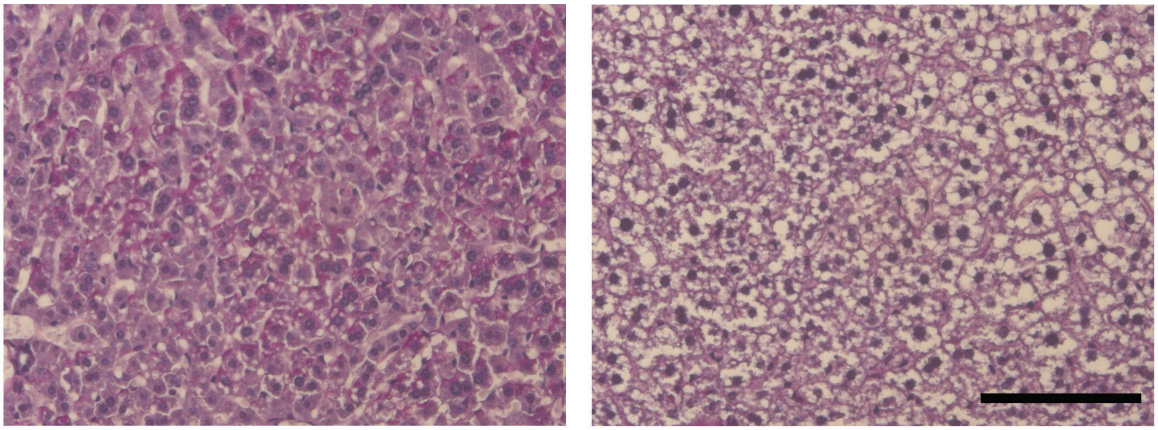

iDTR; M-Cre (+DT) **iDTR; M-Cre (+DT)**

Supplemental Figure 3. DT treatment in iDTR; M-Cre mice is associated with decreased glycogen in the liver.

Liver sections from iDTR; M-Cre (top left panel), DT-treated M-Cre (top right panel), and DT-treated iDTR; M-Cre (bottom two panels) mice were stained with periodic acid-Schiff (PAS, pink) to detect glycogen and hematoxylin (purple) to detect nuclei. Decreased glycogen, indicated by white areas lacking PAS staining, was observed in DT-treated iDTR; M-Cre mouse livers (bottom two panels), but varied among individual DT-treated iDTR; M-Cre mice (bottom left panel vs. bottom right panel). Scale bar = 100 μm.

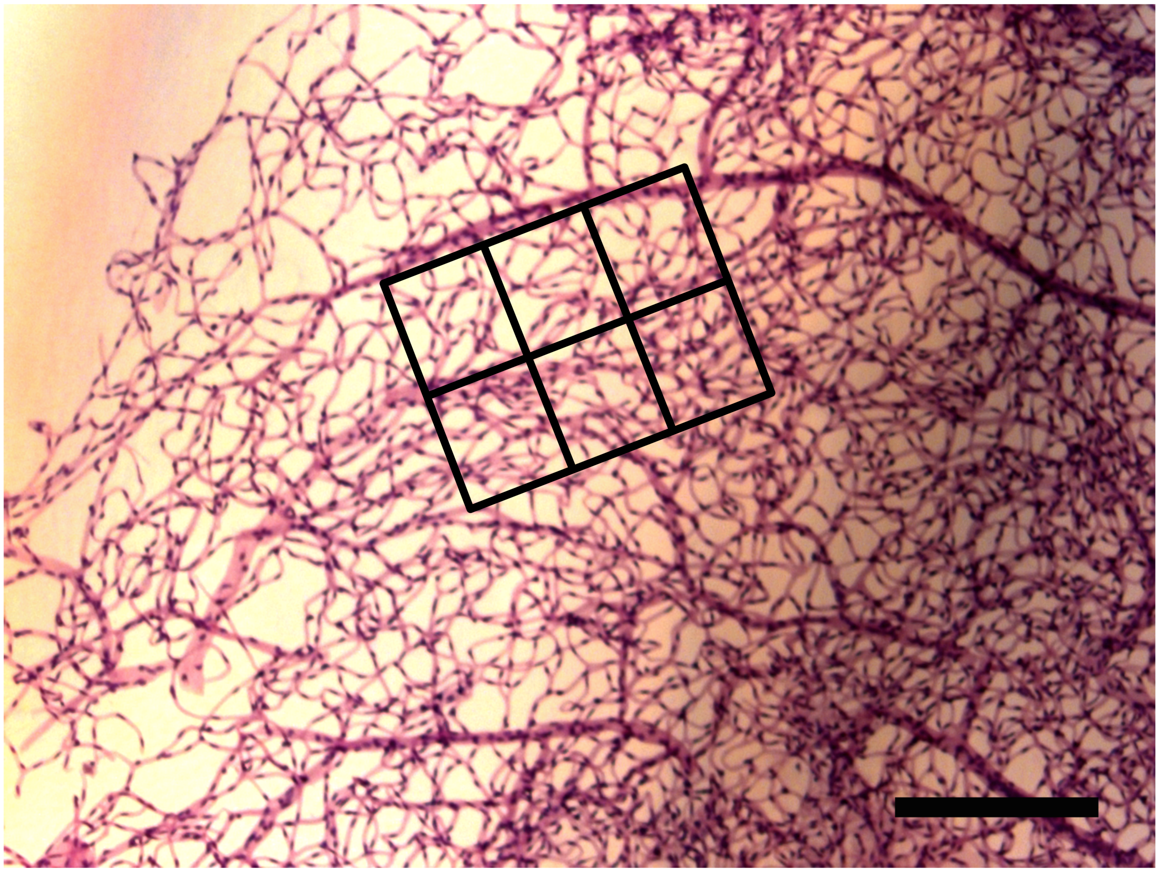

Supplemental Figure 4. Light microscopy image selection for EC, pericyte, and acellular capillary automated quantification.

Images (approximately 175 µm x 125 µm) were taken contiguously in groups of six (black grid) to avoid bias. A minimum of 10 groups of six images was taken per retina. Fields were randomly selected from each group of six images for quantification of ECs, pericytes, and acellular capillaries. Grid is not to scale and is intended only to illustrate the method of image selection used for quantification. Scale bar = 250 µm.